TABLE OF CONTENTS

NOMENCLATURE	v	1/A7
LIST OF APPENDICES	vii	1/A9
LIST OF FIGURES	viii	1/A10
LIST OF TABLES	x	1/A12
SUMMARY	xi	1/A13

CHAPTER

1. INTRODUCTION	1	1/A14
2. DIMENSIONLESS EQUATIONS OF MOTION	3	1/A2
2.1 Three-Dimensional Equations of Motion		
2.2 Dimensionless Equations of Motion		
3. VARIATIONAL FORMULATION	6	1/B8
3.1 Variational Formulation		
3.2 Integrals of the Motion		
4. PLANAR FLIGHT	14	1/B12
4.1 Governing Equations		
4.2 Change of Adjoint Variables		
5. FLAT PLANET SIMPLIFICATION	18	1/C3
5.1 Governing Equations for Flat Planet Model		
6. OPTIMAL TRAJECTORIES FOR FLAT EARTH	22	1/C7
6.1 Maximum Final Speed or Maximum Final Altitude		
6.2 Pull-Up Maneuver with Bounded λ		
6.3 Maximum Range		
6.4 Linearized Singular Lift Control for Maximum Range		

7. OPTIMAL TRAJECTORIES FOR SPHERICAL EARTH 49 1/E13

7.1 Pull-Up Maneuver at Moderate Altitude
7.2 Keplerian Motion Following a Skip Maneuver
7.3 Skip Trajectory for Maximum Final Speed
7.4 Skip Trajectory for Maximum Apogee Altitude
7.5 Skip Trajectory for Maximum Apogee Altitude with Prescribed Apogee Speed
7.6 Skip Trajectory for Maximum Apogee Speed with Prescribed Apogee Altitude
7.7 Skip Trajectory for Maximum Coasting Range
7.8 Glide with Maximum Range

8. THREE-DIMENSIONAL FLIGHT 77 2/A7

8.1 Maximum Cross Range
8.2 The Footprint

9. CONCLUSIONS 97 2/C5

APPENDICES 100 2/C8

REFERENCES 109 2/D3

NAS1.26:3236

FEB 25 1980

COMPLETED

ORIGINAL

NASA Contractor Report 3236

Optimum Reentry Trajectories of a Lifting Vehicle

Jeng-Shing Chern and Nguyen Xuan Vinh

GRANT NSG-1448
FEBRUARY 1980

NASA

121

NASA Contractor Report 3236

Optimum Reentry Trajectories of a Lifting Vehicle

Jeng-Shing Chern and Nguyen Xuan Vinh
The University of Michigan
Ann Arbor, Michigan

Prepared for
Langley Research Center
under Grant NSG-1448

National Aeronautics
and Space Administration

Scientific and Technical
Information Office

1980

TABLE OF CONTENTS

NOMENCLATURE v

LIST OF APPENDICES vii

LIST OF FIGURES viii

LIST OF TABLES x

SUMMARY xi

CHAPTER

1. INTRODUCTION 1

2. DIMENSIONLESS EQUATIONS OF MOTION . . . 3

2.1 Three-Dimensional Equations of Motion
2.2 Dimensionless Equations of Motion

3. VARIATIONAL FORMULATION 9

3.1 Variational Formulation
3.2 Integrals of the Motion

4. PLANAR FLIGHT 14

4.1 Governing Equations
4.2 Change of Adjoint Variables

5. FLAT PLANET SIMPLIFICATION. 18

5.1 Governing Equations for Flat Planet Model

6. OPTIMAL TRAJECTORIES FOR FLAT EARTH 22

6.1 Maximum Final Speed or Maximum Final Altitude
6.2 Pull-Up Maneuver with Bounded λ
6.3 Maximum Range
6.4 Linearized Singular Lift Control for Maximum Range

7. OPTIMAL TRAJECTORIES FOR SPHERICAL EARTH 49

7.1 Pull-Up Maneuver at Moderate Altitude
7.2 Keplerian Motion Following a Skip Maneuver
7.3 Skip Trajectory for Maximum Final Speed
7.4 Skip Trajectory for Maximum Apogee Altitude
7.5 Skip Trajectory for Maximum Apogee Altitude with Prescribed Apogee Speed
7.6 Skip Trajectory for Maximum Apogee Speed with Prescribed Apogee Altitude
7.7 Skip Trajectory for Maximum Coasting Range
7.8 Glide with Maximum Range

8. THREE-DIMENSIONAL FLIGHT 77

8.1 Maximum Cross Range
8.2 The Footprint

9. CONCLUSIONS 97

APPENDICES. 100

REFERENCES 109

NOMENCLATURE

A, B	functions, Eqs (6.33)
C	function, Eq. (6.34)
C_j	constants of integration
C_D	drag coefficient
C_D^*	drag coefficient for maximum lift-to-drag ratio
C_L	lift coefficient
C_L^*	lift coefficient for maximum lift-to-drag ratio
e	eccentricity of orbit
E^*	maximum lift-to-drag ratio
F	ratio of adjoint variables, Eq. (4.6)
g	acceleration of gravity
G	ratio of adjoint variables, Eq. (5.8)
h	altitude
H	Hamiltonian function
J	performance index
k	parameter of atmosphere, $k^2 = \beta r$
k_1, k_2	constants of integration
m	mass of vehicle
N, P, Q	modified adjoint variables, Eqs. (3.8)
p	conic parameter
p_x	adjoint variable associated to state variable x
r	radial distance from center of the planet
R	ratio of apogee distance to radius of atmosphere
s	dimensionless arc length, Eq. (2.7)
S	reference area
t	time
u	dimensionless kinetic energy for flat planet case, Eq. (5.1)
v	dimensionless kinetic energy for spherical planet case, Eq. (2.7)
$\bar{v}_a$	dimensionless kinetic energy at apogee, Eq. (7.26)

w	dimensionless wing loading, used as altitude variable in flat planet case, Eq. (5.1)
y	dimensionless longitudinal range, Eq. (5.2)
Y	longitudinal range
z	dimensionless lateral range
Z	Chapman's modified altitude variable, Eq. (2.7)
β	inverse of height scale
γ	flight path angle
η	u/v , dimensionless dynamic pressure
θ	longitude
λ	normalized lift coefficient, Eq. (2.4)
μ	gravitational constant
ξ	half the range of skip trajectory, Fig. 15
ρ	density of atmosphere
σ	bank angle
ϕ	latitude
ψ	heading

Subscript

a	condition at apogee
b	condition at lowest point of trajectory
f	final condition
i	initial condition
s	condition at switching point
max	maximum condition

LIST OF APPENDICES

APPENDIX A 100

APPENDIX B 102

APPENDIX C 106

LIST OF FIGURES

1. State Variables, Control Variables, and Other Parameters Defined with Respect to Inertial Coordinates, OXYZ. 4

2. Geometry of a Pull-Up Maneuver 23

3. Solution for Pull-Up Maneuver 26

4. Variation of the Optimal Lift Coefficient in Terms of the Flight Path Angle in Pull-Up Maneuver 28

5. Influence of the Initial Speed on Optimum Solution . . . 31

6. Influence of the Initial Flight Path Angle on Optimum Solution 32

7. Optimum Trajectories for Pull-Up Maneuver 34

8. Pull-Up Maneuver with Bounded λ; Trajectories in the Physical Space $\beta(h - h_1)$ vs y, and Variation of the Optimum Bounded Lift Control 36

9. Variation of the Optimum λ for Glide with Maximum Range 40

10. Variation of the Flight Path Angle for Glide with Maximum Range 41

11. Variation of the Dimensionless Dynamic Pressure for Glide with Maximum Range 42

12. Variation of the Optimum Lift Coefficient for Short Range (Small Altitude Drop) Glide 43

13. Solution for the Optimum Pull-Up Maneuver at Low Speed over a Spherical Earth 51

14. Variation of the Optimum Lift Coefficient for Pull-Up Maneuver at Low Speed over a Spherical Earth 52

15. Geometry of a Skip Trajectory 53

16. Variation of the Optimum λ as a Function of the Speed Ratio for Skip Trajectories with Maximum Final Speed . 59

17. Maximum Apogee Distance for a Prescribed Apogee Speed, or Maximum Apogee Speed for a Prescribed Apogee Distance. 63

18. Variation of the Optimum λ for Low Altitude Maximum Range Glide over a Spherical Earth 70

19. Variation of γ for Low Altitude Maximum Range Glide over a Spherical Earth 71

20. Variation of the Altitude and the Speed for Low Altitude Maximum Range Glide over a Spherical Earth 72

21. Variation of the Altitude for Maximum Range Glide from the Reentry Point 74

22. Variation of γ for Maximum Range Glide from the Reentry Point 75

23. Variation of the Optimum λ and the Speed for Maximum Range Glide from the Reentry Point 76

24. The Longitudinal and Cross Ranges as Functions of E^* . 82

25. Variation of the Altitude and the Speed of the Trajectory Generated by the Control Law $\lambda = 1$ and Eq. (8.14) . . 84

26. Variation of the Flight Path Angle and the Bank Control of the Trajectory Generated by the Control Law $\lambda = 1$ and Eq. (8.14). 85

27. Rotation of the Coordinate Axes, Flat Planet Case . . . 90

28. Rotation of the Coordinate Axes, Spherical Planet Case . 92

29. Footprint for $E^* = 1.5$ 95

30. Bank Control for Trajectories Leading to the Footprint, $E^* = 1.5$ 96

C.1. (θ_f', ϕ_f') and (θ_f, ϕ_f) 106

LIST OF TABLES

Table 1. Comparison of Approximate λ_b and Actual λ_b 30

SUMMARY

The success of future permanent space stations depends on the development of a space shuttle vehicle having aerodynamic maneuvering capability. The purpose of this technical report is to investigate the optimum maneuver of such a vehicle reentering a spherical, stationary, and locally exponential atmosphere. The use of Chapman's modified variables and a rescaled lift-drag polar leads to the formulation of a set of dimensionless equations of motion for flight analysis. The resulting equations are exact in the sense that they are also valid for flight in a vacuum. For the vehicle, we only have to specify the most important performance parameter, namely the maximum lift-to-drag ratio E^*. On the other hand, the planetary atmosphere is characterized simply by the so-called Chapman's atmospheric parameter $k^2 = \beta r$.

For planar flight several typical optimum maneuvers are investigated at different altitude ranges, low, moderate and very high. In each case the characteristics of the optimum lift control are discussed.

For three-dimensional flight, the procedure to solve the optimum trajectory for maximum cross range is discussed in detail. Finally, using the equilibrium glide condition the maximum cross ranges for entry from circular speed, for several values of E^*, and the footprint for $E^* = 1.5$ are computed in this reduced problem. A technique of coordinate rotation is used which makes the iteration procedure for solving the footprint of a reentry vehicle much more effective and geometrically meaningful.

CHAPTER 1

INTRODUCTION

The purpose of this report is to investigate the optimum maneuver of a space vehicle having aerodynamic maneuvering capability. The present day space shuttle is an example of such a kind of space vehicle. In the previously published literature, the analyses are either for constant lift-to-drag ratio [1], or usually numerically oriented and confined to the performance of a particular vehicle [3]. In order to maintain the generality of the results, we shall introduce a set of dimensionless variables and a rescaled lift-drag polar, to derive the dimensionless equations of motion for flight analysis inside a spherical, stationary, and locally exponential planetary atmosphere. The resulting equations are exact in the sense that they are also valid for flight in a vacuum and are almost free from all the physical quantities of the vehicle and the planetary atmosphere. For flight at very high altitude with orbital speed, a Newtonian, inverse-squared force field is used. By a simple canonical transformation [5,6], the corresponding equations for low altitude and low speed flight over a flat earth model are obtained.

Two main types of optimum maneuver in a vertical plane will be investigated at three different altitudes, low, moderate, and very

high. In the pull-up type maneuver we either maximize the final speed with the final altitude prescribed, or vice versa. At very high altitude with orbital speed, the maneuver generates the useful skip trajectory. In the gliding type maneuver we maximize the gliding range. The three-dimensional gliding maneuver for maximum cross range will also be discussed and then solved in a reduced problem. The footprint of a reentry vehicle will be assessed.

The organization of the report is as follows. After this introductory chapter, the dimensionless equations of motion for three-dimensional atmospheric flight are derived in Chapter 2. The problem is then formulated as an optimal control problem with the adjoint equations and the control law derived in Chapter 3. In Chapter 4, the equations for planar flight are deduced from the general equations of Chapter 3. Then in Chapter 5 they are transformed into the equivalent form appropriate to a flat earth model. The numerical applications are carried out in Chapters 6, 7, and 8. The case of flight over a flat earth is first analyzed in Chapter 6. The concept of a linearized singular arc [8] is introduced and tested. The case of planar flight over a spherical earth is discussed in detail in Chapter 7. Then in Chapter 8 we discuss the procedure to solve the three-dimensional optimum trajectory. The problem is then simplified and solved with a footprint obtained. The final chapter, Chapter 9, summarizes the main results.

CHAPTER 2

DIMENSIONLESS EQUATIONS OF MOTION

In this chapter, the three-dimensional equations of motion of a nonthrusting, lifting vehicle entering a stationary spherical planetary atmosphere are introduced. Then by using the modified Chapman's variables, a normalized lift coefficient, and a dimensionless arc length as the independent variable, a set of dimensionless state equations are obtained for entry analysis. It will be seen that, by this formulation, the only physical parameter involved is the maximum lift-to-drag ratio, and the planetary atmosphere is simply characterized by a value referred to as Chapman's atmospheric parameter.

2.1 Three-Dimensional Equations of Motion

The equations of motion of a nonthrusting, lifting vehicle entering a stationary spherical planetary atmosphere are

$$\frac{dr}{dt} = V \sin\gamma$$

$$\frac{dV}{dt} = -\frac{\rho S C_D V^2}{2m} - g \sin\gamma$$

$$V\frac{d\gamma}{dt} = \frac{\rho S C_L V^2}{2m}\cos\sigma - \left(g - \frac{V^2}{r}\right)\cos\gamma$$

$$\frac{d\theta}{dt} = \frac{V \cos\gamma \cos\psi}{r \cos\phi} \tag{2.1}$$

$$\frac{d\phi}{dt} = \frac{V \cos\gamma \sin\psi}{r}$$

$$V \frac{d\psi}{dt} = \frac{\rho S C_L V^2}{2m \cos\gamma} \sin\sigma - \frac{V^2}{r} \cos\gamma \cos\psi \tan\phi$$

where t is time, $(r, V, \gamma, \theta, \phi, \psi)$ are state variables and are defined in Figure 1, ρ is density of the atmosphere, S is the reference area of the vehicle, C_D and C_L are the drag and lift coefficients, m is the mass of the vehicle, g is the magnitude of gravitational acceleration, and σ is the bank angle. The flight path angle γ is defined to be

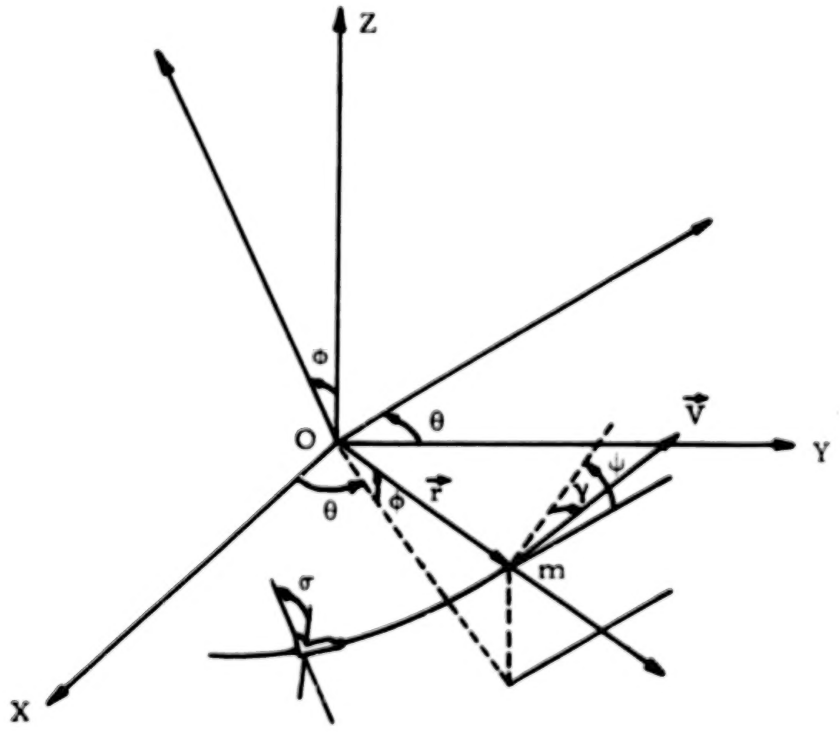

Figure 1.- State Variables, Control Variables, and Other Parameters Defined with Respect to Inertial Coordinate, OXYZ.

positive when the velocity is directed above the horizontal plane. The bank angle σ is taken to be positive for a bank to the left. For flight in a Newtonian force field of a spherical planet, the magnitude of the gravitational acceleration is of the form

$$g = \frac{\mu}{r^2} \tag{2.2}$$

where μ is the gravitational constant. The density of the atmosphere ρ is assumed to be locally exponential, that is, it obeys the differential law

$$\frac{d\rho}{\rho} = -\beta\, dr \tag{2.3}$$

where the inverse scale height β is a function of the distance from the center of the planet r.

There are two control variables, one is the bank angle σ and the other is either the lift coefficient C_L or the drag coefficient C_D. For a given vehicle there is a lift-drag relation; therefore either the lift coefficient C_L or the drag coefficient C_D can be used as the control. We shall use as lift control a normalized lift coefficient λ such that

$$C_L = C_L^* \lambda \tag{2.4}$$

where C_L^* is the lift coefficient corresponding to maximum lift-to-drag ratio E^*. If C_D^* is the corresponding drag coefficient, then

$$C_D = C_D^* f(\lambda) \tag{2.5}$$

where $f(\lambda)$ is the function specifying the chosen drag polar (see Appendix A). When $\lambda = 1$, the flight is at maximum lift-to-drag ratio.

Thus we also have $f(1) = 1$. We shall consider a parabolic drag polar with the simple function

$$f(\lambda) = \tfrac{1}{2}\,(1 + \lambda^2) \tag{2.6}$$

In general, the parameters C_L^*, C_D^*, and E^* are functions of Mach number; but in the hypervelocity regime they are essentially constant.

2.2 Dimensionless Equations of Motion

The following dimensionless variables are introduced,

$$Z = \frac{\rho S C_L^*}{2m}\sqrt{\frac{r}{\beta}}$$

$$v = \frac{V^2}{gr} = \frac{V^2}{\mu/r} \tag{2.7}$$

$$s = \int_0^t \frac{V}{r}\cos\gamma\, dt$$

where Z and v are the modified Chapman's variables [1]. Z is proportional to the atmospheric density ρ and will replace the altitude, while the dimensionless kinetic energy v is a measure of the speed. The remaining dimensionless variable s is the dimensionless arc length. It is monotonically increasing and will replace the time as an independent variable. By using Eqs. (2.4), (2.5), (2.6) and (2.7) in Eqs. (2.1), we have the dimensionless three-dimensional equations of motion

$$\frac{dZ}{ds} = -k^2 Z \tan\gamma$$

$$\frac{dv}{ds} = -\frac{k Z v (1+\lambda^2)}{E^* \cos\gamma} - (2 - v)\tan\gamma$$

$$\frac{d\gamma}{ds} = \frac{k Z \lambda \cos\sigma}{\cos\gamma} + \left(1 - \frac{1}{v}\right)$$

$$\frac{d\theta}{ds} = \frac{\cos\psi}{\cos\phi} \qquad (2.8)$$

$$\frac{d\phi}{ds} = \sin\psi$$

$$\frac{d\psi}{ds} = \frac{k Z \lambda \sin\sigma}{\cos^2\gamma} - \cos\psi \tan\phi$$

where E^* is the maximum lift-to-drag ratio, and k^2 is the dimensionless product βr. These equations are exact and hence are valid for Keplerian motion outside the planetary atmosphere. The only slight simplification is that in the equation for Z, the exact coefficient of $-Z \tan\gamma$ is

$$\bar{k}^2 = k^2 \left(1 - \frac{1}{2k^2} + \frac{1}{2\beta^2}\frac{d\beta}{dr}\right) \qquad (2.9)$$

For a strictly exponential atmosphere, β = constant and

$$\frac{d\beta}{dr} = 0 \qquad (2.10)$$

On the other hand, if an isothermal atmosphere is considered, β/g = constant and

$$\frac{1}{2\beta^2}\frac{d\beta}{dr} = -\frac{1}{k^2} \qquad (2.11)$$

In both cases $\bar{k}^2$ is a function of $k^2 = \beta r$. Chapman has shown that in the reentry range of the altitude, this product is oscillating about and near a mean value [1]. Furthermore, its value is much greater than unity, e.g., for the earth's atmosphere $k^2 \simeq 900$, thus we take

$$\bar{k}^2 \simeq k^2 \qquad (2.12)$$

The Eqs. (2.8) are the state equations for entry analysis. It is seen that the only physical parameter of the vehicle involved is the maximum lift-to-drag ratio E^*. Furthermore, any planetary atmosphere is simply characterized by a properly selected value k^2. This mean value will be referred to as Chapman's atmospheric parameter.

CHAPTER 3

VARIATIONAL FORMULATION

With an adjoint vector introduced, we formulate the problem as an optimal control problem by using the Pontryagin's maximum principle. The control law is derived. The integrals of the motion are obtained. Then there is a change in the adjoint variables to have a better form for the adjoint equations. Finally, the parameters of the problem under different cases are discussed.

3.1 Variational Formulation

The Eqs. (2.8) are the state equations with two control variables, the lift control λ and the bank angle σ. They are subjected to the constraints

$$\begin{aligned} |\lambda| &\leq \lambda_{max} \\ |\sigma| &\leq \sigma_{max} \end{aligned} \tag{3.1}$$

These controls are to be selected to bring the vehicle from a certain prescribed initial condition to a certain partially prescribed final condition, such that a certain function of the final state variables is minimized.

Using the maximum principle, we introduce the adjoint vector $\vec{p}$ to form the Hamiltonian

$$H = -k^2 Z p_Z \tan\gamma - p_v\left[\frac{k Z v (1+\lambda^2)}{E^* \cos\gamma} + (2 - v)\tan\gamma\right]$$

$$+ p_\gamma\left[\frac{k Z \lambda \cos\sigma}{\cos\gamma} + \left(1 - \frac{1}{v}\right)\right] + p_\theta \frac{\cos\psi}{\cos\phi} + p_\phi \sin\psi$$

$$+ p_\psi\left[\frac{k Z \lambda \sin\sigma}{\cos^2\gamma} - \cos\psi \tan\phi\right] \qquad (3.2)$$

where p_x, $x = Z, v, \gamma, \theta, \phi$, and ψ are the adjoint components corresponding to the six state variables, respectively. They are governed by the following adjoint equations

$$\frac{dp_Z}{ds} = k^2 p_Z \tan\gamma + p_v \frac{k v (1+\lambda^2)}{E^* \cos\gamma} - p_\gamma \frac{k \lambda \cos\sigma}{\cos\gamma} - p_\psi \frac{k \lambda \sin\sigma}{\cos^2\gamma}$$

$$\frac{dp_v}{ds} = p_v\left[\frac{k Z (1+\lambda^2)}{E^* \cos\gamma} - \tan\gamma\right] - \frac{p_\gamma}{v^2}$$

$$\frac{dp_\gamma}{ds} = \frac{1}{\cos^2\gamma}\left\{k^2 Z p_Z + p_v\left[\frac{k Z v (1+\lambda^2)\sin\gamma}{E^*} + (2 - v)\right]\right.$$

$$\left. - k p_\gamma Z \lambda \cos\sigma \sin\gamma - 2 k p_\psi Z \lambda \sin\sigma \tan\gamma\right\} \qquad (3.3)$$

$$\frac{dp_\theta}{ds} = 0$$

$$\frac{dp_\phi}{ds} = \frac{\cos\psi}{\cos^2\phi}\left[-p_\theta \sin\phi + p_\psi\right]$$

$$\frac{dp_\psi}{ds} = \frac{\sin\psi}{\cos\phi}\left[p_\theta - p_\psi \sin\phi\right] - p_\phi \cos\psi$$

The solution is then obtained by integrating the two sets of state and adjoint equations, subjected to the end conditions, and at each instant selecting the lift control λ and the bank angle σ such that the Hamiltonian is an absolute maximum.

The Hamiltonian H will be maximum either at the boundary of the control set or at an interior, variable point where

$$\frac{\partial H}{\partial \lambda} = 0 \quad , \quad \frac{\partial H}{\partial \sigma} = 0 \tag{3.4}$$

Explicitly, we have

$$\lambda \cos\sigma = \frac{E^* p_\gamma}{2 v p_v} \quad , \quad \lambda \sin\sigma = \frac{E^* p_\psi}{2 v p_v \cos\gamma} \tag{3.5}$$

3.2 Integrals of the Motion

It is known that the problem has a number of integrals [2-4]. First of all,

$$H = C_0 \tag{3.6}$$

where C_0 is a constant. Then by solving the last three equations of Eqs. (3.3), we have

$$\begin{aligned} p_\theta &= C_1 \\ p_\phi &= C_2 \cos\theta + C_3 \sin\theta \\ p_\psi &= C_1 \sin\phi - \cos\phi\,(C_2 \sin\theta - C_3 \cos\theta) \end{aligned} \tag{3.7}$$

where C_1, C_2, and C_3 are constants of integration.

To simplify the first three equations which are not integrable analytically in Eqs. (3.3), it is convenient to use the modified adjoint variables defined as

$$\begin{aligned} P &= k^2 Z p_Z \\ N &= v p_v \\ Q &= p_\gamma \end{aligned} \tag{3.8}$$

The corresponding modified adjoint equations are then

$$\frac{dP}{ds} = \frac{k^3 Z}{\cos\gamma}\left[\frac{N}{E^*} - \frac{E^*}{4N}\left(Q^2 + \frac{p_\psi^2}{\cos^2\gamma}\right)\right]$$

$$\frac{dN}{ds} = -\frac{1}{v}\left(Q + 2N\tan\gamma\right) \tag{3.9}$$

$$\frac{dQ}{ds} = \frac{1}{\cos^2\gamma}\left\{P + N\left[\frac{k Z \sin\gamma}{E^*} + \frac{(2-v)}{v}\right] - \frac{E^* k Z \sin\gamma}{4N}\left[Q^2 + \frac{3 p_\psi^2}{\cos^2\gamma}\right]\right\}$$

In terms of P, N, and Q, the optimum lift and bank controls become

$$\lambda\cos\sigma = \frac{E^* Q}{2N}$$

$$\lambda\sin\sigma = \frac{E^* p_\psi}{2N\cos\gamma} \tag{3.10}$$

$$\lambda^2 = \frac{E^{*2}}{4N^2}\left(Q^2 + \frac{p_\psi^2}{\cos^2\gamma}\right)$$

and the Hamiltonian becomes

$$-P\tan\gamma - N\left[\frac{k Z}{E^*\cos\gamma} + \frac{(2-v)}{v}\tan\gamma\right] - \frac{(1-v)Q}{v}$$

$$+ \frac{E^* k Z}{4N\cos\gamma}\left(Q^2 + \frac{p_\psi^2}{\cos^2\gamma}\right) + p_\theta\frac{\cos\psi}{\cos\phi} + p_\phi\sin\psi$$

$$- p_\psi\cos\psi\tan\phi = C_0 \tag{3.11}$$

In summary, the optimal solutions of this problem are governed by the Eqs. (2.8) for the state variables, Eqs. (3.7) and (3.9) for the adjoint variables, and Eqs. (3.10) for the controls. It requires six parameters C_1, C_2, C_3, P_i, N_i, and Q_i to satisfy the final and transversality conditions, where P_i, N_i and Q_i are the initial values of P, N, and Q, respectively. The Hamiltonian equation, Eq. (3.11), can be used to check the accuracy of the integration.

For the most practical cases, the arc length s is not prescribed at the final time. Thus $H = C_0 \equiv 0$ and Eq. (3.11) becomes

$$- P\tan\gamma - N\left[\frac{kZ}{E^*\cos\gamma} + \frac{(2-\nu)}{\nu}\tan\gamma\right] - \frac{(1-\nu)Q}{\nu}$$

$$+ \frac{E^* kZ}{4N\cos\gamma}\left(Q^2 + \frac{p_\gamma^2}{\cos^2\gamma}\right) + p_\theta \frac{\cos\psi}{\cos\phi} + p_\phi \sin\psi$$

$$- p_\psi \cos\psi \tan\phi \equiv 0 \qquad (3.12)$$

Using this integral, one of the three equations in Eqs. (3.9) can be deleted. But there are some difficulties in so doing. First, Eq. (3.12) is quadratic in both Q and N. To solve either Q or N from Eq. (3.12) requires frequent change in sign in front of the square root each time the quantity under the square root passes through the value zero. Next, in Eq. (3.12) the coefficient of P is $\tan\gamma$. Whenever γ goes to zero, P cannot be determined. Hence, it is more convenient to use Eq. (3.12) solely to determine one of the three initial values, either P_i or N_i or Q_i, and to check the accuracy of the integration. Anyway, it is obvious that the number of parameters is reduced by one, that is, from six to five.

CHAPTER 4

PLANAR FLIGHT

In this chapter, we deduce the governing equations for the optimum reentry trajectories confined to the plane of a great circle from the general three-dimensional equations of Chapter 3. They are the state equations, the adjoint equations, the control law, and the Hamiltonian integral. Then by a change of adjoint variables, we obtain a handy equation for the control variable λ, and the number of parameters is reduced by one.

4.1 Governing Equations

For entry trajectories in the plane of a great circle, we have

$$\sigma = \phi = \psi = 0 \tag{4.1}$$

and the independent variable s is simply the range angle θ. The state equations and the modified adjoint equations are reduced to

$$\begin{aligned}
\frac{dZ}{d\theta} &= -k^2 Z \tan\gamma \\
\frac{dv}{d\theta} &= -\frac{k Z v (1+\lambda^2)}{E^* \cos\gamma} - (2 - v)\tan\gamma \qquad (4.2) \\
\frac{d\gamma}{d\theta} &= \frac{k Z \lambda}{\cos\gamma} + \left(1 - \frac{1}{v}\right)
\end{aligned}$$

and

$$\frac{dP}{d\theta} = \frac{k^3 Z}{\cos\gamma}\left[\frac{N}{E^*} - \frac{E^* Q^2}{4N}\right]$$

$$\frac{dN}{d\theta} = -\frac{1}{v}(Q + 2N\tan\gamma) \qquad (4.3)$$

$$\frac{dQ}{d\theta} = \frac{1}{\cos^2\gamma}\left\{P + N\left[\frac{kZ\sin\gamma}{E^*} + \frac{(2-v)}{v}\right] - \frac{E^* k Z Q^2 \sin\gamma}{4N}\right\}$$

respectively. The optimum lift control is either $|\lambda| = \lambda_{max}$ or a variable λ such that

$$\lambda = \frac{E^* Q}{2N} \qquad (4.4)$$

The Hamiltonian integral becomes

$$-P\tan\gamma - N\left[\frac{kZ}{E^*\cos\gamma} + \frac{(2-v)}{v}\tan\gamma\right] - \frac{(1-v)Q}{v} + \frac{E^* k Z Q^2}{4N\cos\gamma} = -C_1 \qquad (4.5)$$

where C_1 is the same constant of integration as in Eqs. (3.7).

In general, this is a three-parameter problem, with P_i, N_i, and Q_i as the three parameters. For the special case where the range angle θ is not prescribed at the final time, i.e., θ_f is free, $C_1 \equiv 0$ and it becomes a two-parameter problem.

4.2 Change of Adjoint Variables

From the expression of Eq. (4.4), it is seen that a simplification can be made if we use λ as a new variable. Another variable which will be seen to be useful is

$$F = \frac{P}{N} \qquad (4.6)$$

Using (F, N, λ) as a new set of variables to replace the modified

adjoint variables (P, N, Q), and taking the derivative of Eqs. (4.4) and (4.6) with respect to θ, we have

$$\frac{dF}{d\theta} = \frac{k^3 Z (1-\lambda^2)}{E^* \cos\gamma} + \frac{2F}{E^* v} (\lambda + E^* \tan\gamma)$$

$$\frac{dN}{d\theta} = -\frac{2N}{E^* v} (\lambda + E^* \tan\gamma) \qquad (4.7)$$

$$\frac{d\lambda}{d\theta} = \frac{k Z (1-\lambda^2) \sin\gamma}{2\cos^2\gamma} + \frac{2\lambda (\lambda + E^* \tan\gamma)}{E^* v} + \frac{E^*}{2\cos^2\gamma} \left(F - 1 + \frac{2}{v}\right)$$

The Hamiltonian integral Eq. (4.5) in terms of (F, N, λ) becomes

$$\frac{k Z (1-\lambda^2)}{E^* \cos\gamma} + \frac{2(1-v)\lambda}{E^* v} + \left(F - 1 + \frac{2}{v}\right) \tan\gamma = \frac{C_1}{N} \qquad (4.8)$$

In Eqs. (4.7), it is seen that the first and third equations are independent of N. It can be shown that N_i, the initial value of N, is free whenever the final value of N doesn't appear in the transversality conditions. Thus the second equation of Eqs. (4.7) can be deleted. It becomes a two-parameter problem for the general case. For the special case if θ_f is free, $C_1 \equiv 0$ and it is simply a one-parameter problem. The Hamiltonian integral for this special case is, from Eq. (4.8),

$$\frac{k Z (1-\lambda^2)}{E^* \cos\gamma} + \frac{2(1-v)\lambda}{E^* v} + \left(F - 1 + \frac{2}{v}\right) \tan\gamma = 0 \qquad (4.9)$$

As has been mentioned in Section 3.2, there are difficulties in using Eq. (4.9) to solve for λ or F. To solve for λ from Eq. (4.9), we have to determine the sign in front of the square root and change this sign each time the quantity under the square root passes through

zero. At that instant the equation has a double root

$$\lambda_1 = \lambda_2 = \frac{(1 - v)\cos\gamma}{k Z v} \tag{4.10}$$

From the third equation of Eqs. (4.2), it is seen that this corresponds to $d\gamma/d\theta = 0$. Physically, the flight path angle passes through a maximum or a minimum and the trajectory has an inflection point at this instant. This behavior is typical in an optimal trajectory. Therefore it is more convenient to obtain the optimum λ directly from integration. On the other hand to solve for F from Eq. (4.9) will become impractical whenever γ is approaching and passing through the value zero. Hence, Eq. (4.9) will be used solely to compute the initial value F_i in terms of λ_i and to check the accuracy of the integration.

CHAPTER 5

FLAT PLANET SIMPLIFICATION

The equations we have derived in the preceding chapter are the optimum equations for the general case of planar flight. They are to be used when the speed of the vehicle is of the order of orbital speed, $v \simeq 1$, which occurs at high altitude where the value of Z is small. They are, of course, also valid at low altitude and low speed. But in this case, without compromising the accuracy, it is simpler to use the equations within the framework of a flat planet model. These equations are to be deduced in this chapter.

5.1 Governing Equations for Flat Planet Model

It is interesting to know that by a proper change of variables we can deduce the dimensionless equations for the flat planet case from the general equations of planar flight in the preceding chapter. At low speed and low altitude, it is more convenient to use the following dimensionless variables

$$w = \frac{2m\beta}{\rho S C_L^*} \quad , \quad u = \frac{V^2}{g/\beta} \quad , \quad y = \beta Y \qquad (5.1)$$

where w is the dimensionless wing loading which will replace the altitude, u is the new dimensionless kinetic energy to represent the

speed, and y is the dimensionless linear downrange. The relationships between the two sets of dimensionless variables (Z, v, θ) in Eqs. (2.7) (where s has been replaced by θ in planar flight case) and (w, u, y) in Eqs. (5.1) are

$$Z = \frac{k}{w} \quad , \quad v = \frac{u}{k^2} \quad , \quad \theta = \frac{y}{k^2} \tag{5.2}$$

Since the value of k^2 is much larger than u, e.g., for the earth's atmosphere $k^2 \simeq 900$ and u is of the order of unity at low speed, we have

$$k^2 >> u \tag{5.3}$$

This is the flat planet condition. Upon substituting Eqs. (5.2) into Eqs. (4.2) and using Eq. (5.3), we have

$$\begin{aligned} \frac{dw}{dy} &= w \tan\gamma \\ \frac{du}{dy} &= -\frac{u(1+\lambda^2)}{E^* w \cos\gamma} - 2\tan\gamma \\ \frac{d\gamma}{dy} &= \frac{\lambda}{w\cos\gamma} - \frac{1}{u} \end{aligned} \tag{5.4}$$

These are the state equations for flat planet model. We will obtain identical equations by starting out from the classical equations for flight over a flat planet and using Eqs. (5.1) in them. It is seen that, although an exponential atmosphere is still used for this case, the characteristic parameter k^2 of the atmosphere is removed from the equations. Hence, the flight behavior is independent of any particular atmosphere.

Again, we can use Eqs. (5.4) to form the Hamiltonian and derive the optimum equations, as has been done in Chapter 3. It is more elegant and informative to use the condition of a canonical transformation as a handy tool to effect the transformation from the old to the new variables [5,6]. This, coupled with the condition of Eq. (5.3), will lead directly to the equations for the optimal control of the flat planet case.

For a transformation from the variables (Z, v, θ) with Hamiltonian H to the new variables (w, u, y) with the Hamiltonian $\mathscr{H}$ to be canonical, we have the necessary and sufficient condition that the quantity

$$(p_Z\, dZ + p_v\, dv - H\, d\theta) - (p_w\, dw + p_u\, du - \mathscr{H}\, dy) = dU \qquad (5.5)$$

be an exact differential. In particular, for dU = 0, and using Eqs. (5.2), we have

$$H = k^2 \mathscr{H}$$

$$p_Z = -\frac{w^2 p_w}{k} \qquad (5.6)$$

$$p_v = k^2 p_u$$

p_γ remains unchanged. By using Eqs. (5.2) and (5.6) and the condition (5.3) in the Hamiltonian integral (4.8), we get the Hamiltonian integral for the flat planet case

$$\frac{1-\lambda^2}{E^* w \cos\gamma} + \frac{2\lambda}{E^* u} - \left(G - \frac{2}{u}\right)\tan\gamma = \frac{C_1}{u\, p_u} \qquad (5.7)$$

where again $C_1 = -\mathscr{H}$ is a constant of integration with $C_1 = 0$ for the

free range case. The variable G in Eq. (5.7) is the analogue of the variable F in Eq. (4.8), and is defined as

$$G = \frac{w p_w}{u p_u} \tag{5.8}$$

Similarly, performing the same transformation and using the same condition on the first and third equations of Eqs. (4.7), we have

$$\begin{aligned} \frac{dG}{dy} &= -\frac{(1-\lambda^2)}{E^* w \cos\gamma} + \frac{2G}{E^* u}(\lambda + E^* \tan\gamma) \\ \frac{d\lambda}{dy} &= \frac{(1-\lambda^2)\tan\gamma}{2w\cos\gamma} + \frac{2\lambda}{E^* u}(\lambda + E^* \tan\gamma) - \frac{E^*}{2\cos^2\gamma}\left(G - \frac{2}{u}\right) \end{aligned} \tag{5.9}$$

Again, this is a two-parameter problem in general. It will be reduced to a one-parameter problem when y_f is free and $C_1 = 0$. The Hamiltonian integral for this special case is

$$\frac{1-\lambda^2}{E^* w \cos\gamma} + \frac{2\lambda}{E^* u} - \left(G - \frac{2}{u}\right)\tan\gamma = 0 \tag{5.10}$$

CHAPTER 6

OPTIMAL TRAJECTORIES FOR FLAT EARTH

In this chapter, two categories of optimum trajectories are computed numerically using the equations derived in the preceding chapter for a flat planet model. The first category of optimum trajectories is for the pull-up maneuver. We either maximize the final speed with a prescribed final altitude or vice versa. The final flight path angle can be either prescribed or free. We consider both cases of unconstrained λ and constrained λ. The second category is for the glide trajectory which maximizes the final range with prescribed final altitude, final speed, and/or final flight path angle. Since the equations used are independent of the planet and its atmosphere, so are the results. But to have some idea about the physical quantities of the flight, we use the flat earth model and its atmosphere as an example to get dimensional quantities from the dimensionless results. In the last section of this chapter, the linearized singular control technique is introduced and tested. It is shown to be useful in reducing computational work.

6.1 Maximum Final Speed or Maximum Final Altitude

In this case, it is proposed to find the optimum lift control to bring the vehicle from the initial condition

$$y = y_i = 0 \quad , \quad w = w_i \quad , \quad u = u_i \quad , \quad \gamma = \gamma_i \tag{6.1}$$

to the condition at the final instant y_f such that either

$$w = w_f \quad , \quad u = u_f = \text{maximum} \tag{6.2}$$

or,

$$u = u_f \quad , \quad w = w_f = \text{maximum} \tag{6.3}$$

We call this the pull-up type maneuver. A sketch of this type of trajectory is presented in Figure 2. The condition of Eq. (6.2) is to maximize the final speed with a prescribed final altitude, while the

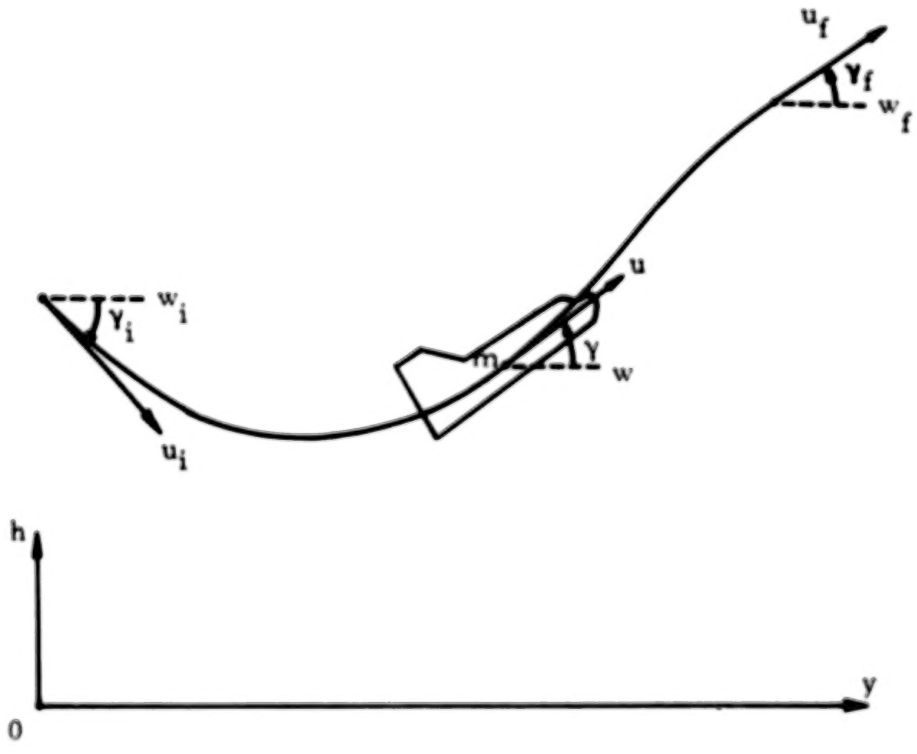

Figure 2. - Geometry of a Pull-Up Maneuver.

condition of Eq. (6.3) is to maximize the final altitude with a prescribed final speed. They are equivalent, and it will be shown that their solutions are obtained through a single formulation. We shall assume that the final range is free, thus $C_1 = 0$. Since this is a one parameter problem, we can use Eq. (5.10).

As has been explained before, to avoid the difficulties in using Eq. (5.10) to solve for either λ or G, we shall integrate both of the Eqs. (5.9) along with the state equations, Eqs. (5.4). For the five initial values required, since the initial state (w_i, u_i, γ_i) is given, we need only the two initial values λ_i and G_i to start the integration. We set λ_i to be the only parameter of this problem, and obtain G_i from Eq. (5.10). This can be done except when $\gamma_i = 0$. The case with $\gamma_i = 0$ will be discussed later in this section.

For the numerical computation, we shall use the initial state

$$(w_i, u_i, \gamma_i) = (.5, .5, -\frac{1}{E^*}) \qquad (6.4)$$

Although a specific set of values has been used, it is found that the optimum lift control has a general typical behavior. For the maximum lift-to-drag ratio E^*, we shall use $E^* = 10$ which is typical for a fighter aircraft, and $E^* = 4.5$ which is somewhat higher than the value of a shuttle vehicle at low speed. To maximize the final speed with a prescribed final altitude, we start the integration with a guessed λ_i, and stop it at $w = w_f$. If the final flight path angle γ_f is prescribed, this value is used to adjust λ_i until the condition is met.

The resulting trajectory is the optimal for maximizing u_f with the prescribed w_f and γ_f satisfied. If γ_f is free, then by the transversality condition, $p_{\gamma_f} = 0$. From the first equation of Eqs. (3.5), after being transformed to the form for the flat planet case, we have at the final instant

$$\lambda_f = \frac{E^* p_{\gamma_f}}{2 u_f p_{u_f}} = 0 \tag{6.5}$$

This condition is used to adjust λ_i for the free γ_f case. The result is the overall best since the final flight path angle is also optimized.

A similar procedure is used to find the optimum trajectory for the case of maximum final altitude with a prescribed final speed.

Since the problem has one arbitrary parameter, namely the initial value λ_i, the family of optimum trajectories is generated by simply integrating the Eqs. (5.4) and (5.9) for different values of λ_i until $\lambda_f = 0$. The results for $E^* = 10$ and 4.5 are presented in Figure 3, which is plotted in the ratio w/w_i versus the ratio V/V_i. The solid lines are the different optimum trajectories leading to the terminal boundary represented by the dashed line. From the definition of w in Eq. (5.1), if an exponential atmosphere is used, the actual altitude change is simply

$$\Delta h = h_f - h_i = \frac{1}{\beta} \log \left(\frac{w_f}{w_i} \right) \tag{6.6}$$

For any prescribed change in altitude, we can evaluate the corresponding minimum speed reduction along the dashed line. Conversely,

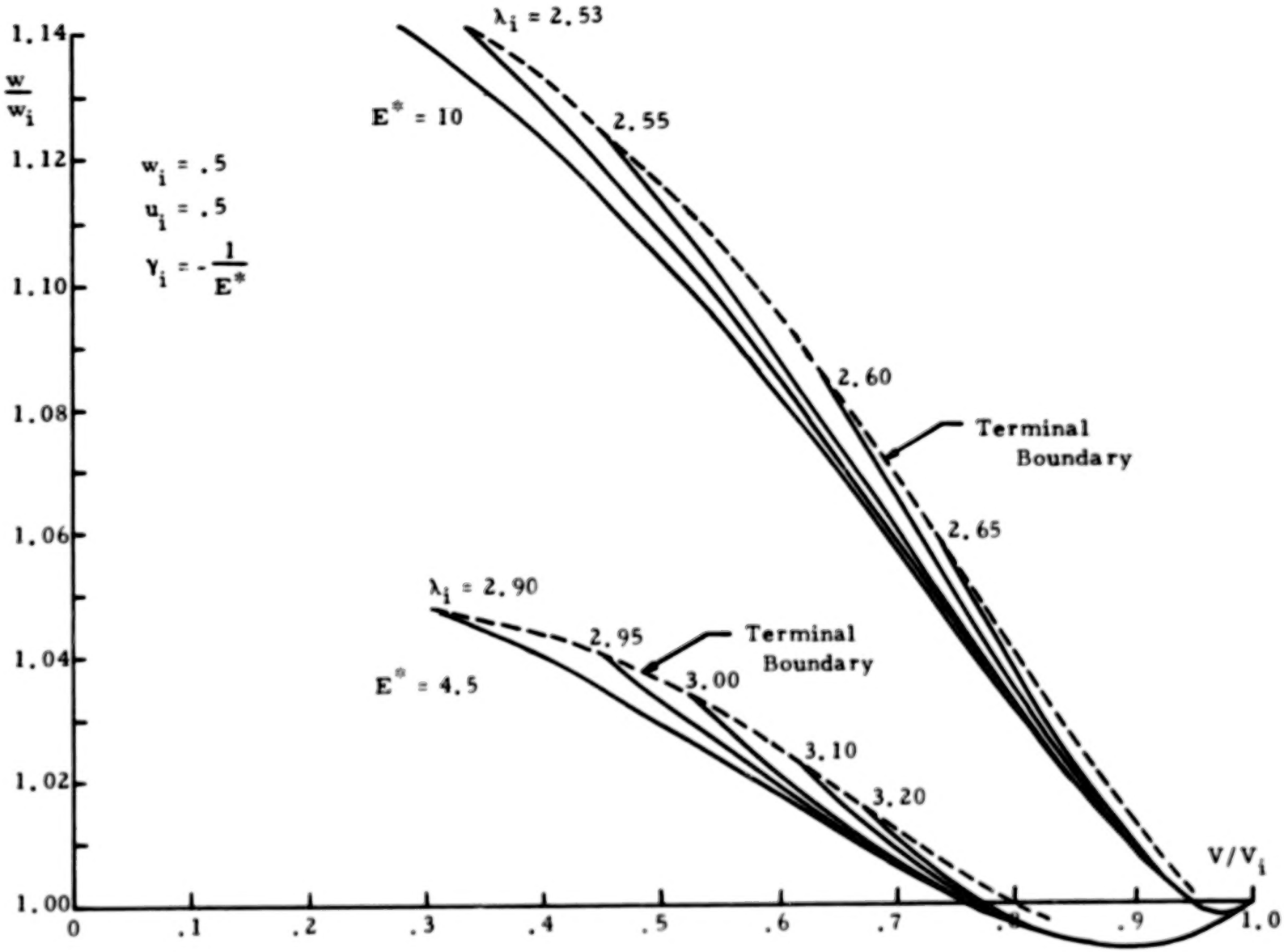

Figure 3.-Solution for Pull-Up Maneuver.

we can evaluate the maximum altitude gain if $w_f/w_i > 1$, or the minimum altitude loss if $w_f/w_i < 1$, for any prescribed speed reduction.

Although the figure is plotted for a specific initial state given in Eq. (6.4), the use of dimensionless variables allows a general discussion of the influence of different physical characteristics of the vehicle on its performance. For a numerical example, with $u_i = .5$ and taking $g = 9.81$ m/sec^2, $1/\beta = 7162$ m, the initial speed is 187.43 m/sec or 674.7 km/hr. Assume a prescribed reduction in the speed, say $V_f/V_i = .7$. Then flying optimally, the maximum final altitude is identified in Figure 3 along the dashed line of $E^* = 10$ to be $w_f/w_i = 1.07$. From Eq. (6.6) this represents an altitude gain of 484.57 meters. The initial altitude with $w_i = .5$ is

$$\rho_i = 4\beta \left(\frac{m}{SC_L^*}\right) \tag{6.7}$$

which is a function of the wing loading m/SC_L^*. For a higher wing loading, the same gain in the altitude can only be achieved at a lower altitude. In other words, small wing loading favors the pull-up maneuver.

Figure 4 presents the variation of the normalized lift coefficient λ as a function of the flight path angle γ for several optimal trajectories. Higher values of λ_i correspond to smaller speed reductions. It is interesting to notice that when $\gamma = 0$, that is, when the vehicle is at the lowest point (or bottom) of the trajectory, the λ for different

BLANK PAGE

BLANK PAGE

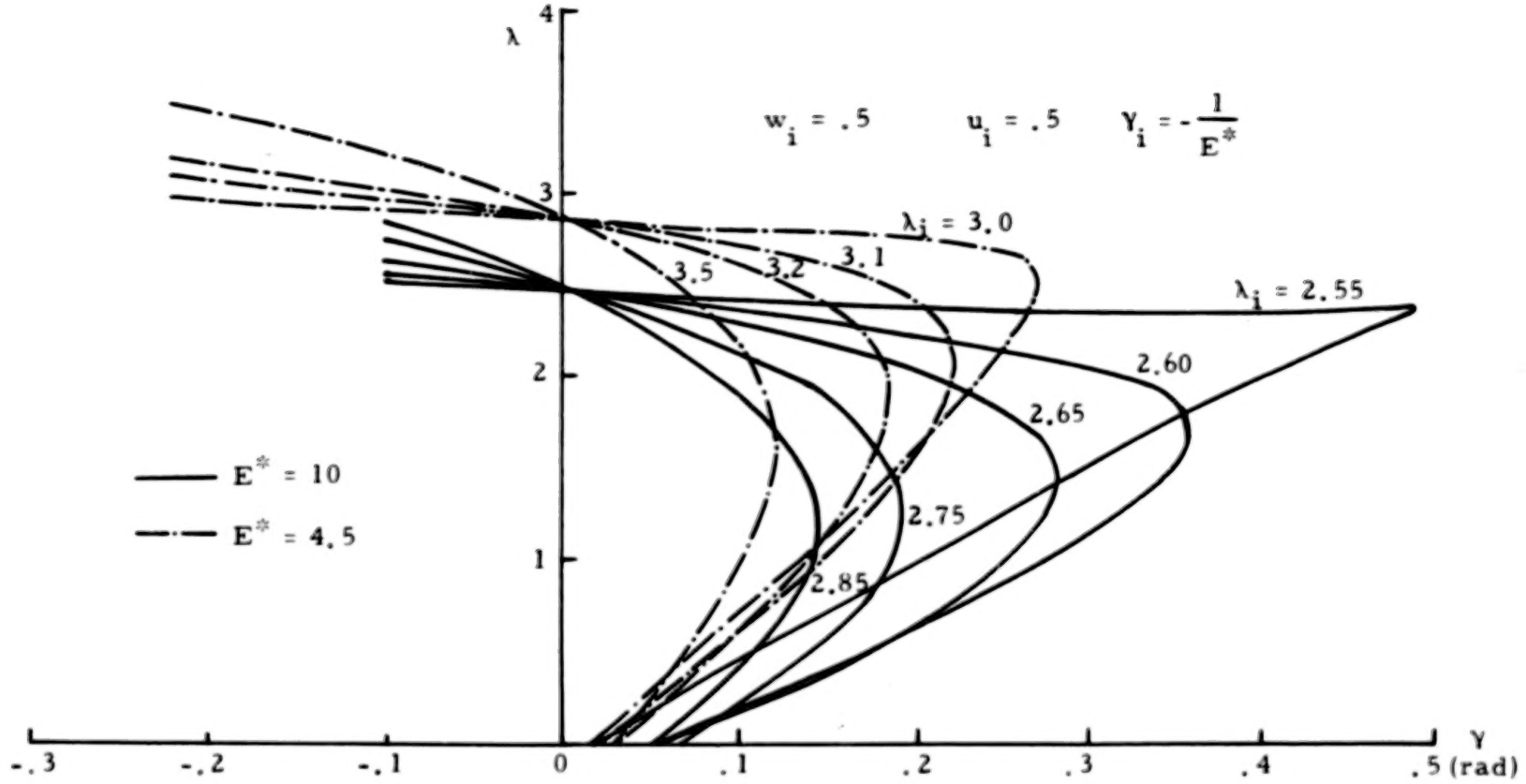

Figure 4. - Variation of the Optimal Lift Coefficient in Terms of the Flight Path Angle in Pull-Up Maneuver.

trajectories with the same E^* have nearly the same value λ_b. From the Hamiltonian integral Eq. (5.10) with $\gamma = 0$, we have

$$\left(\frac{u}{w}\right)_b = \frac{2\lambda_b}{\lambda_b^2 - 1} \tag{6.8}$$

On the other hand, from the definition of u and w in Eqs. (5.1), we have

$$\frac{u}{w} = \frac{1}{g}\left(\frac{\rho V^2}{2}\right)\left(\frac{S C_L^*}{m}\right) \tag{6.9}$$

Therefore, if λ_b is nearly the same for all trajectories, the corresponding dynamic pressure $(\frac{1}{2}\rho V^2)_b$ is nearly the same, which in turn means that the indicated speed at the lowest point is nearly the same. Furthermore, at the lowest point, the normal acceleration as felt by the pilot is the opposite of the acceleration due to the lift force, which in terms of λ_b is

$$\left(\frac{a_N}{g}\right)_b = \left(\frac{u}{w}\right)_b \lambda_b = \frac{2\lambda_b^2}{\lambda_b^2 - 1} \tag{6.10}$$

Thus it is also nearly the same for all trajectories regardless of the final condition achieved.

It is possible to obtain an approximate analytical expression for λ_b by considering a particular trajectory in Figure 4 which shows a near constant value of λ from $\gamma = \gamma_i$ to $\gamma = 0$. From the second equation of Eqs. (5.9), since $d\lambda/dy \simeq 0$ at $\gamma = 0$, we have

$$E^*(uG - 2)_b = \frac{4\lambda_b^2}{E^*} \tag{6.11}$$

Secondly, from the Hamiltonian integral Eq. (5.10) at the initial

instant,

$$E^* (uG - 2)_i \tan \gamma_i = \frac{u_i (1 - \lambda_i^2)}{w_i \cos \gamma_i} + 2\lambda_i \qquad (6.12)$$

It is confirmed by the numerical results that the product uG also varies slowly. Thus

$$\lambda_i \simeq \lambda_b \ , \quad (uG - 2)_i \simeq (uG - 2)_b \qquad (6.13)$$

Combining Eqs. (6.11), (6.12), and (6.13) gives the quadratic equation for evaluating λ_b

$$\left[\left(\frac{u}{w}\right)_i + \frac{4}{E^*} \sin \gamma_i\right] \lambda_b^2 - 2\lambda_b \cos \gamma_i - \left(\frac{u}{w}\right)_i = 0 \qquad (6.14)$$

The values of λ_b obtained from this equation is in excellent agreement with the numerical results, as shown in Table 1.

Table 1. Comparison of Approximate λ_b and Actual λ_b

$(u/w)_i$ variable, $\gamma_i = -1/E^*$

	$(u/w)_i$	.6	.8	1.0	1.2	1.4
$E^* = 10$	Approx. λ_b	3.833	2.972	2.491	2.188	1.982
	Actual λ_b	3.825	2.964	2.487	2.186	1.981
	$(u/w)_i$	.6	.8	1.0	1.2	1.4
$E^* = 4.5$	Approx. λ_b	-	3.598	2.861	2.434	2.159
	Actual λ_b	-	3.635	2.879	2.456	2.172

To assess the influence of the initial speed, we use the same values $w_i = .5$ and $\gamma_i = -1/E^*$, and generate several families of optimum trajectories using $u_i = .3, .4, .5, .6$, and $.7$. The solutions, that is, the terminal boundaries of different families, are presented in Figure 5. It is obvious that higher altitude gain is obtained with higher initial speed.

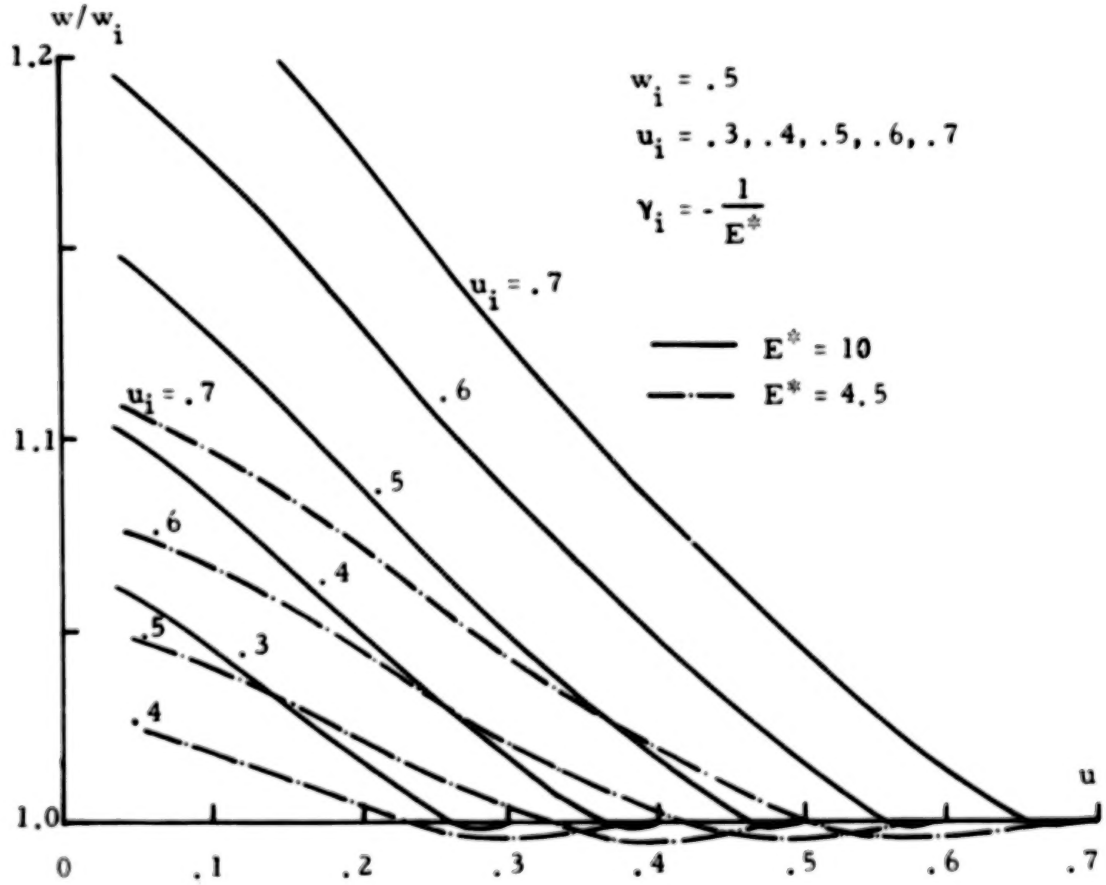

Figure 5. - Influence of Initial Speed on Optimum Solution.

Finally, using the same values $w_i = .5$ and $u_i = .5$, we vary the γ_i to analyze its effect on performance. The solutions are presented in Figure 6. Obviously, the performance improves as γ_i increases and becomes positive. One interesting observation is that when $\gamma_i = 0$, that is when the maneuver starts horizontally, λ_i can be solved from Eq. (5.10),

$$\lambda_i = \left(\frac{w}{u}\right)_i + \sqrt{1 + \left(\frac{w}{u}\right)_i^2} \tag{6.15}$$

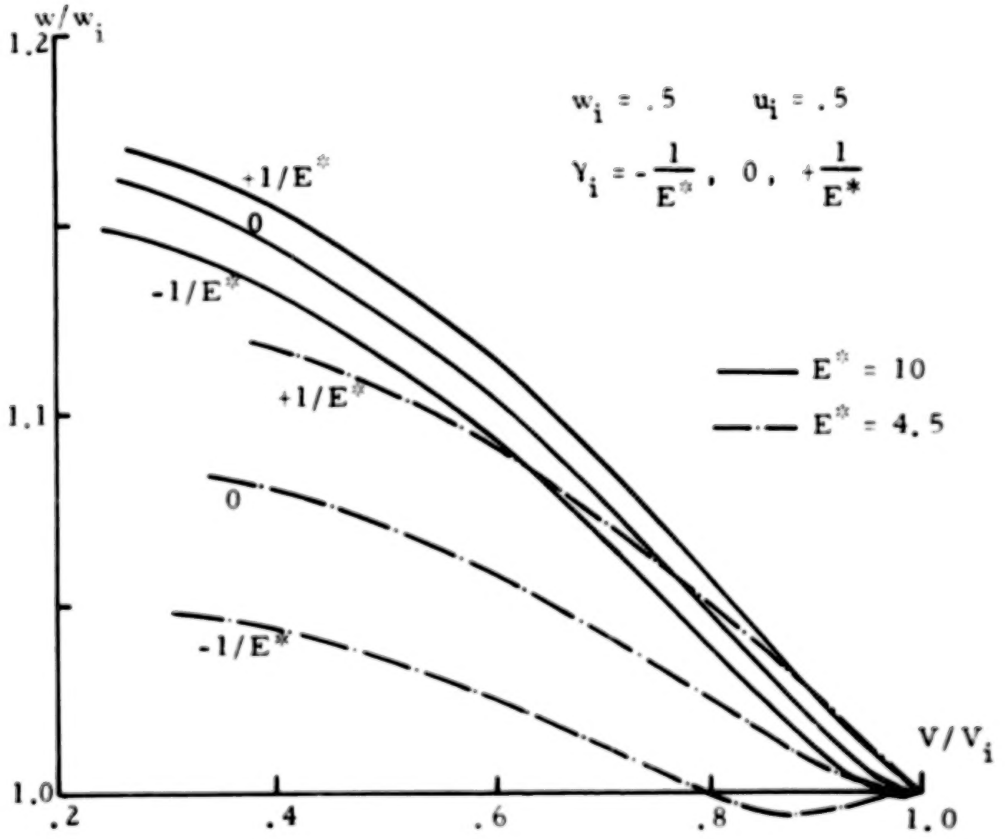

Figure 6. - Influence of Initial Flight Path Angle on Optimum Solution.

Thus it is solely a function of the initial dynamic pressure $(u/w)_i$ (or the initial indicated speed), and has the same value for all trajectories. In the example here its value is 2.4142. This also means that λ_i can no longer be a parameter in this case. To generate the family of optimum trajectories, we have to use either G_i or $(d\lambda/dy)_i$ as a parameter.

6.2 Pull-Up Maneuver with Bounded λ

In the preceding section, to display the behavior of the lift coefficient along an optimum trajectory, we put no restriction on its upper limit. This is of no problem for vehicles with high maximum lift-to-drag ratio since the optimum λ is within a reasonable limit. But for vehicles with low maximum lift-to-drag ratio, as in the case of the reentry vehicle, the optimum λ may be unacceptable since it can exceed the stalling lift coefficient λ_{max}.

To discuss the behavior of the optimum trajectory in the case of bounded λ, we refer to Figure 7 which plots different optimum trajectories in the (w,y) space for $E^* = 10$. Trajectories for higher final altitude (lower final speed) are started with lower λ_i. The variation of λ has been [illegible]ated in Figure 4. Let us assume that the upper bound of λ is $\lambda_{max} = 2.75$. Then from Figure 4, all trajectories with $\lambda_i \leq 2.75$ are pure variable λ trajectories since the condition $\lambda = \lambda_{max}$ is never reached. On the other hand, to generate the remaining optimum trajectories, we must start with $\lambda = \lambda_{max}$ for a

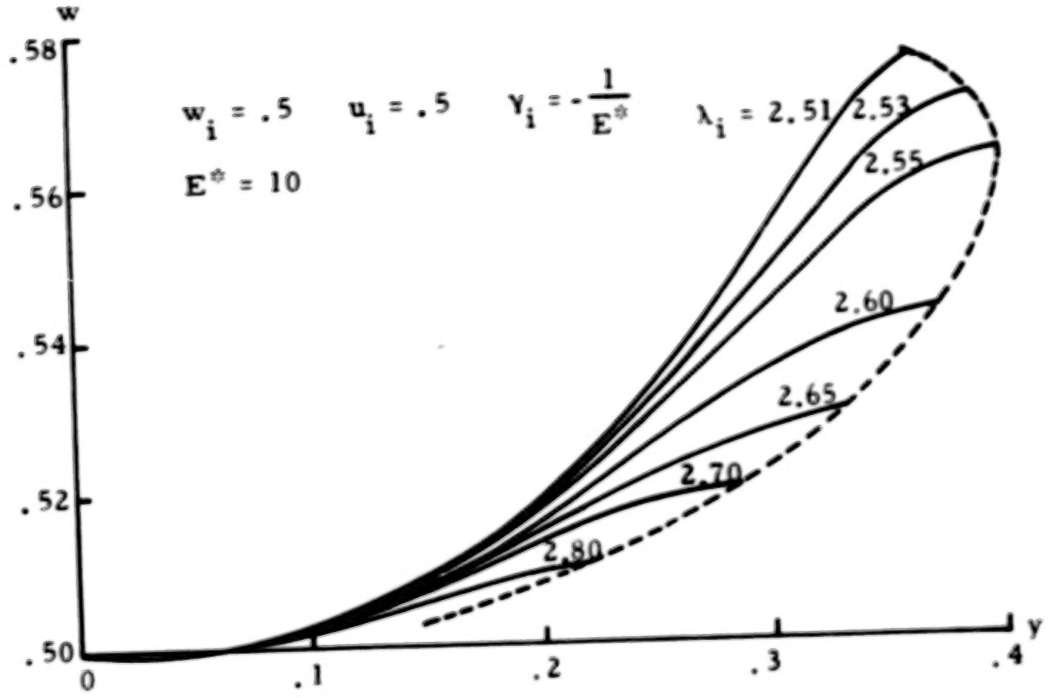

Figure 7.- Optimum Trajectories for Pull-Up Maneuver.

certain distance and then switch to variable λ. The integration starts with the state equations only using $\lambda = \lambda_{max}$, then at a certain point called the switching point with the state (w_s, u_s, γ_s), we use the variational equations, that is the state equations and the equations for λ and G, as before and continue the integration until $\lambda_f = 0$. We notice that in this example $\lambda_{max} > \lambda_b$, the initial derivative of λ $(d\lambda/dy)_i$ with $\lambda_i = \lambda_{max}$ is negative. To generate the family of optimum trajectories, we can switch at any point where $d\lambda/dy$ is negative. But to solve a particular problem with a prescribed w_f or u_f, the switching point has to be found such that the final condition $w = w_f$ or $u = u_f$ is satisfied.

Next, we consider the same case of Figure 4 with $E^* = 10$, but now we have $\lambda_{max} = 2.0$. Then all trajectories must start with $\lambda = \lambda_{max}$. Since $\lambda_{max} < \lambda_b$ in this example, $d\lambda/dy$ is positive initially. The constant $\lambda = \lambda_{max}$ subarc must continue for a certain distance until $d\lambda/dy \leq 0$, which occurs after passage through the lowest point in this example. Thus all the switches occur along the ascending arc, with the constant λ subarc longer for higher altitude gain (smaller final speed) trajectory.

To give an explicit example, we solve the problem for the following initial and end conditions,

$$w_i = .5\,, \quad u_i = .5\,, \quad \gamma_i = -1/E^* \quad \text{with} \quad E^* = 10; \qquad V_f/V_i = .7\,, \quad w_f = \text{maximum}\,, \quad \gamma_f = \text{free} \tag{6.16}$$

The physical trajectories are plotted in Figure 8. For the trajectory without lift constraint, it is found that $\lambda_i = 2.628314$ leading to a final value $w_f = 0.53457$ corresponding to a gain in altitude of $h_f - h_i = 478.81$ meters. If the constraint $\lambda_{max} = 2.55 > \lambda_b$ is enforced, the trajectory starts with $\lambda = \lambda_{max}$ until $w_s = .49935$, and switches to variable λ. The switch occurs during the descending phase. The final altitude is $w_f = 0.53450$ and corresponding to a gain in altitude of $h_f - h_i = 477.87$ meters. On the other hand, with the constraint $\lambda_{max} = 2.0 < \lambda_b$, the switch occurs at $w_s = .50877$, at a point along the ascending arc. We obtain $w_f = .53402$ which corresponds to a gain in altitude of $h_f - h_i = 471.44$ meters. The variation of the

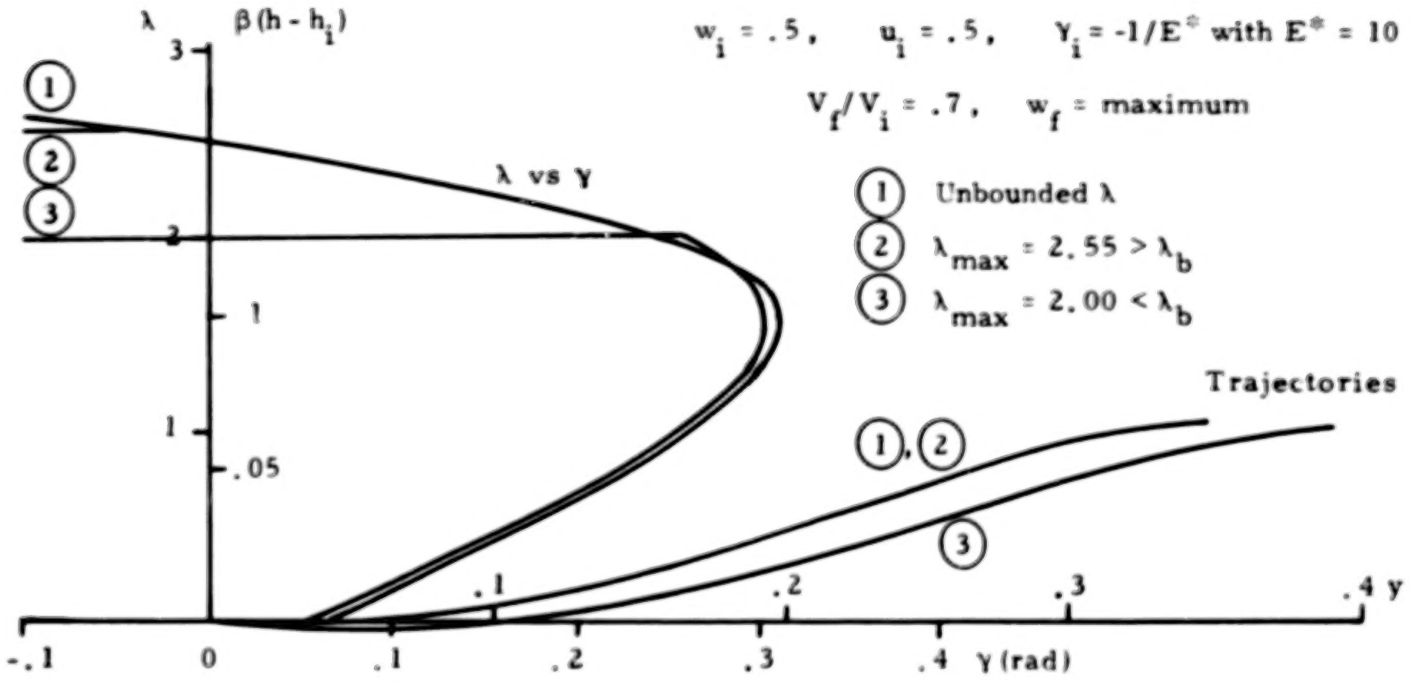

Figure 8. - Pull-Up Maneuver with Bounded λ; Trajectories in the Physical Space β (h - h_i) vs y, and Variation of the Optimum Bounded Lift Control.

normalized lift coefficient λ for these three trajectories is also presented in Figure 8.

6.3 Maximum Range

In this case, it is proposed to find the optimum lift control λ to glide the vehicle from the initial condition until the final condition

$$w = w_f \quad , \quad u = u_f \quad , \quad \gamma = \gamma_f \tag{6.17}$$

such that the final range y_f is maximized. Since y_f is not free, $C_1 \neq 0$, and the Hamiltonian integral Eq. (5.7) is inoperative in our formulation. We still have the same differential system, that is, Eqs. (5.4) and (5.9), the difference here is that we have two arbitrary parameters λ_i and G_i. The differential system is integrated with a set of guessed values λ_i and G_i until the prescribed final altitude $w = w_f$ is reached. The other two prescribed final values u_f and γ_f are used to adjust the values of λ_i and G_i. If the final angle is free, the condition on γ_f is replaced by the transversality condition $\lambda_f = 0$.

The advantage of using the variables λ and G to replace the adjoint variables is that their numerical values are nearly constant. This is because in glide for maximum range, both γ and u vary slowly so that $d\gamma/dy \simeq 0$ and $du/dy \simeq 0$, and we have

$$\lambda = \frac{w \cos \gamma}{u}$$
$$-\tan \gamma = \frac{u(1+\lambda^2)}{2E^* w \cos \gamma} \tag{6.18}$$

Hence

$$- \tan \gamma = \frac{1+\lambda^2}{2E^*\lambda} \tag{6.19}$$

In this so-called steady state approximation, the range is maximized by selecting the lift coefficient λ to minimize the glide angle $-\gamma$. This leads to the selection $\lambda = 1$, that is, to glide at maximum lift-to-drag ratio. Then we have the minimum glide angle

$$- \tan \gamma = \frac{1}{E^*} \tag{6.20}$$

Of course, this solution is only approximate. The real optimum solution is obtained by a lift modulation. Nevertheless, the steady state solution provides an educated guess for the behavior of λ and G. First, using $\lambda = 1$ and Eq. (6.20) in the first equation of Eqs. (5.9), we deduce that $dG/dy \simeq 0$. This means that G is nearly constant during the glide. Furthermore, using $\lambda = 1$ and Eq. (6.20) in the second equation of Eqs. (5.9) and noticing that $d\lambda/dy \simeq 0$, we have $G \simeq 4$ since $u \simeq u_i = .5$. In summary, the range of values for λ_i is close to 1 and the range of values for G_i is close to 4. In other words, the optimum trajectories are very sensitive to the initial values λ_i and G_i, especially when E^* is large.

The results are presented in Figures 9, 10, and 11 for the case of fighter aircraft with $E^* = 10$. Each figure presents several optimum trajectories with different final altitude. To restrict the plot to a one-parameter family of trajectories, we impose the condition $u_f = w_f$ at the final instant. For each trajectory, that is,

for each prescribed final altitude w_f, the corresponding initial value of the normalized lift coefficient λ_i is also labelled in the figures. For comparison, in each figure we plot in a dashed line the steady state trajectory, that is, the trajectory generated by using $\lambda = 1$.

Figure 9 gives the variation of λ as a function of y for different altitude drops. It is seen that, for large altitude drop, optimum glide is effected at near maximum lift-to-drag ratio, i.e., $\lambda \simeq 1$, except for the initial phase and the final phase. Also, we assume that γ_f is free, thus $\lambda_f = 0$.

Figure 10 gives the variation of $-\gamma$ as a function of y. For large altitude drop, it is steadily increasing at a very slow rate except for the initial and the final phases. Hence, as an approximation, along this portion of the optimum trajectory γ is nearly constant.

Figure 11 gives the variation of the dimensionless dynamic pressure $\eta = u/w$. For large altitude drop, it is nearly constant and slightly less than unity during the main portion of the glide. To find this near constant value, we take $\lambda = 1$ in Eqs. (6.18) and have

$$\eta = \frac{E^*}{\sqrt{1 + E^{*2}}} \tag{6.21}$$

For $E^* = 10$, this value is $\eta = .99504$ and is slightly less than the optimum value of η which is near $\eta = .9965$.

Concerning the actual performance, namely the maximized range, the $\lambda = 1$ trajectory gives a good approximation for large

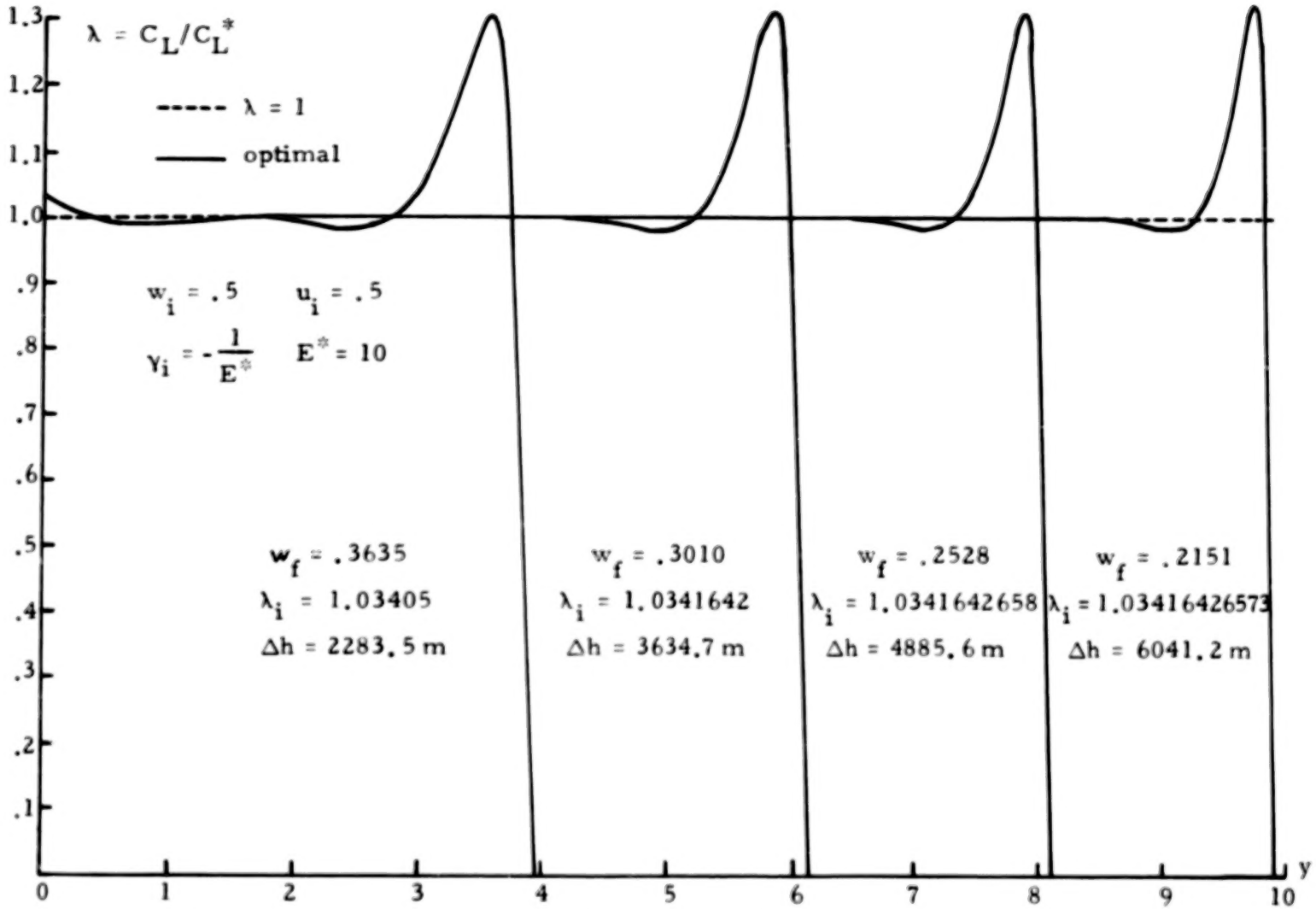

Figure 9. - Variation of the Optimum λ for Glide with Maximum Range.

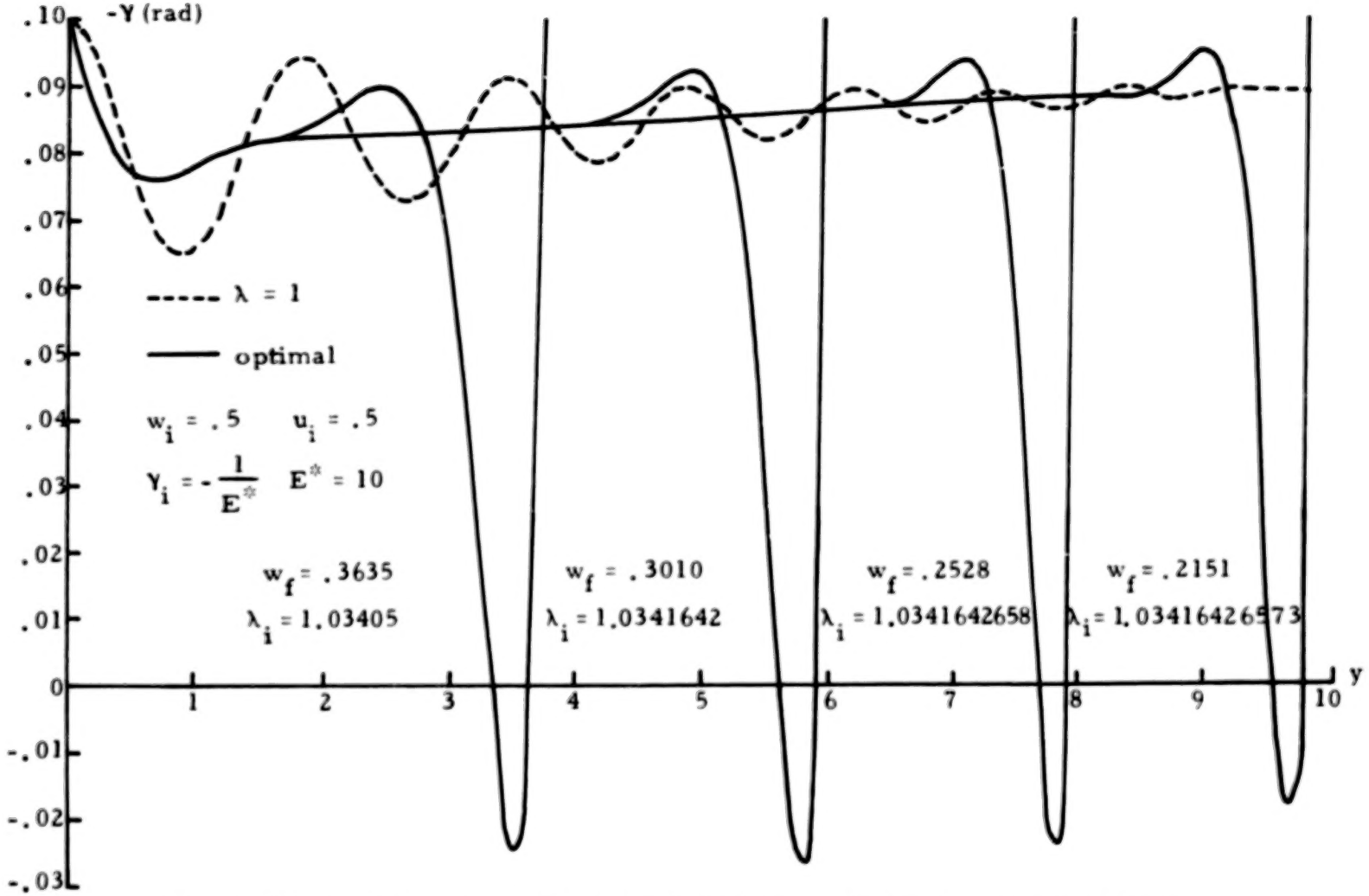

Figure 10.- Variation of the Flight Path Angle for Glide with Maximum Range.

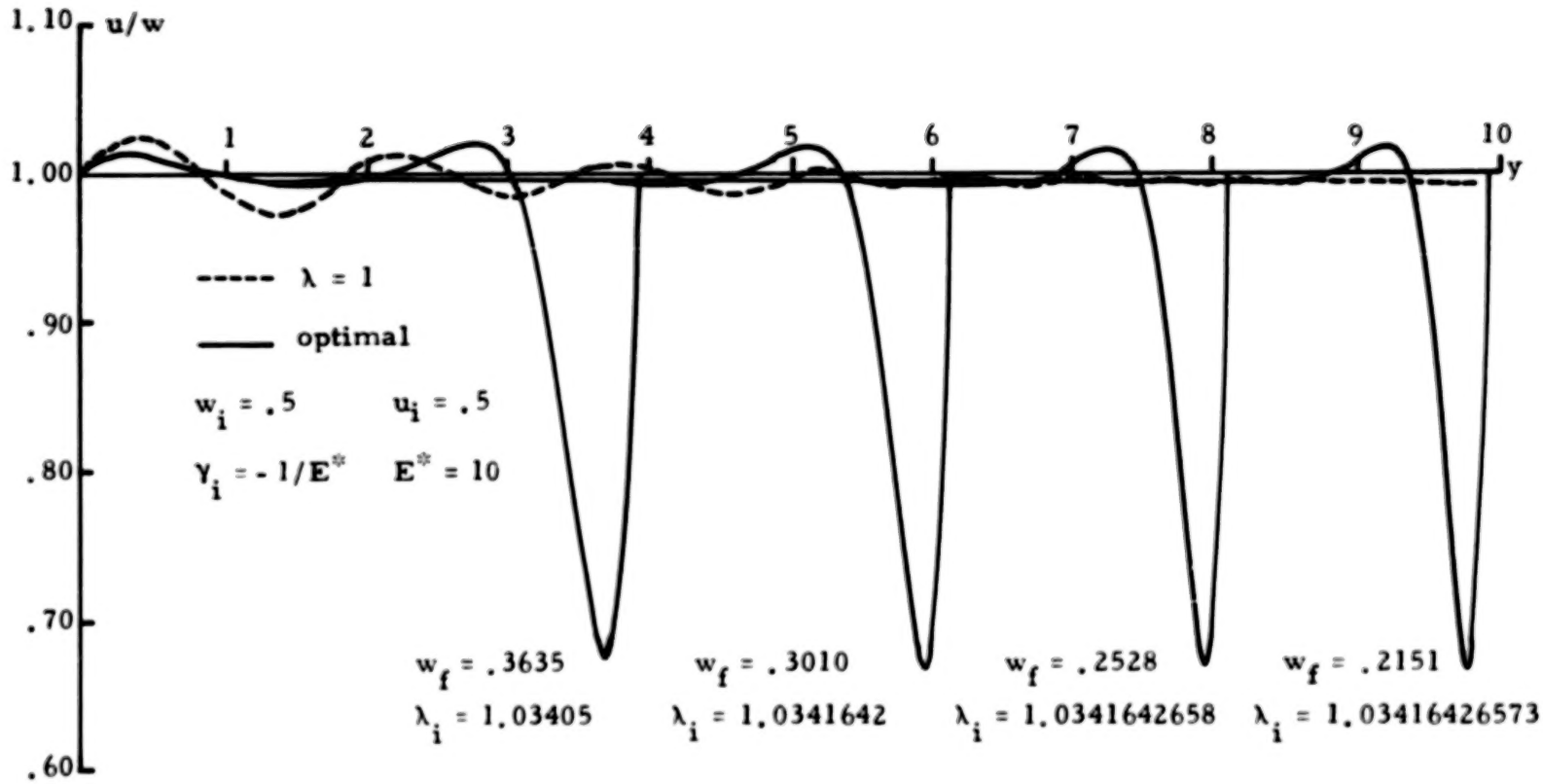

Figure 11.-Variation of the Dimensionless Dynamic Pressure for Glide with Maximum Range.

altitude drop. Its range is within 1% of the optimum range. A better approximation is to use constant dynamic pressure glide. This also has the advantage of flying with constant indicated speed. The value of η is given approximately by Eq. (6.21), and is purely a function of the maximum lift-to-drag ratio E^*.

In contrast with long range glide, the optimum glide for small altitude drop is not close to the glide with $\lambda = 1$. This is shown in Figure 12 where again the dashed line represents the $\lambda = 1$ trajectory. The short range problem is closely related to the problem of a pull-up maneuver with prescribed range. In this respect, we have the final

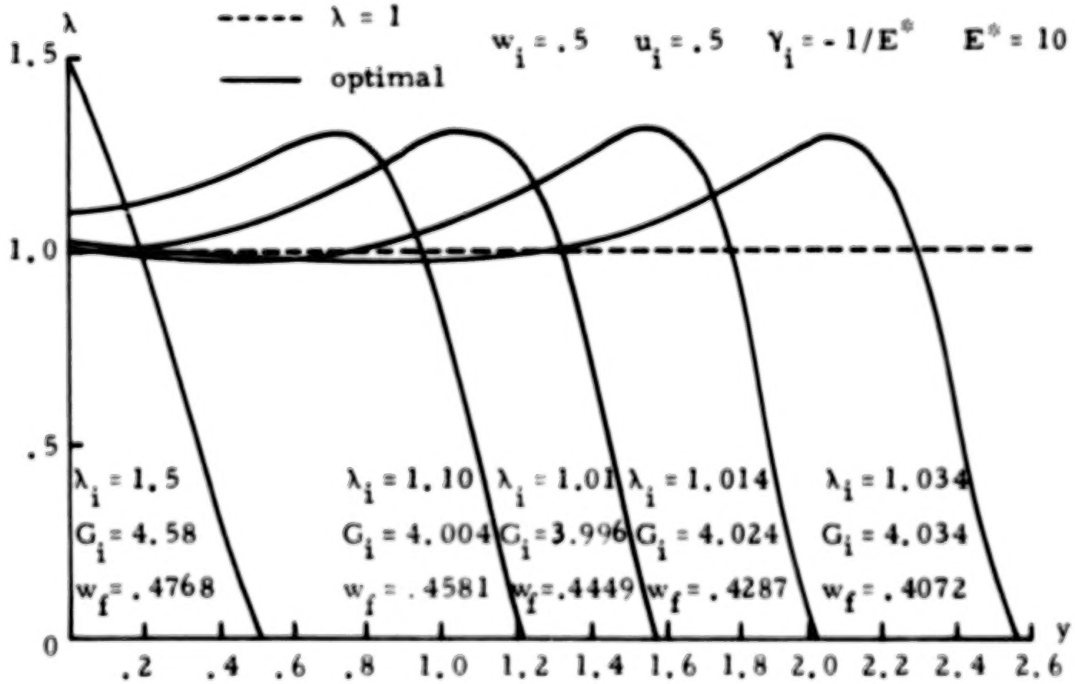

Figure 12. - Variation of the Optimum Lift Coefficient for Short Range (Small Altitude Drop) Glide.

condition either

$$w_f, \gamma_f, y_f = \text{prescribed}, \quad u_f = \text{maximum} \tag{6.22}$$

or

$$u_f, \gamma_f, y_f = \text{prescribed}, \quad w_f = \text{maximum} \tag{6.23}$$

We terminate the integration at $y = y_f$, and use the other two prescribed final values to find the two initial values λ_i and G_i. If γ_f is free, the final condition in γ is replaced by the condition $\lambda_f = 0$.

6.4 Linearized Singular Lift Control for Maximum Range

An inspection of the data presented in Figure 9 clearly shows the difficulty encountered in the numerical computation. More explicitly, for large altitude drop, the initial value λ_i has to be found with great accuracy for the final condition to be identically satisfied. It is seen that, except for the initial maneuver and the final maneuver, the lift control nearly follows the same line. This line can be considered as a singular arc familiar to the problem in which the control is linear. To reduce the computation work, if this singular arc can be found, one can follow the line until near the end and then compute separately the last arc where again, the control undergoes drastic change.

In general, let us consider an optimum control problem with the Hamiltonian

$$H = H(\vec{p}, \vec{x}, u, t) \tag{6.24}$$

where u is a scalar control subject to the constraint

$$u_{min} \leq u \leq u_{max} \tag{6.25}$$

To maximize the Hamiltonian, we either use $u = u_{min}$ or $u = u_{max}$, or an interior variable u such that

$$\frac{\partial H}{\partial u} = 0 \tag{6.26}$$

In general, the solution of Eq. (6.26) provides the optimum control

$$u^* = u^*(\vec{p}, \vec{x}, t) \tag{6.27}$$

This control is of the Euler-Lagrange type and u^* can be expressed explicitly in terms of the state vector $\vec{x}$ and possibly the time t and some constants of integration provided that the adjoint vector $\vec{p}$ can be expressed in terms of the same variables. This, in turn, requires the analytical integration of the equations for the adjoint vector $\vec{p}$. But, unfortunately, for most realistic cases it is not possible.

Now, let us assume that we know an approximate law for the optimum control, say

$$u^* \simeq u_0(\vec{x}, t) \tag{6.28}$$

Then by Taylor's series, we can expand the maximized Hamiltonian near the value $u = u_0$ to have

$$H^* = H(\vec{p}, \vec{x}, u_0, t) + \left(\frac{\partial H}{\partial u}\right)_0 (u^* - u_0) + \cdots \tag{6.29}$$

If u_0 is near the optimum value, the difference $\epsilon = u^* - u_0$ is small and, by retaining only the first order we have the approximate H^* which is now linear in u. Again, for this linearized problem, the

optimum solution is either $u = u_{min}$ or $u = u_{max}$ or a variable u when the coefficient of the linear control, called the switching function, vanishes identically. That is

$$\left(\frac{\partial H}{\partial u}\right)_0 = 0 \qquad (6.30)$$

Here, since we have assumed that u is not on the boundary, it is of the variable type. We have Eq. (6.30) which provides a relation between the state variables and the adjoint variables. This relation is exact in the linearized problem, but is approximate in the original non-linear problem. The accuracy of this approximation is of the order of ϵ. In the linearized problem, the Eq. (6.30) is valid as long as the control is of the interior type. Hence, we can take its derivative with respect to the independent variable t, to generate another relation between $\vec{x}$ and $\vec{p}$. It is known that we can take the derivative successively until the linear control appears for the first time, with an even derivative. The linear control can then be deduced explicitly. Then in the case where it can be expressed explicitly in terms of the state variables by using the additional relations obtained, we have an approximate but explicit law for the optimum control.

As an example for our present case here, from the steady state and the numerical analyses we have found a good approximation for the lift control λ. It is $\lambda_0 = 1$. We shall call this the zeroth order solution. By applying the linearizing technique on this problem, we can obtain the approximate law for the control

$$\lambda_1 = \frac{w \cos \gamma}{u} \tag{6.31}$$

We call this the first order solution. Then if we apply the linearizing technique once again, based on the first order solution which is a better approximation than the zeroth order, we finally have

$$\lambda_2 = \frac{w \cos \gamma}{u} \frac{A}{B} \tag{6.32}$$

where

$$\begin{aligned} A = {} & E^{*2} u^2 [6 \tan^2 \gamma - 4u (1 - \tan^2 \gamma) + 2u^2 \tan^2 \gamma + (1 + u) C] \\ & - 2E^* u (3 + u) (2 + C) w \sin \gamma + 2C (2 + C) w^2 \cos^2 \gamma \\ B = {} & E^{*2} u^2 [2 (1 + u) \tan^2 \gamma - 4u - C] - 2E^* u (4 + C) w \sin \gamma \\ & + 8 w^2 \cos^2 \gamma \end{aligned} \tag{6.33}$$

with

$$C = 1 - \frac{u^2}{w^2 \cos^2 \gamma} \tag{6.34}$$

Eq. (6.32) gives the explicit second order solution for the lift control. The details of the derivation of λ_1 and λ_2 will be given in Appendix B. For the first order solution, from the third equation of (5.4) we see that using the near optimum law (6.31), the flight path angle is maintained constant, a fact which can be observed in Figure 10. It is an improved approximation as long as the zeroth order solution $\lambda_0 = 1$ is accurate. Then for the second order solution (6.32), we have tested it numerically, and it gives excellent results. Using the initial values of the No. 2 trajectory in Figures 9, 10, and 11, we start the integration optimally. Then at $y = 2.4$ it is switched to the

explicit control law (6.32). The integration keeps on going, and the trajectory is generated by using this approximate control law. As compared with the nearly linear portion of the optimum trajectory No. 4 in Figures 9, 10, and 11, the two lift coefficients, approximate and optimum, agree to four significant digits, and the two trajectories generated are identical.

CHAPTER 7

OPTIMAL TRAJECTORIES FOR SPHERICAL EARTH

As in the case of the flat earth, we shall consider two types of optimum maneuvers. The first type is the pull-up maneuver, and the second one is of the gliding type. The optimum trajectory can be initiated from the top of the atmosphere. In some cases the pull-up maneuver gives the skip trajectory. Since the state equations we have derived for the spherical planet case, the Eqs. (4.2), are exact, they are also valid for the Keplerian motion of the vehicle after skipping out of the planetary atmosphere. In the other cases, the vehicle may reenter the planetary atmosphere after a coasting flight to initiate a new skip trajectory until effective entry at low speed. We shall consider both cases. The computation is done with the value $k^2 = 900$ for the earth atmosphere. For the maximum lift-to-drag ratio, a reasonable value $E^* = 3$ is considered since the flight is effected at high speed. Again, the maximum lift-to-drag ratio trajectory, that is, the $\lambda = 1$ trajectory, is used for comparison in the gliding type optimum trajectory.

7.1 Pull-Up Maneuver at Moderate Altitude

This is the same problem as discussed in Section 6.1. The differential system consists of the Eqs. (4.2) and the Eqs. (4.7). The initial condition is

$$\theta = 0, \quad Z = Z_i, \quad v = v_i, \quad \gamma = \gamma_i \tag{7.1}$$

It is proposed to find the optimum lift control to bring the vehicle from this initial condition to the final instant θ_f such that either

$$Z = Z_f, \quad v = v_f = \text{maximum} \tag{7.2}$$

or

$$v = v_f, \quad Z = Z_f = \text{minimum} \tag{7.3}$$

The final range θ_f is assumed to be free and hence $C_1 = 0$. Since the second equation of Eqs. (4.7) can be deleted, the only arbitrary parameter is λ_i and F_i can be obtained from Eq. (4.9). If the final flight path angle γ_f is prescribed, it is used to find the required initial value λ_i. If γ_f is free, we have the transversality condition $\lambda_f = 0$.

The problem considered here involves relatively low speed and altitude, and we shall take the initial values as

$$Z_i = .5, \quad v_i = .15, \quad \gamma_i = -\frac{1}{2E^5} \tag{7.4}$$

At high altitude where $Z_i \simeq 0$, and v_i is of the order of orbital speed, $v_i \simeq 1$, this type of maneuver leads the vehicle to skip out of the atmosphere. This case will be analyzed in detail later.

The problem is solved by the same routine as discussed in the case of the flat earth. The results are summarized in Figure 13. It is plotted as $\beta(h - h_i)$ versus V/V_i, where h is the actual altitude and V is the actual speed. By the definition of Eqs. (2.7) for Z, if an exponential atmosphere is used, the actual altitude change is

$$\Delta h = h_f - h_i = \frac{1}{\beta} \log\left(\frac{Z_i}{Z_f}\right) \tag{7.5}$$

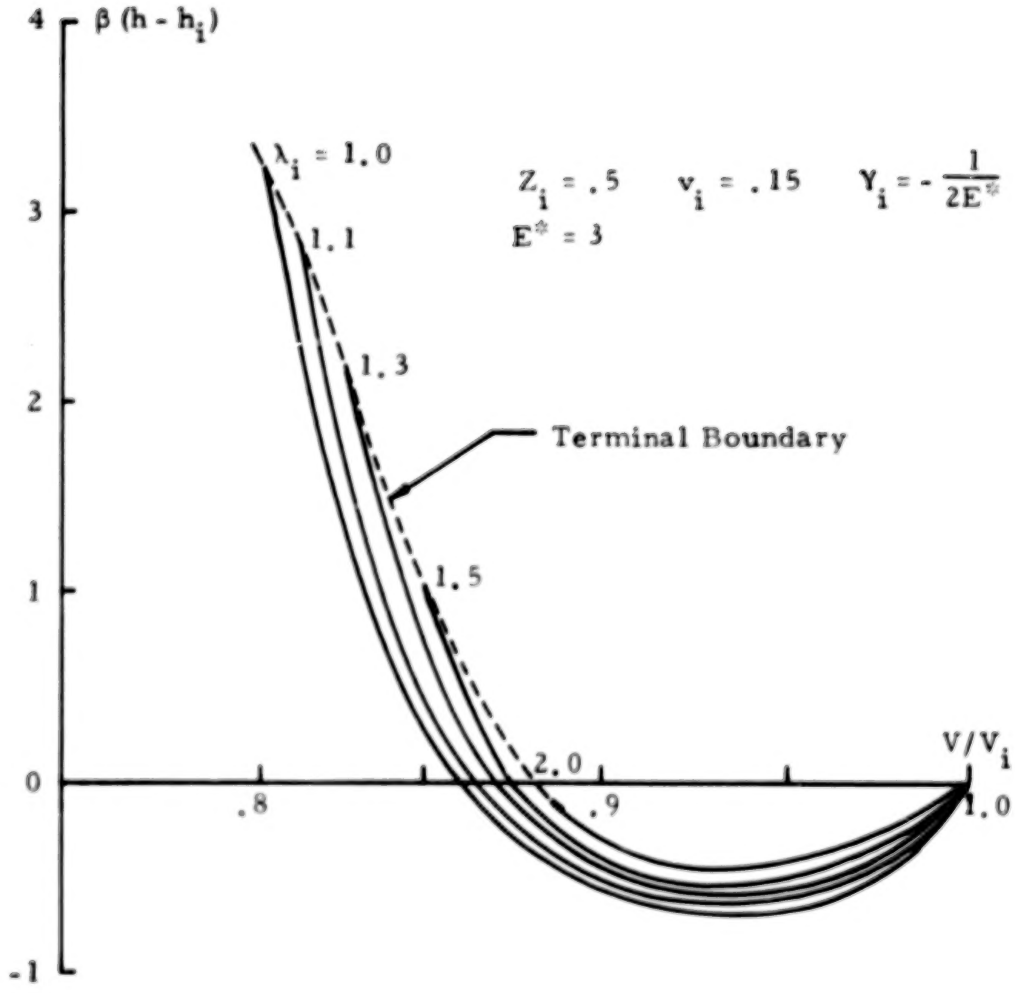

Figure 13.- Solution for the Optimum Pull-Up Maneuver at Low Speed over a Spherical Earth.

Again, the different solid lines are the optimum trajectories leading to the final boundary plotted in dashed line.

The variation of the normalized lift coefficient λ as a function of the flight path angle γ for different trajectories is presented in Figure 14. The behavior is the same as in the flat earth case, but the values of λ at the lowest point, $\gamma = 0$, are not so nearly the same. The difference is more due to the fact that the value of the maximum lift-to-drag ratio E^* used is relatively low rather than due to the additional centrifugal acceleration term which is included in the spherical planet equations.

7.2 Keplerian Motion Following a Skip Maneuver

In a skip trajectory, the vehicle enters the atmosphere at very high altitude with a speed at orbital magnitude and uses its

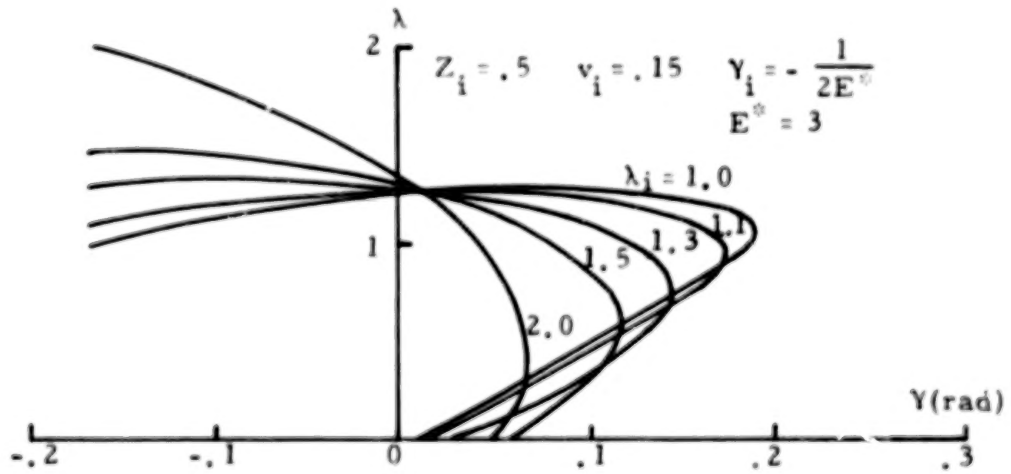

Figure 14.- Variation of the Optimum Lift Coefficient for Pull-Up Maneuver at Low Speed over a Spherical Earth.

lifting capability to negotiate a turn. It is then ejected from the atmosphere. This maneuver is depicted in Figure 15.

The skip maneuver is an important maneuver. It can be used to achieve maximum range or to assist a climb to orbital altitude with maximum residual speed, hence minimizing the required characteristic velocity for orbit insertion. In the three-dimensional maneuver,

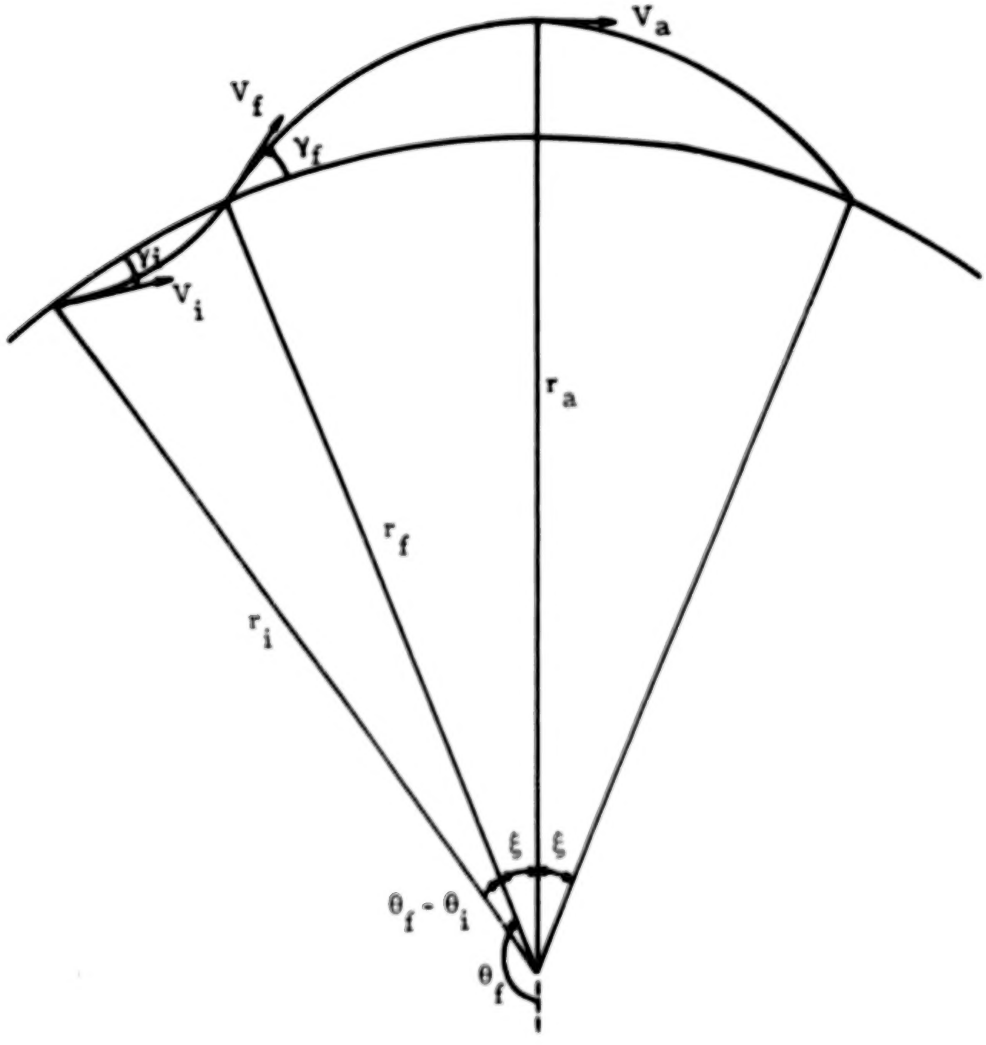

Figure 15.- Geometry of a Skip Trajectory.

it can be used to change the orbital plane. The first order solution for constant lift-to-drag ratio with the centrifugal and gravity accelerations neglected has been obtained in the classical literature [1]. An accurate second order solution for open loop guidance of skip trajectory has also been obtained [7]. In this chapter, we shall analyze the optimum solution with lift modulation using the exact equations.

The equations we have derived are valid for flight in the vacuum by taking the limit $Z \to 0$. But to initiate atmospheric flight we must start with some nonzero initial value Z_i. We shall adopt the convention that atmospheric entry is initiated when the acceleration due to atmospheric lift is equal to a certain small fraction of the gravity acceleration. From the definitions of Z and v in (2.7), the dimensionless acceleration due to a lift force with $C_L = C_L^*$, is

$$\frac{a}{g} = \sqrt{\beta r}\ Z v \tag{7.6}$$

For the earth atmosphere, $\beta r = 900$. Taking $a/g = .015$, i.e., 1.5%, with an initial speed equal to the orbital speed, $v_i = 1$, we have $Z_i = .0005$. We shall use this value as the value of Z at the top of the sensible atmosphere. For higher altitude with $Z < Z_i$, the flight is considered as in the vacuum and Keplerian motion applies.

As shown in Figure 15, the initial point (r_i, V_i, γ_i) is considered as the entry point, and the final point $(r_f = r_i, V_f, \gamma_f)$ is

considered as the exit point. Between the two points is the atmospheric skip trajectory, while beyond the exit point the flight is in the vacuum. Once in the vacuum, the vehicle climbs to the highest point (r_a, V_a, $\gamma_a = 0$), the apogee of the Keplerian orbit. Because of the obvious symmetry, the range angle ξ between the exit point and the apogee is half of the range angle for the coasting portion of the trajectory in vacuum. We shall be concerned with the maximizing of either the apogee distance r_a, or the apogee speed V_a, or the coasting range angle 2ξ. Hence, it is necessary to express these elements in terms of the variables at the exit point where atmospheric flight terminates. These relations can easily be obtained by using the classical Keplerian equations. However, we shall derive the pertinent equations from the general equations (4.2).

With $Z \to 0$, and using the equation for the variation of the radial distance to replace the first equation of (4.2) since it is inoperative, we have

$$\frac{dr}{d\theta} = r \tan\gamma$$

$$\frac{dv}{d\theta} = -(2 - v)\tan\gamma \qquad (7.7)$$

$$\frac{d\gamma}{d\theta} = -\frac{(1 - v)}{v}$$

From the second and third equations of (7.7),

$$\frac{dv}{d\gamma} = \frac{v(2 - v)}{1 - v}\tan\gamma \qquad (7.8)$$

Upon integrating this equation, we have

$$v(2 - v)\cos^2\gamma = (1 - e^2) \tag{7.9}$$

where the right hand side represents a constant of integration.

Next, from the first and second equations of (7.7),

$$\frac{dr}{dv} = \frac{-r}{2 - v} \tag{7.10}$$

Its integration gives

$$\frac{r}{a} = 2 - v \tag{7.11}$$

where a is another constant of integration. Returning to the definition of v, $v = r V^2/\mu$, it is easily seen that Eq. (7.11) expresses the conservation of energy and a is the semimajor axis of the Keplerian orbit. Furthermore, combining the two integrals (7.9) and (7.11) and again using the definition of v, we have

$$r^2 V^2 \cos^2\gamma = \mu p \tag{7.12}$$

where

$$p = a(1 - e^2) \tag{7.13}$$

Equation (7.12) expresses the conservation of angular momentum, and it is now clear that e is the eccentricity of the orbit while p is the semilatus rectum. Now, consider the derivative

$$\frac{d}{d\theta}\left(\frac{p}{r}\right) = -\frac{p}{r^2}\frac{dr}{d\theta} = -\frac{p}{r}\tan\gamma \tag{7.14}$$

where we have used the first equation of (7.7). By taking the

derivative again and simplifying, we have

$$\frac{d^2}{d\theta^2}\left(\frac{p}{r}\right) = \left(\frac{p}{r}\right)\left[-1 + \frac{1}{v\cos^2\gamma}\right] \tag{7.15}$$

Using the definition of v and the integral (7.12) in Eq. (7.15), we finally have the differential equation for the orbit

$$\frac{d^2}{d\theta^2}\left(\frac{p}{r}\right) + \left(\frac{p}{r}\right) = 1 \tag{7.16}$$

The general solution of this equation is

$$\frac{p}{r} = 1 + A\cos\theta + B\sin\theta \tag{7.17}$$

where A and B are constants of integration. Starting the angular variable at the perigee, $\theta = 0$, $dr/d\theta = 0$, $r = a(1 - e)$, and we obtain the polar equation of the orbit

$$\frac{p}{r} = 1 + e\cos\theta \tag{7.18}$$

Hence, we have derived the classical equations for Keplerian motion from our general equations (4.2). With these equations, we can deduce the performance indices for optimization in the following sections.

7.3 Skip Trajectory for Maximum Final Speed

Again, we assume that θ_f is free. Thus $C_1 = 0$, and we can use Eq. (4.9). It is a one-parameter problem. Referring to Figure 15, the vehicle enters the atmosphere at the initial point with the

initial condition

$$(Z_i , v_i , \gamma_i) = (.0005 , 1.0 , \text{variable}) \tag{7.19}$$

It is proposed to find the optimum lift modulation such that at the exit point

$$Z_f = Z_i , \quad \gamma_f = \text{free} , \quad v_f = \text{maximum} \tag{7.20}$$

Since γ_f is free, we again have $\lambda_f = 0$. We integrate the Eqs. (4.2) and the first and third equations of (4.7), from the initial state, with a guessed λ_i and a F_i solved from Eq. (4.9). Then we use the condition $\lambda_f = 0$ to find the correct value of λ_i.

The variation of the optimum lift coefficient as a function of the speed ratio V/V_i is presented in Figure 16 for several initial flight path angles γ_i. It is clear that less negative γ_i gives higher final speed. For all the trajectories computed, the optimum lift coefficient slightly increases at the beginning and then decreases continuously to the final value $\lambda_f = 0$.

7.4 Skip Trajectory for Maximum Apogee Altitude

In this problem, it is proposed to use optimum lift modulation to bring the vehicle to the exit point such that subsequent climb in the vacuum leads to a maximum height. Since θ_f is free, $C_l = 0$, and therefore the only parameter is λ_i. From Eq. (7.11) we have

$$\frac{r_a}{r_f} = \frac{2 - v_a}{2 - v_f} \tag{7.21}$$

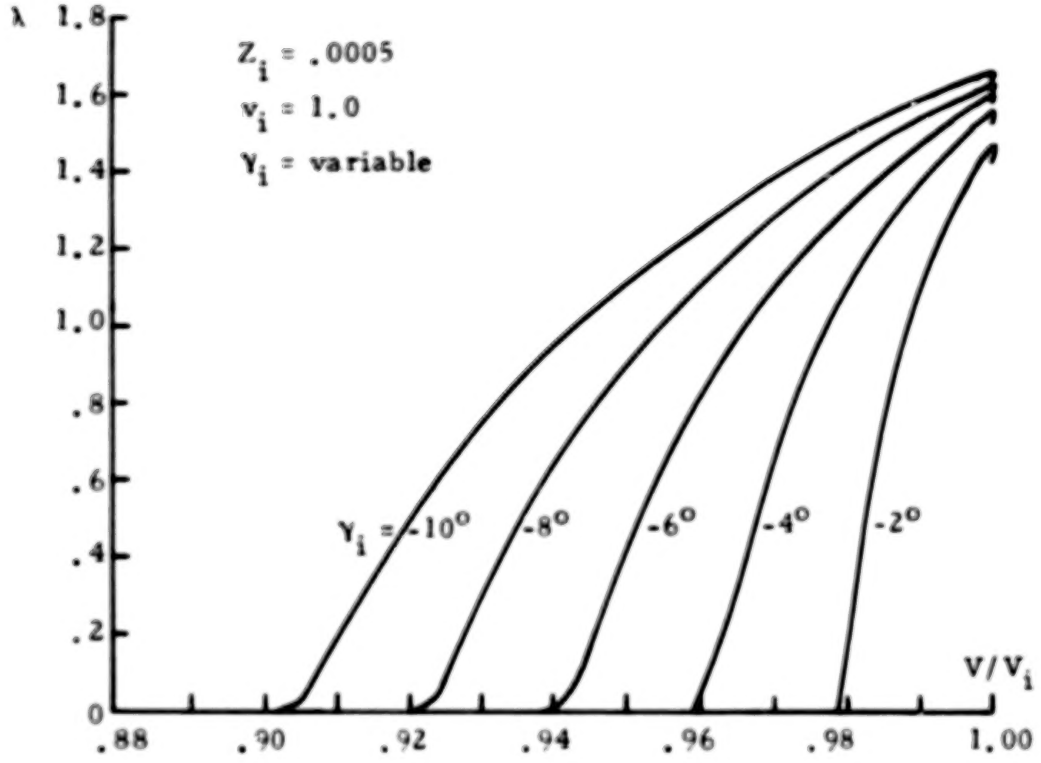

Figure 16.-Variation of the Optimum λ as a Function of the Speed Ratio for Skip Trajectories with Maximum Final Speed

As $r_f = r_i$, maximizing r_a is equivalent to maximizing r_a/r_f or, to minimizing $-r_a/r_f$. On the other hand, from Eq. (7.9),

$$v_a(2 - v_a) = v_f(2 - v_f)\cos^2\gamma_f \tag{7.22}$$

Solving for v_a from this equation and substituting into Eq. (7.21), we have

$$J = -\frac{r_a}{r_f} = \frac{1}{v_f - 2}\left[1 + \sqrt{1 - (2 - v_f)v_f\cos^2\gamma_f}\right] \tag{7.23}$$

Equivalent expression in terms of the energy was given in [10].

Since J is a function of v_f and γ_f, we have at the final time

$$p_{v_f} = -\frac{\partial J}{\partial v_f} \quad , \quad p_{\gamma_f} = -\frac{\partial J}{\partial \gamma_f} \tag{7.24}$$

Upon using the relation of Eq. (6.5), we have the following transversality condition

$$\lambda_f = \frac{E^* (2 - v_f)^2 \sin\gamma_f \cos\gamma_f}{2\left[1 - (2 - v_f)\cos^2\gamma_f + \sqrt{1 - (2 - v_f) v_f \cos^2\gamma_f}\right]} \tag{7.25}$$

This condition is used to find the initial value λ_i for the optimum trajectory. Finally, the corresponding max (r_a/r_f) can be obtained from Eq. (7.23).

This problem has been solved, and we have the following results

$$Z_i = .0005 \quad , \quad v_i = 1.0 \quad , \quad \gamma_i = -8^\circ$$

$$Z_f = .0005 \quad , \quad v_f = .377 \quad , \quad \gamma_f = 43.36^\circ$$

$$\lambda_i = -.70225 \quad , \quad \lambda_f = 2.04406 \quad , \quad \max\left(\frac{r_a}{r_f}\right) = 1.12308$$

In this flight program, the initial lift coefficient is negative. It appears that the optimum trajectory starts with a plunge toward the dense atmosphere with a slight increase in the speed, and then uses the lift to rotate the velocity vector upward with a relatively high exit angle, to achieve the absolute maximum apogee height. This maneuver is purely an academic exercise. It incurs excessively high acceleration. The value of Z at the bottom of the flight path is

$Z_b = 4.7795$. This represents a dip into the atmosphere with a distance $\Delta h = (1/\beta) \log (Z_b/Z_i) = 65,641.5$ meters. In practice, we shall have the following problem.

7.5-Skip Trajectory for Maximum Apogee Altitude with Prescribed Apogee Speed.

This is a more realistic formulation of the previous problem. Specifically, we seek to maximize the apogee altitude while prescribing a residual apogee speed V_a.

Let

$$R = \frac{r_a}{r_f} \quad , \qquad \bar{v}_a = \frac{V_a^2}{\mu/r_f} \tag{7.26}$$

Hence, we minimize $J = 1/R$ with a prescribed $\bar{v}_a$. From Eqs. (7.21) and (7.26), we have

$$\frac{1}{R} = 1 + \tfrac{1}{2}\bar{v}_a - \tfrac{1}{2} v_f \tag{7.27}$$

From this relation it is obvious that to minimize $1/R$ we simply maximize the final speed v_f. But this time, besides maximizing v_f, the prescribed V_a (or $\bar{v}_a$) must also be achieved. Since $v_a = r_a V_a^2/\mu = R\bar{v}_a$, by using this relation and Eq. (7.27) for $1/R$ in Eq. (7.22), we have

$$\frac{\bar{v}_a}{v_f \cos^2 \gamma_f} - (1 + \tfrac{1}{2}\bar{v}_a - \tfrac{1}{2} v_f)^2 = 0 \tag{7.28}$$

This is the final condition to be satisfied so that the prescribed $\bar{v}_a$ can be achieved. The procedure to solve this problem is the same

as that in the preceding section, but here we use Eq. (7.28) to search for the correct initial value λ_i.

As this is a one-parameter problem, we can obtain the totality of solutions simply by varying the parameter λ_i. Then at the end of the integration where $Z_f = Z_i$, Eq. (7.28) is used to solve for $\bar{v}_a$ and Eq. (7.27) for R. Figure 17 presents the solution for several values of γ_i. For each value of γ_i there is an absolute maximum apogee distance corresponding to the problem solved in the preceding section. For any other prescribed $\bar{v}_a$ which is different from this point, the maximized apogee distance is lower. The case of $\bar{v}_a = 0$ corresponds to vertical ascent in a vacuum, and hence for a trajectory leading to $\gamma_f = \pi/2$. Of course, this case is unrealistic.

7.6 Skip Trajectory for Maximum Apogee Speed with Prescribed Apogee Altitude

This is a trajectory with practical importance. It is proposed to use optimum lift modulation to bring the vehicle to the exit point such that the subsequent ascent in the vacuum will lead the vehicle to a prescribed apogee altitude r_a with a maximized residual speed V_a. Clearly, this leads to minimizing the characteristic velocity ΔV for orbit insertion.

By eliminating $\bar{v}_a$ between Eqs. (7.27) and (7.28) we have

$$R^2(2 - v_f) - 2R + v_f \cos^2\gamma_f = 0 \qquad (7.29)$$

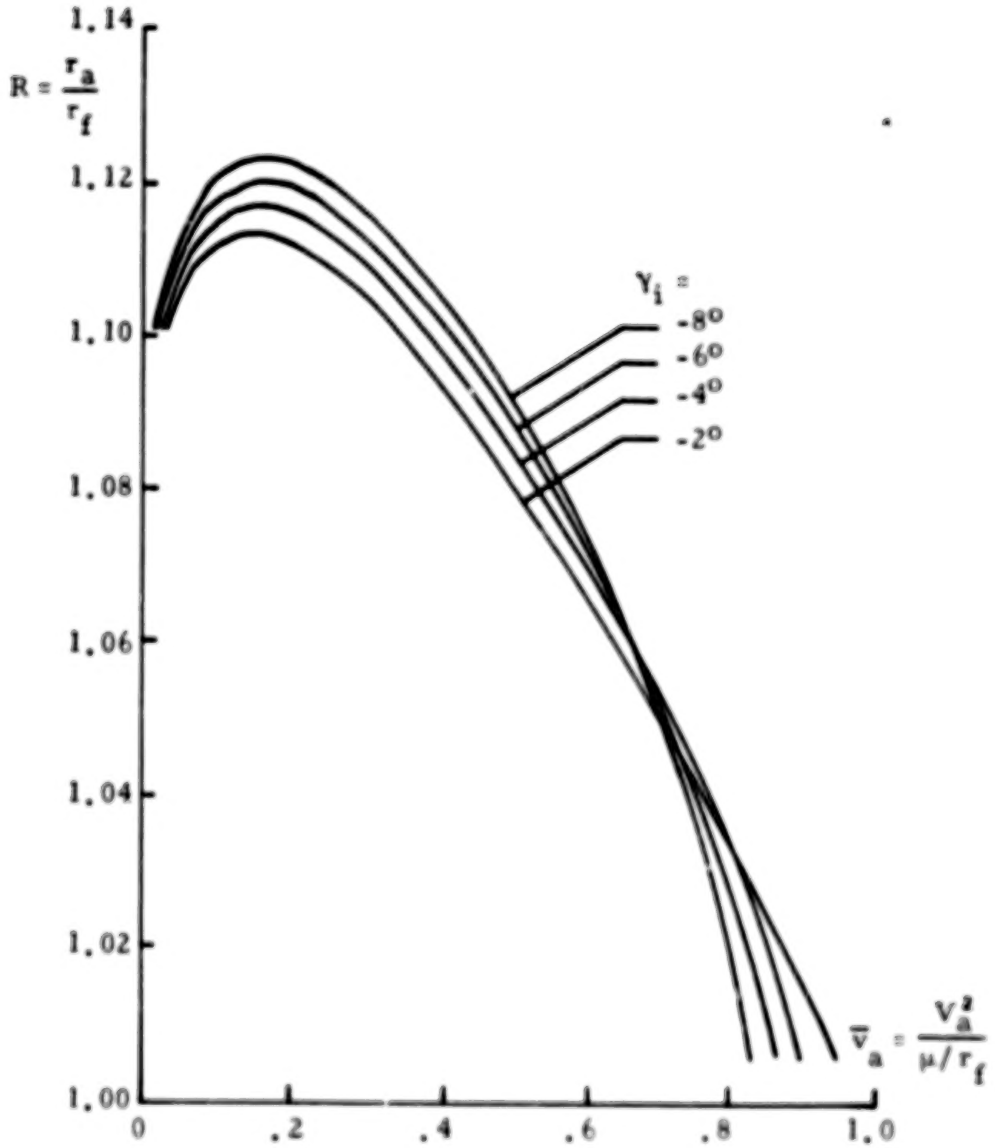

Figure 17.- Maximum Apogee Distance for a Prescribed Apogee Speed, or Maximum Apogee Speed for a Prescribed Apogee Distance.

For a prescribed r_a, the ratio R is specified. The procedure to obtain the optimum solution is the same as in Section 7.4, except that in here Eq. (7.29) is used to adjust the initial value λ_i. For the totality of the solutions, it is exactly the same as has been plotted in Figure 17. But this time, the value r_a/r_f is prescribed while the corresponding value $\bar{v}_a$ is maximized. We notice that there exists a range of r_a/r_f that gives two trajectories both satisfying the necessary condition for optimality. The optimum trajectory is the one corresponding to higher value of $\bar{v}_a$.

7.7 Skip Trajectory for Maximum Coasting Range

Again, we refer to Figure 15. For the initial condition we are still using Eq. (7.19). In this problem, it is proposed to find the optimum lift control to negotiate a skip trajectory such that after its exit from the atmosphere, the vehicle coasts ballistically in the vacuum to achieve a maximum coasting range 2ξ. We first solve this problem by assuming that the final value θ_f at the exit point is free, hence $C_1 = 0$. This is suggested by the fact that at orbital speed with small value of γ_i, the coasting range 2ξ is significantly larger and more sensitive to change than the atmospheric skip range $(\theta_f - \theta_i)$. The next case to be addressed is the maximization of the total range from the initial point, $(\theta_f - \theta_i) + 2\xi$.

From Figure 15, it is seen that $\xi = \pi - \theta_f$. Therefore, we obtain from Eq. (7.18)

$$\cos \xi = \frac{1}{e}\left(1 - \frac{p}{r_f}\right) \tag{7.30}$$

By writing the Eq. (7.9) at the exit point and solving for e, we have

$$e = \sqrt{1 - (2 - v_f)\, v_f \cos^2 \gamma_f} \tag{7.31}$$

Then by using Eq. (7.31) and the Eq. (7.11) at the exit point in the relation (7.13), it gives

$$p = r_f v_f \cos^2 \gamma_f \tag{7.32}$$

Upon substituting Eqs. (7.31) and (7.32) into Eq. (7.30), it becomes

$$\cos \xi = \frac{1 - v_f \cos^2 \gamma_f}{\sqrt{1 - (2 - v_f) v_f \cos^2 \gamma_f}} \tag{7.33}$$

For the first case we maximize 2ξ. It is equivalent to minimizing $\cos \xi$ and thus $J = \cos \xi$. Since J is a function of the two final variables v_f and γ_f, we again have the relations (7.24). The transversality condition is then

$$\lambda_f = \frac{E^* [1 - v_f - \tan^2 \gamma_f]}{2 \tan \gamma_f} \tag{7.34}$$

This is the condition used to search for the exact value λ_i. The initial state used and the results obtained are

$$Z_i = .0005 , \qquad v_i = 1.0 , \qquad \gamma_i = -4^\circ$$

$$Z_f = .0005 , \qquad v_f = .87475 , \qquad \gamma_f = 6.02^\circ$$

$$\lambda_i = .2925$$

$$\theta_f - \theta_i = .17646$$

$$2\xi_{max} = 1.18958$$

To show the optimality character of this trajectory, we integrate the state equations (4.2) using a constant lift coefficient, λ = constant. The best constant λ which gives the maximum coasting range is found to be $\lambda = 1.024$, and the results are

$$Z_f = .0005\,, \qquad v_f = .90876\,, \qquad \gamma_f = 3.58^o$$

$$\theta_f - \theta_i = .20633$$

$$2\xi_{max} = 1.07743$$

It shows that using optimum lift modulation we have an improvement of 10.41% in the coasting range as compared to the best solution obtained with a constant lift coefficient.

We now solve the second case, in which we maximize the total range from the initial point to the end of the coasting flight. That is, we maximize the following performance index

$$J = (\theta_f - \theta_i) + 2\cos^{-1}\left[\frac{1 - v_f\cos^2\gamma_f}{\sqrt{1 - (2 - v_f)\,v_f\cos^2\gamma_f}}\right] \qquad (7.35)$$

This time, the final range is not free and hence $C_1 \neq 0$. There are two parameters to be found, λ_i and F_i. Actually C_1 is equal to p_{θ_f},

and from Eq. (7.35) we have, for a maximization problem,

$$p_{\theta_f} = \frac{\partial J}{\partial \theta_f} = 1 \tag{7.36}$$

Thus $C_1 = 1$. Furthermore, we also have

$$p_{v_f} = \frac{\partial J}{\partial v_f} \quad , \qquad p_{\gamma_f} = \frac{\partial J}{\partial \gamma_f} \tag{7.37}$$

Upon using the relations (7.37) in Eq. (6.5), it gives exactly the same λ_f as given by Eq. (7.34). Therefore, Eq. (7.34) is also a transversality condition for this case. We need one more transversality condition because this case has two parameters. It comes from the Hamiltonian integral (4.8) at the final time. With $C_1 = 1$ and the p_{v_f} given in Eq. (7.37), we finally have

$$\frac{k Z_f v_f (1 - \lambda_f^2)}{E^* \cos \gamma_f} + \frac{(1 - v_f)\lambda_f}{E^*} + \left(1 - \frac{v_f}{2} + v_f F_f\right) \tan \gamma_f = 0 \tag{7.38}$$

The problem is solved and this time it is found that

$$Z_f = .0005 \ , \qquad v_f = .88101 \ , \qquad \gamma_f = 5.63^o$$

$$\lambda_i = .57921 \ , \qquad F_i = 3.6873$$

$$\theta_f - \theta_i = .18173$$

$$2\xi = 1.18692$$

The total range obtained is $J = (\theta_f - \theta_i) + 2\xi = 1.36865$, which is slightly higher than the total range $J = 1.36604$ of the first case where only the coasting range 2ξ is maximized.

For all the skip trajectories solved above, it has been assumed that beyond the altitude $Z = .0005$, the flight is in a vacuum. The corresponding altitude is given, through the atmospheric density, by

$$\frac{\rho S C_L^*}{2m} \sqrt{\frac{r}{\beta}} = .0005 \tag{7.39}$$

For most vehicle characteristics, the resulting altitude is generally high enough such that beyond this altitude the subsequent trajectory is practically Keplerian. For better accuracy, one can take a smaller Z. The computational procedure remains unchanged.

7.8 Glide with Maximum Range

The maximum range obtained previously concerns the range with one skip. We now generate the optimum control to maximize the total range for a descent from an initial altitude Z_i to a final altitude Z_f. The problem is first solved for the case of a relatively low initial altitude. A reasonable set of initial values is

$$(Z_i, v_i, \gamma_i) = (.5, .15, -\frac{1}{2E^*}) \tag{7.40}$$

with again $E^* = 3$. This can be considered as the gliding flight following a ballistic entry of a shuttle vehicle. The vehicle enters the earth atmosphere at the reentry altitude $Z_e \simeq 0$, with a speed $v_e \simeq 1$ and a certain reentry angle γ_e. Then at the end of the ballistic phase, the vehicle rotates to reduce the angle of attack,

hence generating a lifting force and using lift modulation to glide to a final altitude with a maximum range. The case of gliding from the entry point will be analyzed in the last part of this section.

The numerical computation is carried out exactly as in the flat earth case. We integrate the state equations, Eqs. (4.2), the first equation of (4.7) for F, and the third equation of (4.7) for λ, from the initial state (7.40) and two guessed values F_i and λ_i. At a prescribed final altitude the integration is terminated, and the other two prescribed final values v_f and γ_f are used for adjusting the F_i and λ_i. If γ_f is not prescribed, then the condition on γ_f is replaced by the condition $\lambda_f = 0$. In order to generate a one-parameter family of optimum trajectories, we impose the final condition

$$\sqrt{\beta r}\, Z_f\, v_f = 1 \tag{7.41}$$

Physically, this means that the final acceleration due to a lift force with $C_L = C_L^*$ is equal to the gravity acceleration. For each prescribed Z_f, the corresponding v_f is obtained from this condition.

Figure 18 presents the variation of the optimum lift coefficient. It is seen that λ oscillates about the value of unity and tends to this value near the end of a long range glide which corresponds to a large altitude drop. Figure 19 presents the variation of the flight path angle while the variations of the altitude and the speed are depicted in Figure 20.

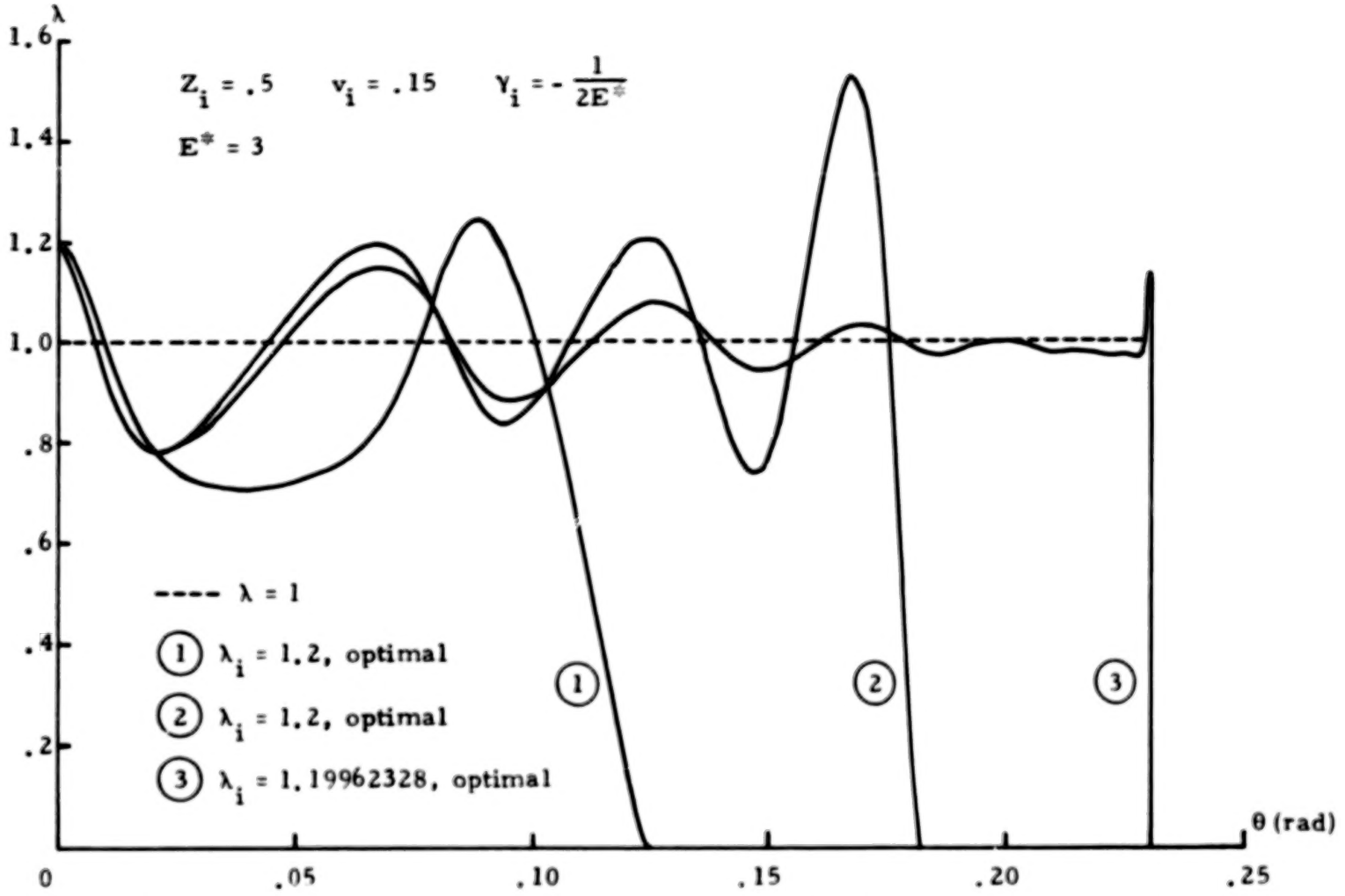

Figure 18. -Variation of the Optimum λ for Low Altitude Maximum Range Glide over a Spherical Earth.

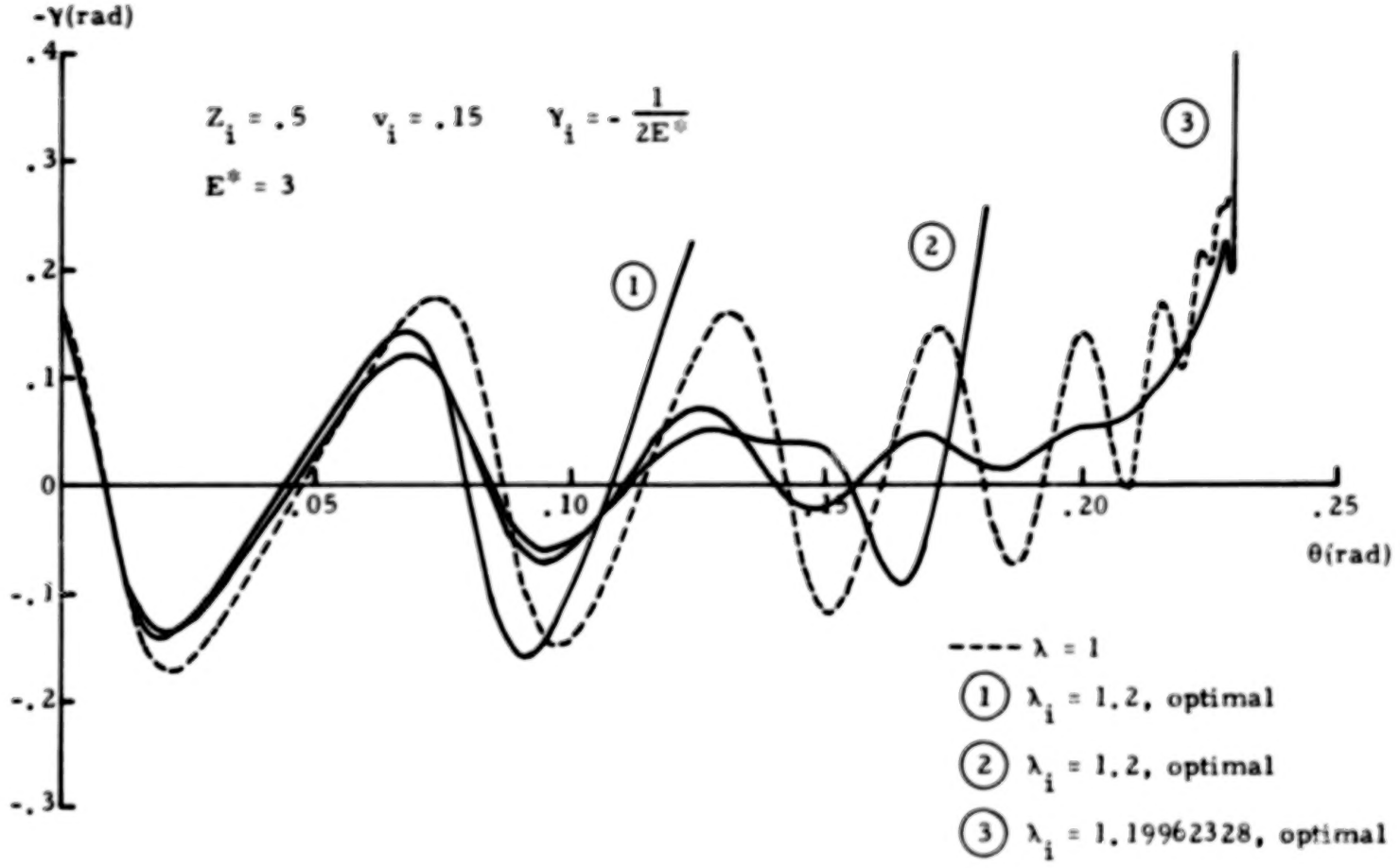

Figure 19. - Variation of γ for Low Altitude Maximum Range Glide over a Spherical Earth.

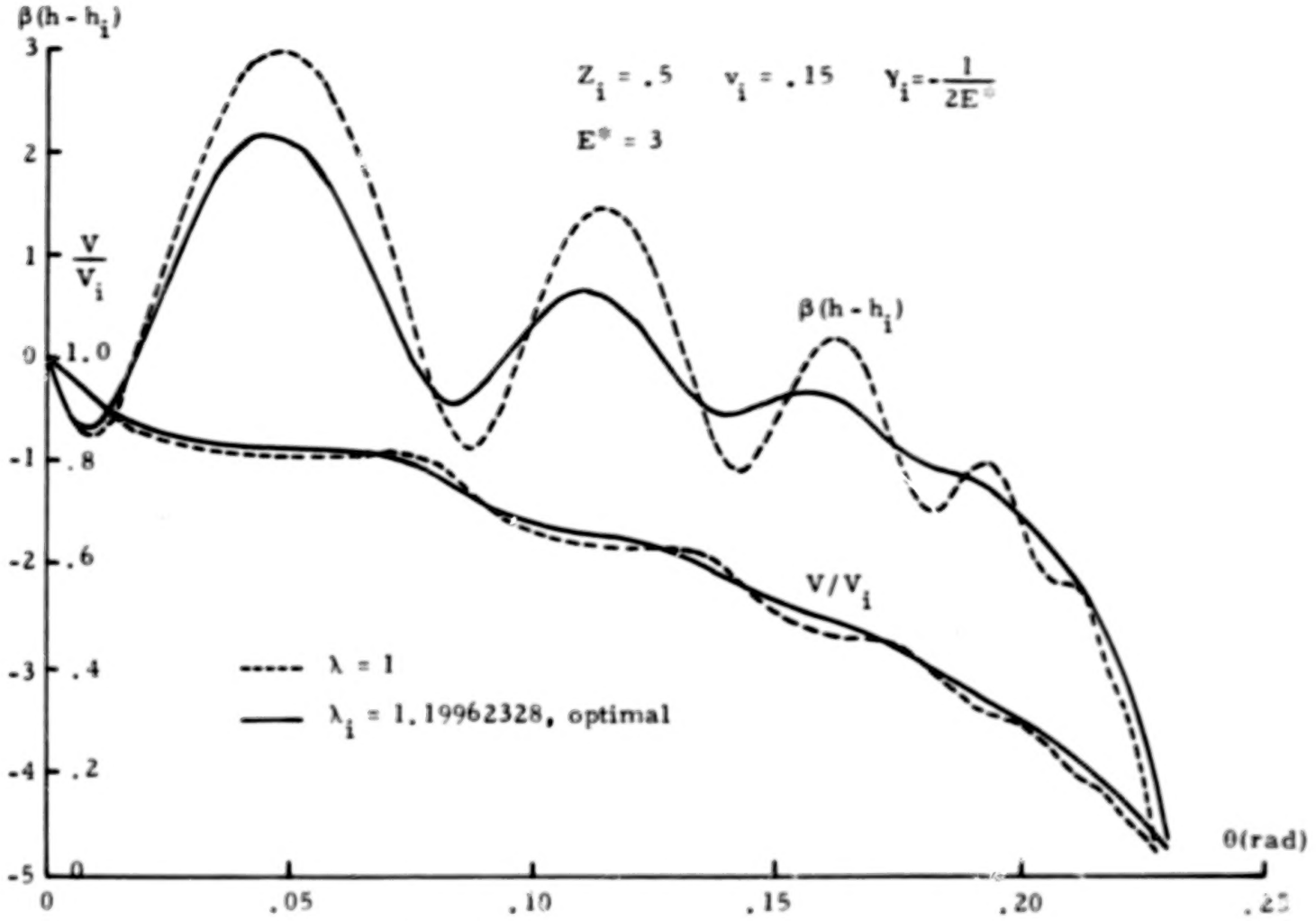

Figure 20. -Variation of the Altitude and the Speed for Low Altitude Maximum Range Glide over a Spherical Earth.

For the case of glide starting from the entry point, a typical initial condition is

$$(Z_i, v_i, \gamma_i) = (.0005, 1.0, -4^{\circ}) \tag{7.42}$$

The final condition to be satisfied is

$$Z = Z_f, \qquad v = v_f, \qquad \gamma_f = \text{free} \tag{7.43}$$

The variation of the altitude as a function of the range for the optimal trajectory is plotted in Figure 21 as a solid line. The variation of the flight path angle is plotted in Figure 22. Finally, Figure 23 presents the variations of the optimum lift control and the speed. Again, the optimum lift control oscillates and tends to the lift control for maximum lift-to-drag ratio, $\lambda = 1$.

In both cases above, the trajectory generated by using maximum lift-to-drag ratio, $\lambda = 1$, is plotted in the dashed line for comparison. Besides an improvement in the range of about 2%, the oscillation in altitude along the optimum trajectory is less severe. We can also see a more desirable behavior of the flight path angle along the optimum trajectory. It also yields a more smooth variation in the deceleration. The oscillation of the optimum trajectory results from an exchange between the kinetic energy and the potential energy. At high speed, a skip to near vacuum contributes significantly to the range.

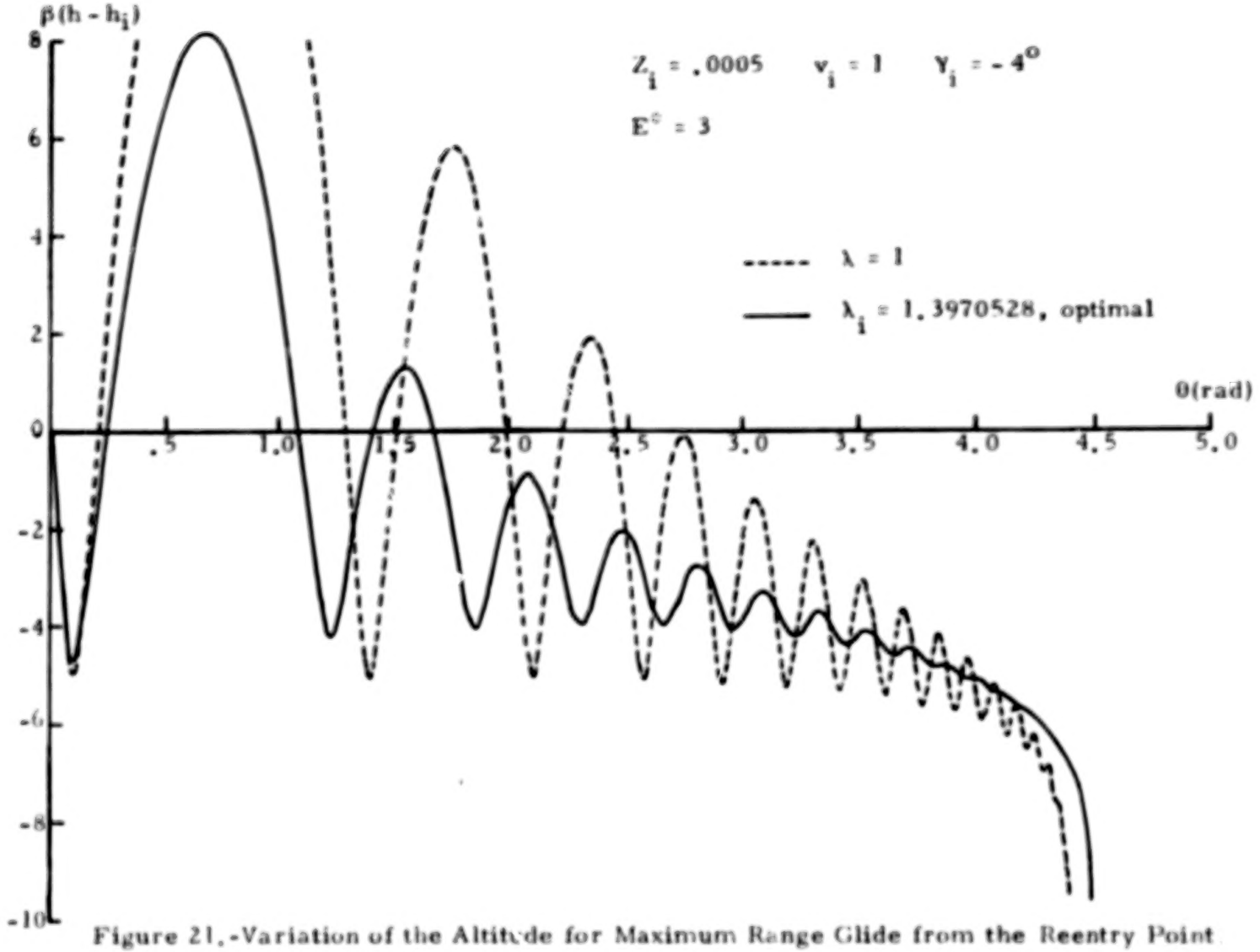

Figure 21.-Variation of the Altitude for Maximum Range Glide from the Reentry Point

TABLE OF CONTENTS

NOMENCLATURE	v	1/A7
LIST OF APPENDICES	vii	1/A9
LIST OF FIGURES	viii	1/A10
LIST OF TABLES	x	1/A12
SUMMARY	xi	1/A13

CHAPTER

1. INTRODUCTION	1	1/A14
2. DIMENSIONLESS EQUATIONS OF MOTION	3	1/A2
2.1 Three-Dimensional Equations of Motion		
2.2 Dimensionless Equations of Motion		
3. VARIATIONAL FORMULATION	6	1/B8
3.1 Variational Formulation		
3.2 Integrals of the Motion		
4. PLANAR FLIGHT	14	1/B12
4.1 Governing Equations		
4.2 Change of Adjoint Variables		
5. FLAT PLANET SIMPLIFICATION	18	1/C3
5.1 Governing Equations for Flat Planet Model		
6. OPTIMAL TRAJECTORIES FOR FLAT EARTH	22	1/C7
6.1 Maximum Final Speed or Maximum Final Altitude		
6.2 Pull-Up Maneuver with Bounded C_L		
6.3 Maximum Range		
6.4 Linearized Singular Lift Control for Maximum Range		

7. OPTIMAL TRAJECTORIES FOR SPHERICAL EARTH 49 1/E13

7.1 Pull-Up Maneuver at Moderate Altitude
7.2 Keplerian Motion Following a Skip Maneuver
7.3 Skip Trajectory for Maximum Final Speed
7.4 Skip Trajectory for Maximum Apogee Altitude
7.5 Skip Trajectory for Maximum Apogee Altitude with Prescribed Apogee Speed
7.6 Skip Trajectory for Maximum Apogee Speed with Prescribed Apogee Altitude
7.7 Skip Trajectory for Maximum Coasting Range
7.8 Glide with Maximum Range

8. THREE-DIMENSIONAL FLIGHT 77 2/A7

8.1 Maximum Cross Range
8.2 The Footprint

9. CONCLUSIONS 97 2/C5

APPENDICES 100 2/C8

REFERENCES 109 2/D3

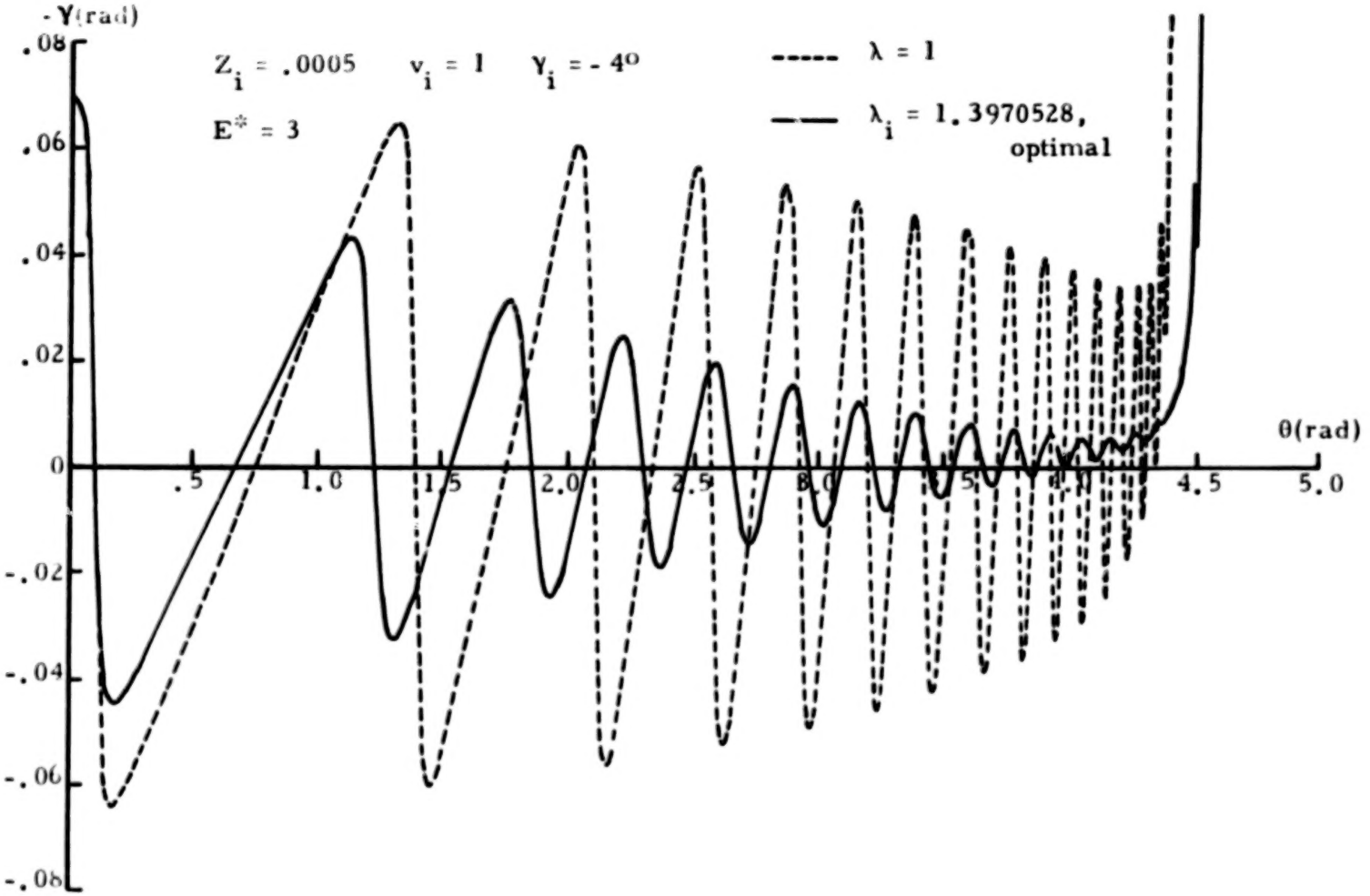

Figure 22.- Variation of γ for Maximum Range Glide from the Reentry Point.

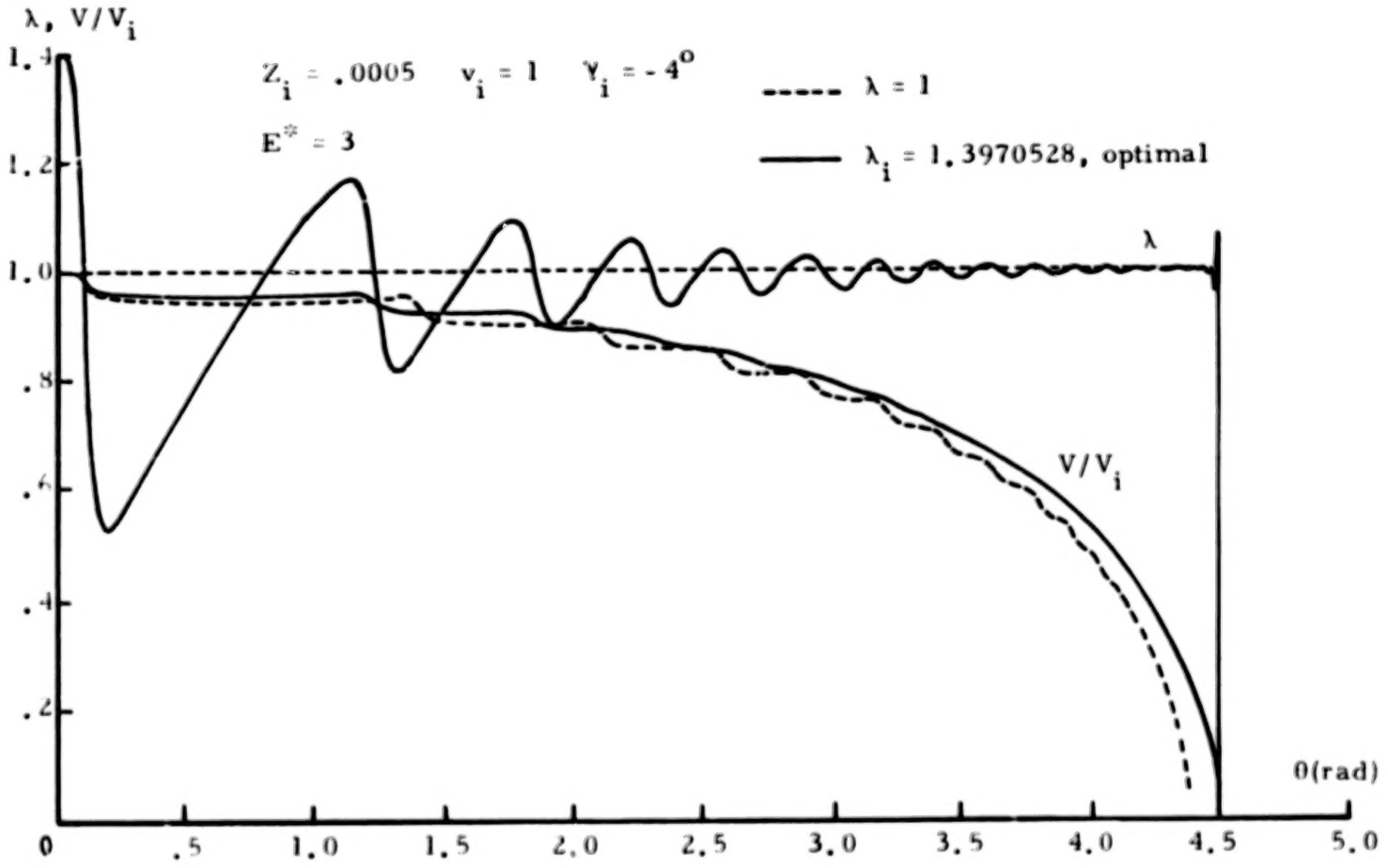

Figure 23.- Variation of the Optimum λ and the Speed for Maximum Range Glide from the Reentry Point.

CHAPTER 8

THREE-DIMENSIONAL FLIGHT

Two elements are of interest in three-dimensional flight; one is the maximum cross range, the other is the footprint. In this chapter, we shall discuss the procedure to solve the absolute maximum cross range. We will see that it is a three-parameter problem. Then by using the equilibrium glide condition as a simplifying device, we shall compute the footprint of a gliding entry vehicle on the surface of a planet. A technique of coordinate rotation is used to make the iteration much more effective.

8.1 Maximum Cross Range

It is proposed to find the lift and bank modulation to maximize the final latitude ϕ_f while the final longitudinal range θ_f is free. For an initially circular orbit, if the position of departure is free, the reachable domain will then be a zone between the latitudes $-\phi_{max}$ and $+\phi_{max}$. If $\phi_{max} = \pi/2$, the reachable domain is the entire surface of the planet.

Since the final arc length s_f is free, we have $C_0 = 0$ in Eq. (3.6). The final condition in the state variables will be

$$Z = Z_f, \quad v = v_f, \quad \gamma = \gamma_f = \text{free}, \quad \theta = \theta_f = \text{free},$$
$$\psi = \psi_f = \text{free}, \quad \phi = \phi_f = \text{maximum} \tag{8.1}$$

The Eqs. (3.7) at the final time then can be written as

$$\begin{aligned} p_\theta &\equiv C_1 = 0 \\ p_{\psi_f} &= -\cos\phi_f (C_2 \sin\theta_f - C_3 \cos\theta_f) = 0 \\ p_{\phi_f} &= C_2 \cos\theta_f + C_3 \sin\theta_f = 1 \end{aligned} \tag{8.2}$$

Solving for the constants of integration C_2 and C_3 we obtain the solutions for p_ψ and p_ϕ,

$$\begin{aligned} p_\psi &= \cos\phi \sin(\theta_f - \theta) \\ p_\phi &= \cos(\theta_f - \theta) \end{aligned} \tag{8.3}$$

We also have, since γ_f is free,

$$Q_f = p_{\gamma_f} = 0 \tag{8.4}$$

The Hamiltonian integral (3.11) becomes

$$-P\tan\gamma - N\left[\frac{kZ}{E^* \cos\gamma} + \frac{(2-v)}{v}\tan\gamma\right] - \frac{(1-v)Q}{v}$$
$$+ \frac{E^* k Z}{4N\cos\gamma}\left(Q^2 + \frac{p_\psi^2}{\cos^2\gamma}\right) + p_\phi \sin\psi - p_\psi \cos\psi \tan\phi = 0 \tag{8.5}$$

Thus for the specified final condition (8.1), the procedure to obtain the optimum solution is as follows. Starting from a certain initial state, say

$$(Z_i, v_i, \gamma_i, \theta_i, \phi_i, \psi_i) = (.0005, 1.0, -4^o, 0, 0, 0) \qquad (8.6)$$

with a given value of E^*, we integrate the state equations (2.8) along with the adjoint equations (3.9), using the control law (3.10) and the Eqs. (8.3) for p_ψ and p_ϕ. There are three parameters, namely, the final longitudinal range θ_f and two of the three initial values P_i, N_i, and Q_i since one of them can be obtained from the Hamiltonian integral (8.5). These parameters are to be selected such that when the integration is stopped at $\theta = \theta_f$, the two prescribed final values Z_f and v_f and one transversality condition (8.4) are all satisfied. The resulting trajectory will be the optimum trajectory for maximum cross range.

A simplification can be made by using the so-called equilibrium glide condition, assuming that the glide angle is small and stays nearly constant. This is expressed as

$$\gamma \simeq 0 \quad , \quad \frac{d\gamma}{ds} \simeq 0 \qquad (8.7)$$

By substituting into the equation for γ in (2.8), we have

$$kZ = \frac{1 - v}{\lambda v \cos \sigma} \qquad (8.8)$$

This equation is used to evaluate the altitude Z. Thus we have the following reduced set of state equations

$$\frac{dv}{ds} = -\frac{(1+\lambda^2)(1-v)}{E^*\lambda\cos\sigma}$$

$$\frac{d\theta}{ds} = \frac{\cos\psi}{\cos\phi}$$

$$\frac{d\phi}{ds} = \sin\psi \qquad (8.9)$$

$$\frac{d\psi}{ds} = \frac{(1-v)}{v}\tan\sigma - \cos\psi\tan\phi$$

The Hamiltonian of the reduced problem is

$$H = -p_v\left[\frac{(1+\lambda^2)(1-v)}{E^*\lambda\cos\sigma}\right] + p_\theta\left[\frac{\cos\psi}{\cos\phi}\right] + p_\phi\sin\psi + p_\psi\left[\frac{(1-v)}{v}\tan\sigma - \cos\psi\tan\phi\right] \qquad (8.10)$$

Then, it is clear that the optimum lift control is

$$\lambda = \pm 1 \qquad (8.11)$$

that is the glide is effected at maximum lift-to-drag ratio. For the bank control, we either have

$$|\sigma| = \sigma_{max}$$

or an interior bank control such that

$$\sin\sigma = \frac{E^* p_\psi}{2 v p_v} \qquad (8.12)$$

We notice that the integrals (3.7) are still valid for this case. Hence, with $C_1 = 0$, $C_0 = 0$, we can write the Hamiltonian integral of (8.10) in

the form

$$-\frac{2\,p_v(1-v)}{E^*\cos\sigma}+p_\phi\sin\psi+p_\psi\left[\frac{(1-v)\tan\sigma}{v}-\cos\psi\tan\phi\right]=0 \qquad (8.13)$$

Using the optimal law (8.12) to eliminate p_v and the Eqs. (8.3) for p_ψ and p_ϕ, we have the explicit law for the bank angle

$$\tan\sigma=\frac{(1-v)}{v}\,\frac{\cos\phi\sin(\theta_f-\theta)}{\cos(\theta_f-\theta)\sin\psi-\cos\psi\sin\phi\sin(\theta_f-\theta)} \qquad (8.14)$$

The problem is thus reduced to a one-parameter problem in the parameter θ_f. In this formulation the stopping condition is no longer Z_f but the final speed v_f.

For numerical computation, we use the control law (8.14) to integrate the full set of exact state equations (2.8) with a guessed value for the final longitudinal range θ_f. This value is to be adjusted such that, at the final time when $\theta=\theta_f$, the prescribed final condition $v=v_f=.001$ is satisfied. The initial state used is (8.6) except that the initial speed is 0.99 instead of 1.0. The purpose of this change is to give a defined σ value at the initial instant. The maximum value of the bank angle is selected to be 85°. Figure 24 presents the maximum cross range solved by using the reduced control law (8.14), as a function of the maximum lift-to-drag ratio E^*. The dashed lines represent the results of the gliding trajectory with $\lambda=1$ and $\sigma=45^\circ$ where the bank angle is switched to 0° when the heading angle ψ reaches the limiting value 90°. The improvement in the

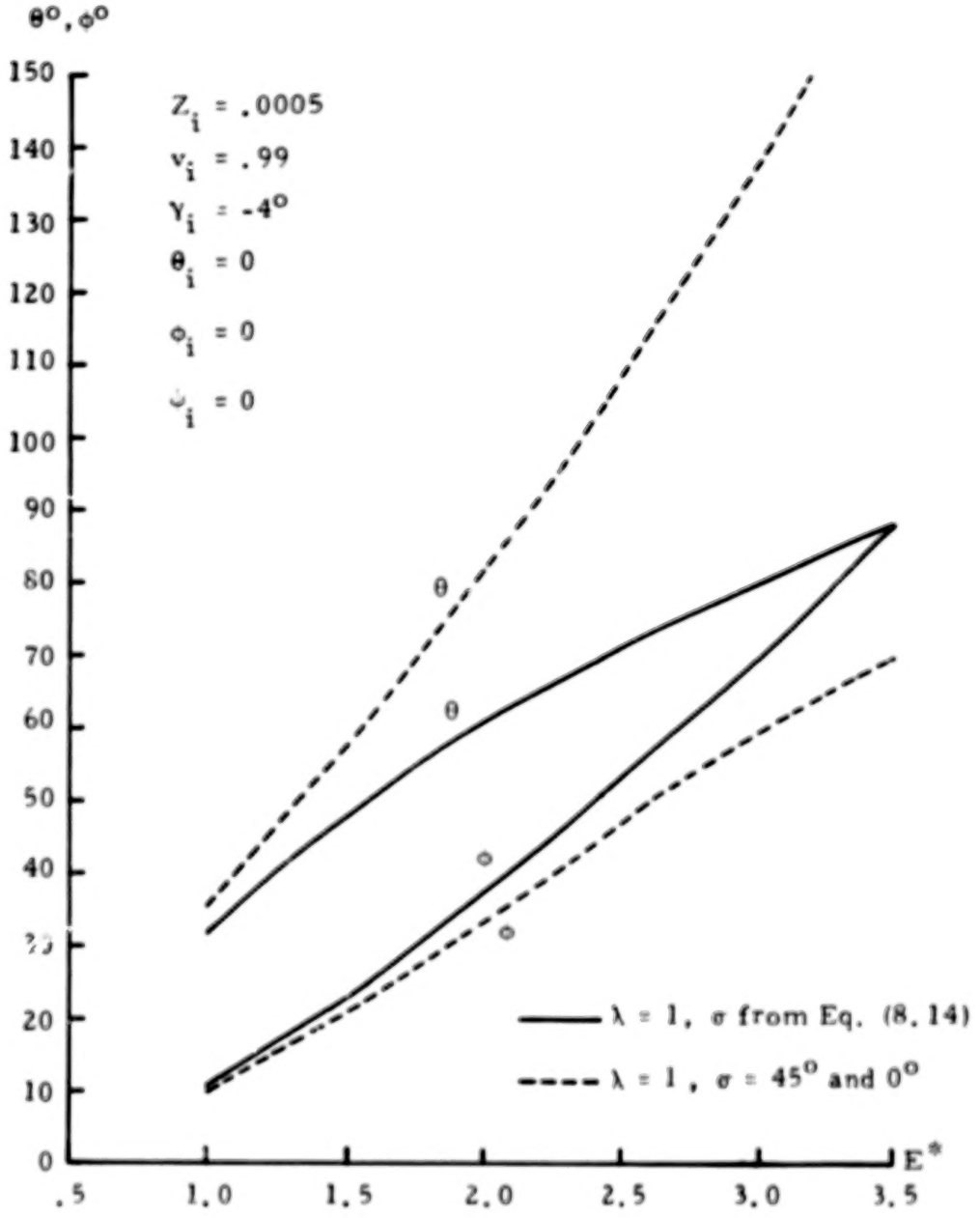

Figure 24. - The Longitudinal and Cross Ranges as Functions of E^*.

cross range is easily seen. We can also see that for vehicles with a maximum lift-to-drag ratio E^* greater than the value 3.5, the maximum cross range is larger than 90° and the reachable domain of the vehicle is the whole surface of the earth if it has an initially circular

orbit and the point of departure is not specified. For all the trajectories, the final altitudes are about the same with $Z_f \simeq 30$, which corresponds to an altitude drop of about 80 km from the initial point. The final flight path angles vary with E^*, with larger E^* giving flatter flight path angles. For example, for $E^* = 1.5$ the final flight path angle is $\gamma_f = -23.5^\circ$ for both control laws Eq. (8.14) and $\sigma = 45^\circ$ and 0°; for $E^* = 3.5$, it is $\gamma_f = -11.0^\circ$. Figure 25 presents the variation of the altitude and the speed of the trajectory generated by the lift control $\lambda = 1$ and the bank control (8.14) while Figure 26 presents the variation of the flight path angle and the bank angle, for the maximum lift-to-drag ratio $E^* = 1.5$.

8.2 The Footprint

As has been mentioned before, if the reentry vehicle is initially in a circular orbit and the position for leaving the orbit is not prescribed, then the reachable domain on the surface of the earth will be a zone between the latitude $-\phi_{max}$ and ϕ_{max}. The footprint of a reentry vehicle is defined as the curve limiting the reachable domain on the surface of the earth if the reentry point is specified. This problem is even more complicated since we have to find the maximum cross range for each prescribed final longitudinal range θ_f. As the final longitudinal range is no longer free, $p_\theta \equiv C_1 \neq 0$. In Eqs. (3.7), if we divide all the equations with C_1, they become

BLANK PAGE

BLANK PAGE

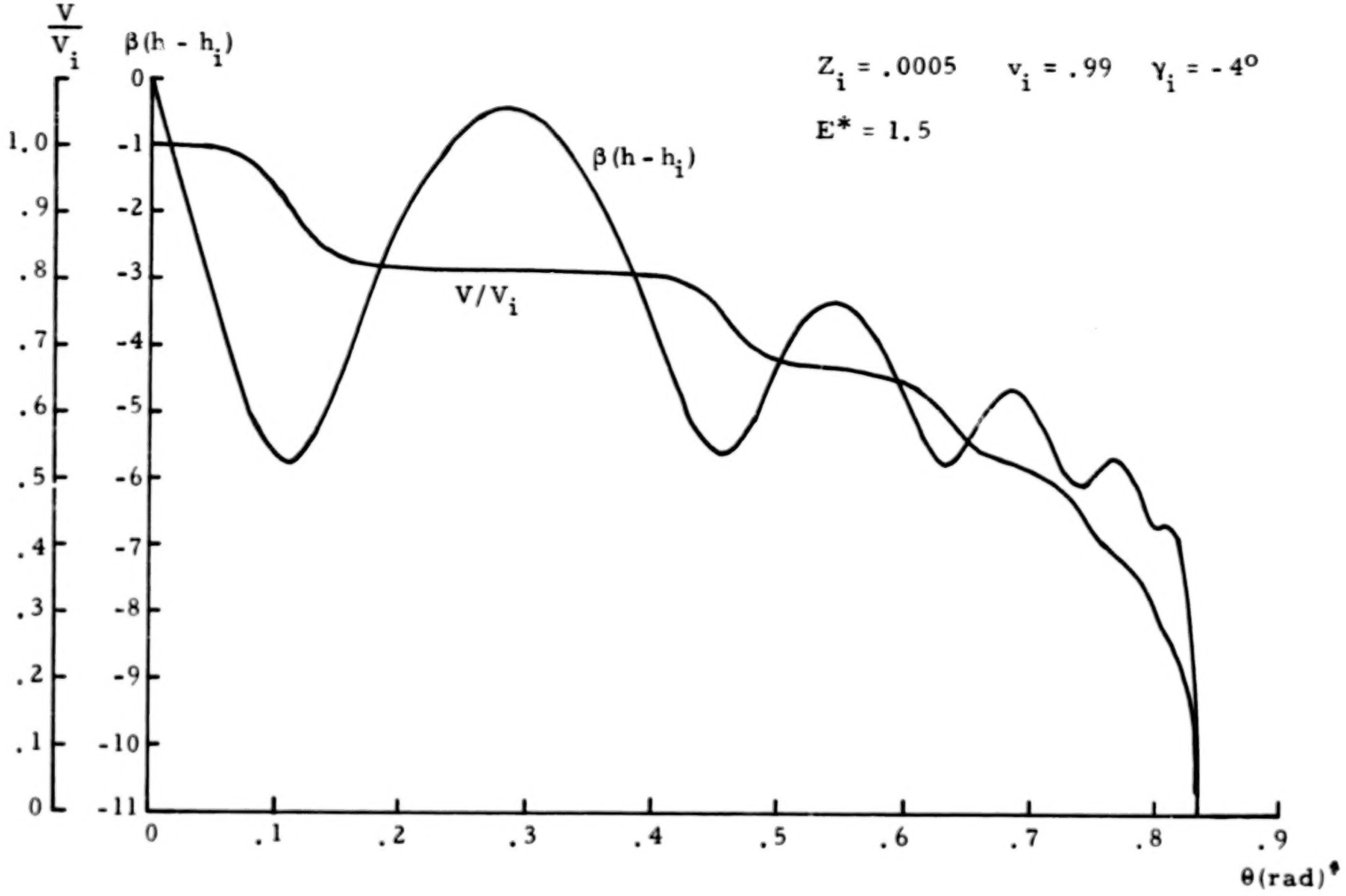

Figure 25.- Variation of the Altitude and the Speed of the Trajectory Generated by the Control Law $\lambda = 1$ and Eq. (8.14).

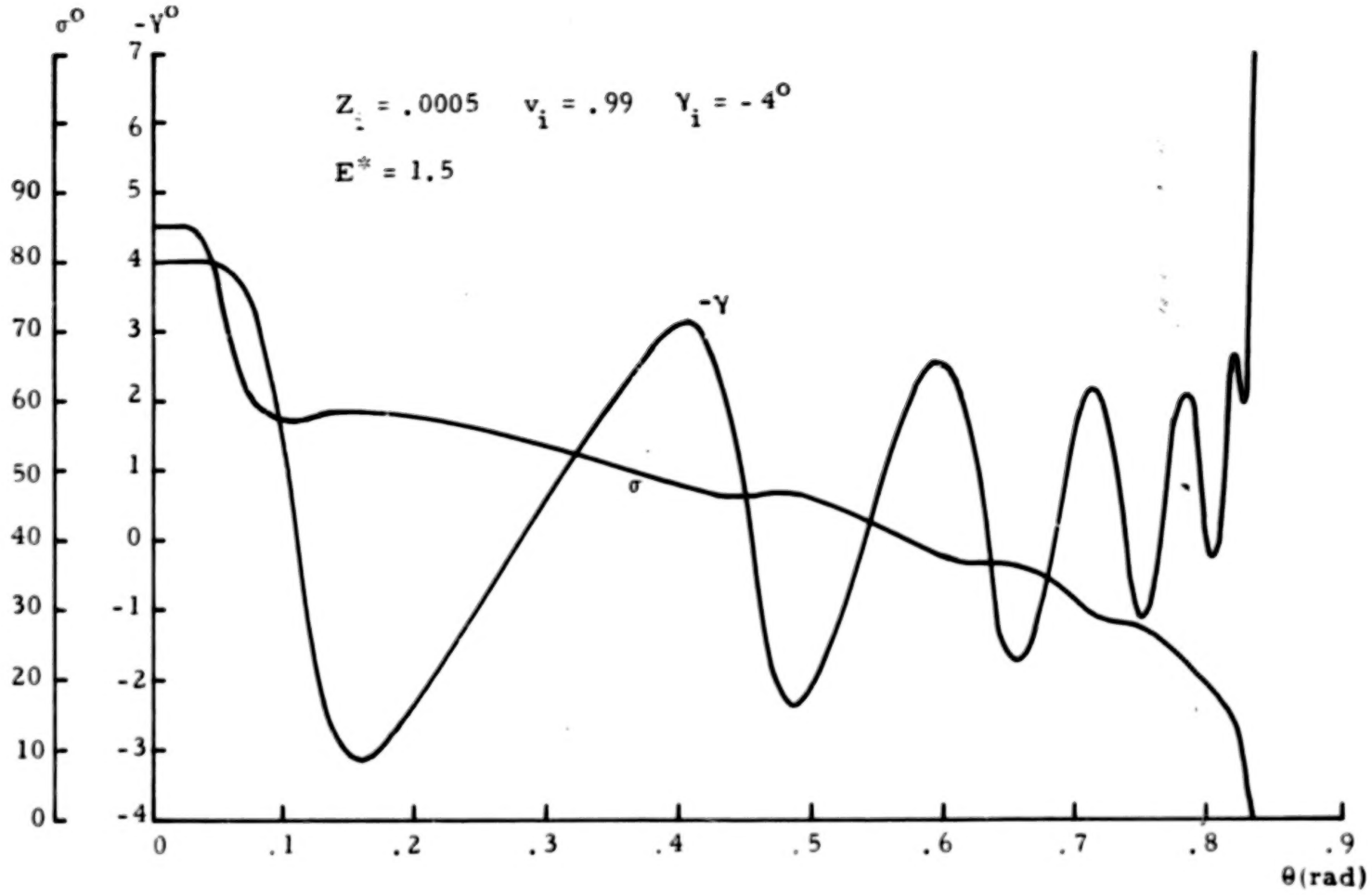

Figure 26.-Variation of the Flight Path Angle and the Bank Control of the Trajectory Generated by the Control Law $\lambda = 1$ and Eq. (8.14).

$$\frac{p_\theta}{C_1} = 1$$

$$\frac{p_\phi}{C_1} = \frac{C_2}{C_1}\cos\theta + \frac{C_3}{C_1}\sin\theta \qquad (8.15)$$

$$\frac{p_\psi}{C_1} = \sin\phi - \cos\phi\left(\frac{C_2}{C_1}\sin\theta - \frac{C_3}{C_1}\cos\theta\right)$$

Similarly, Eqs. (3.9) can be rewritten in the form

$$\frac{d}{ds}\left(\frac{P}{C_1}\right) = \frac{k^3 Z}{\cos\gamma}\left\{\frac{1}{E^*}\left(\frac{N}{C_1}\right) - \frac{E^*}{4\,(N/C_1)}\left[\left(\frac{Q}{C_1}\right)^2 + \frac{1}{\cos^2\gamma}\left(\frac{p_\psi}{C_1}\right)^2\right]\right\}$$

$$\frac{d}{ds}\left(\frac{N}{C_1}\right) = -\frac{1}{v}\left[\left(\frac{Q}{C_1}\right) + 2\left(\frac{N}{C_1}\right)\tan\gamma\right] \qquad (8.16)$$

$$\frac{d}{ds}\left(\frac{Q}{C_1}\right) = \frac{1}{\cos^2\gamma}\left\{\left(\frac{P}{C_1}\right) + \left(\frac{N}{C_1}\right)\left[\frac{k Z \sin\gamma}{E^*} + \frac{2-v}{v}\right]\right.$$
$$\left. - \frac{E^* k Z \sin\gamma}{4\,(N/C_1)}\left[\left(\frac{Q}{C_1}\right)^2 + \frac{3}{\cos^2\gamma}\left(\frac{p_\psi}{C_1}\right)^2\right]\right\}$$

In terms of the new variables p_ϕ/C_1, etc., the Hamiltonian integral (3.11) becomes

$$-\left(\frac{P}{C_1}\right)\tan\gamma - \left(\frac{N}{C_1}\right)\left[\frac{k Z}{E^*\cos\gamma} + \frac{(2-v)}{v}\tan\gamma\right] - \frac{(1-v)}{v}\left(\frac{Q}{C_1}\right)$$
$$+ \frac{E^* k Z}{4\,(N/C_1)\cos\gamma}\left[\left(\frac{Q}{C_1}\right)^2 + \frac{1}{\cos^2\gamma}\left(\frac{p_\psi}{C_1}\right)^2\right] + \frac{\cos\psi}{\cos\phi} + \left(\frac{p_\phi}{C_1}\right)\sin\psi$$
$$- \left(\frac{p_\psi}{C_1}\right)\cos\psi\tan\phi = 0 \qquad (8.17)$$

where again $C_0 = 0$ since the final arc length is always free. The control law is, from Eqs. (3.5),

$$\lambda \cos\sigma = \frac{E^*(Q/C_1)}{2(N/C_1)} \quad , \quad \lambda \sin\sigma = \frac{E^*(p_\psi/C_1)}{2(N/C_1)\cos\gamma} \qquad (8.18)$$

The Eqs. (8.15) - (8.18) combined with the state equations (2.8) are the equations for solving the exact footprint of a reentry vehicle from a specified departure point. There are four parameters in this problem; they are (C_2/C_1), (C_3/C_1), and two of the three initial values $(P/C_1)_i$, $(N/C_1)_i$, and $(Q/C_1)_i$ since one of them can be obtained from the Hamiltonian integral (8.17). Among them, one can be used as a scanning parameter since we want to solve the whole footprint. Hence, it is a three-parameter problem. For a typical example, a vehicle is initially at the specified point (8.6). To find the exact footprint we pick a scanning parameter and guess the other three parameters, and start the integration of Eqs. (2.8) and (8.16) along with the using of Eqs. (8.15) and (8.18). The three guessed parameters are to be adjusted such that when the integration is stopped at the final time with $v = v_f$, the prescribed $Z = Z_f$ and $\gamma = \gamma_f$ and the transversality condition

$$\left(\frac{p_\psi}{C_1}\right)_f = 0 \qquad (8.19)$$

are all satisfied. Then by varying the scanning parameter the footprint can be solved. If the final flight path angle is not prescribed, the condition $\gamma = \gamma_f$ will be replaced by another transversality condition, namely $(Q/C_1)_f = 0$.

In the preceding section we have obtained ϕ_{max} by using the equilibrium glide simplification. We shall use the same device in this section again. The control law (8.12) is still valid in this case. By using it in the Hamiltonian integral (8.10), an explicit law for the bank angle is found to be

$$\tan \sigma = \frac{A}{B} \tag{8.20}$$

where

$$A = \left(\frac{1 - v}{v}\right) \frac{p_\psi}{C_1}$$

$$B = \frac{\cos \psi}{\cos \phi} + \frac{p_\phi}{C_1} \sin \psi - \frac{p_\psi}{C_1} \sin \psi \tan \phi \tag{8.21}$$

From the second and third equations of (3.7) since $C_1 \neq 0$, we have

$$\frac{p_\psi}{C_1} = \sin \phi - \cos \phi (k_1 \sin \theta - k_2 \cos \theta)$$

$$\frac{p_\phi}{C_1} = k_1 \cos \theta + k_2 \sin \theta \tag{8.22}$$

where

$$k_1 = \frac{C_2}{C_1} \quad , \quad k_2 = \frac{C_3}{C_1} \tag{8.23}$$

Hence, there are two parameters k_1 and k_2 in the problem. However this is a one-parameter problem since either k_1 or k_2 can be a scanning parameter. For the transversality condition since the final heading angle ψ_f is still free in this case, we have $p_{\psi_f} = 0$ or from the first equation of (8.22),

$$\sin\phi_f - \cos\phi_f (k_1 \sin\theta_f - k_2 \cos\theta_f) = 0 \qquad (8.24)$$

The procedure to solve the footprint is as follows. Using the explicit control law (8.20) in the full set of exact state equations (2.8), the integration is started from the initial state (8.6) with $v_i = .99$ instead of 1.0. For the two parameters k_1 and k_2 we pick k_1 as the scanning parameter and adjust k_2 such that when the specified value $v = v_f$ is reached, the transversality condition (8.24) is also satisfied. By varying k_1 and doing the same adjustment on k_2 for each value of k_1, the whole footprint is solved. Although in this reduced problem the final altitude is not specified, according to the numerical results it is acceptable in general.

A technique of coordinate rotation has been introduced by Fave [9] for a flat planet model. Its application in the spherical planet model enables us to use the control law (8.14) which corresponds to $C_1 = 0$ for solving the footprint. We shall illustrate the technique in the flat earth case at first, and then use it in the spherical earth case. In Figure 27, let M_i y z be the initial coordinate axes and $M_i M_f$ be an optimal trajectory leading to the final point M_f on the footprint C for a given longitudinal range y_f. Let M_i y' z' be the rotated coordinate system with the axis M_i y' parallel to the tangent of the footprint C at the point M_f. Since the footprint is the same if the initial condition is maintained, if we use the new

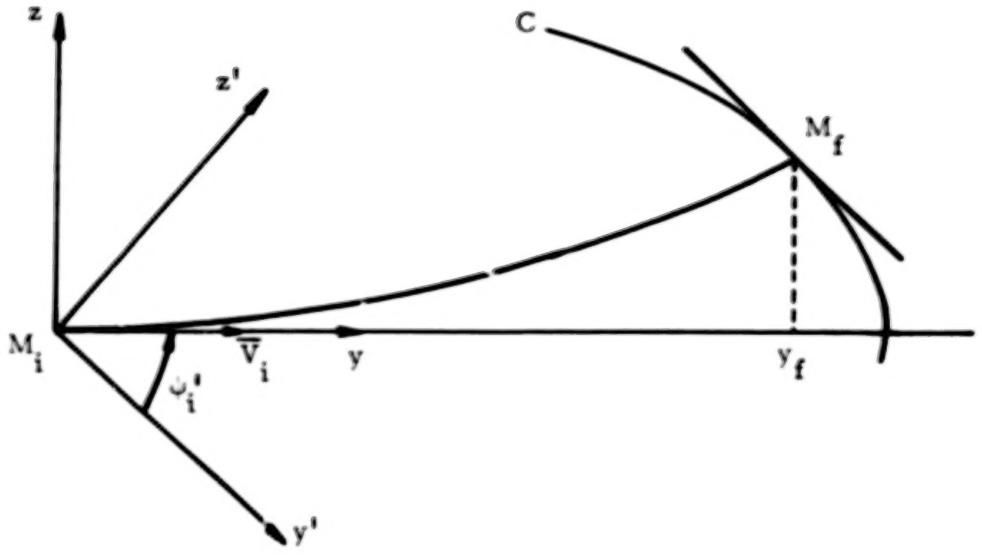

Figure 27.- Rotation of the Coordinate Axes, Flat Planet Case.

axes $M_i y' z'$ to find the point M_f on the footprint, we have the problem of maximizing z' while y' is free. As the axis My' is not known a priori, we have a new parameter, namely the initial heading angle ψ_i' with respect to the new axes. Besides the new parameter ψ_i', we also have another parameter y_f' on the new axes. These two new parameters correspond to the parameters k_1 and k_2 in Eqs. (8.22), but they are geometrical quantities on the rotated axes. The parameter ψ_i' is the initial heading angle with respect to the rotated axes. It will be clear later on that, if we consider the upper half of the footprint and translate the rotated axes to the points on the footprint, we will see that the maximum longitudinal range point corresponds to the value $\psi_i' = 90^\circ$. Then, as the new axes are moving

along the footprint, the ψ_i' angle is decreasing from 90^o to 0^o and then to -90^o. The $\psi_i' = 0^o$ corresponds to the maximum lateral range point of the footprint, and the $\psi_i' = -90^o$ is the point where the slope of the footprint fails to be continuous. On the other hand, the other new parameter y_f' is the value of y' where the maximization of z' occurs. Hence, for the two new parameters we can pick ψ_i' as the scanning parameter. For each value of ψ_i' from $+90^o$ to -90^o, the y_f' is adjusted such that the final condition is satisfied. Then, from the values (y_f', z_f') and the angle ψ_i', we can compute the coordinates (y_f, z_f) of the resulting point on the original axes M_i y z by using the relations

$$y_f = y_f' \cos\psi_i' + z_f' \sin\psi_i'$$

$$z_f = -y_f' \sin\psi_i' + z_f' \cos\psi_i'$$

By varying the ψ_i' from $+90^o$ to -90^o, the footprint can be obtained very systematically and effectively.

For the spherical earth model, the rotation of the coordinate axes must be performed on the surface of a sphere, since all the coordinate axes must lie along a great circle. The equations for coordinate transformation are not apparent and their derivation is more elaborate. Again, in Figure 28, $M_i\,\theta\,\phi$ is the original coordinate system and $M_i M_f$ is an optimal trajectory leading to a point M_f on the footprint C for a given longitudinal range θ_f. There is a tangent of the footprint C at the point M_f. At point M_i and parallel

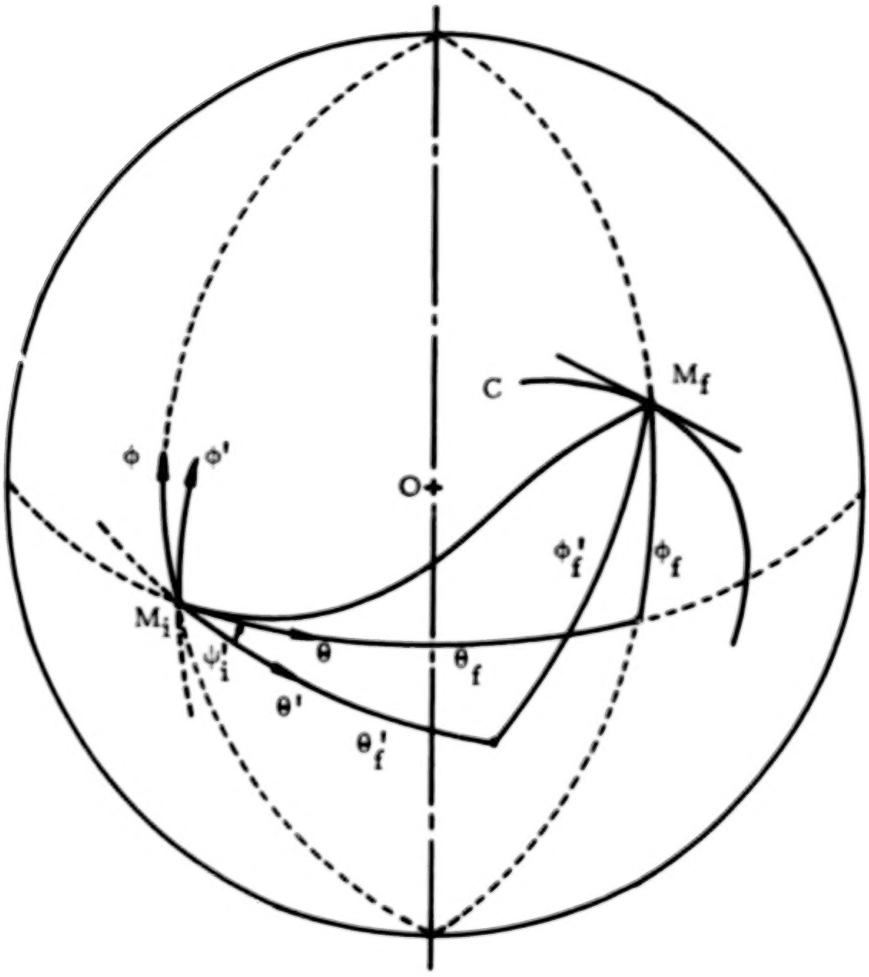

Figure 28.- Rotation of the Coordinate Axes, Spherical Planet Case.

to this line we can draw a straight line which , together with the center of the sphere determines the great circle plane for the rotated axis $M_i \theta'$. The rotated axis $M_i \phi'$ is then on a great circle passing through the point M_i and perpendicular to the great circle of axis $M_i \theta'$. Hence, $M_i \theta' \phi'$ is the rotated coordinate system for the point M_f on the footprint. Referring to this new axes system, the optimal

trajectory $M_i M_f$ has an initial heading angle ψ_i', but the point M_f is the absolute maximum lateral range point. Thus, with respect to the new axes $M_i \theta' \phi'$ we are maximizing ϕ' with θ' free, and the explicit control law (8.14) can be used. For convenience, Eq. (8.14) is rewritten on the new axes $M_i \theta' \phi'$ as follows

$$\tan\sigma = \frac{(1-v)}{v} \frac{\cos\phi' \sin(\theta_f' - \theta')}{\cos(\theta_f' - \theta')\sin\psi' - \cos\psi' \sin\phi' \sin(\theta_f' - \theta')} \quad (8.25)$$

For each value of ψ_i' from $+90^\circ$ to -90°, we guess θ_f' and integrate the state equations (2.8) from the initial condition (8.6) with $v_i = .99$ instead of 1.0 by using the explicit control law (8.25). Then we adjust θ_f' such that when the integration is stopped at $\theta' = \theta_f'$ the final speed $v_f = .001$ is satisfied. The results (θ_f', ϕ_f') obtained from this iteration are the values on the rotated axes $M_i \theta' \phi'$. The formulas to translate them to the values referring to the original axes are

$$\tan\theta_f = \tan\theta_f' \cos\psi_i' + \frac{\tan\phi_f' \sin\psi_i'}{\cos\theta_f'}$$

$$\sin\phi_f = \sin\phi_f' \cos\psi_i' - \sin\theta_f' \cos\phi_f' \sin\psi_i' \quad (8.26)$$

These formulas are derived in Appendix C, using the spherical trigonometrical relations. To construct the footprint, we start from the value $\psi_i' = 90^\circ$ which corresponds to the maximum longitudinal range point of the footprint. As ψ_i' is decreasing from 90° to 0°,

which corresponds to the global maximum cross range point, the portion of the footprint to the right of the global ϕ_{max} point is obtained. The portion to the left is constructed by ψ_i' ranging from 0^o to -90^o. Figure 29 shows the footprint for the maximum lift-to-drag ratio $E^* = 1.5$. The trajectories leading to the points on the footprint are also depicted with the corresponding values of ψ_i' and θ_f' given. This technique of rotating the coordinates is not applicable to the short arc to the left end of the footprint beyond $\psi_i' = -90^o$. For all trajectories from $\psi_i' = 90^o$ to -90^o, the bank angle is always positive, that is, to the left, or zero. But for the short arc beyond $\psi_i' = -90^o$ we have to bank the vehicle to the right at first, and then to the left at a certain switching point. Figure 30 presents the bank control as a function of the longitudinal range θ for the trajectories. The maximum bank angle is $\sigma_{max} = 85^o$. For trajectories with long longitudinal ranges, the bank angle is near zero initially. It increases to certain value and then decreases to zero finally. For trajectories with short longitudinal ranges, the bank control hits the σ_{max} for a while and then decreases to zero finally. Again, the final altitude is not considered. But for all the trajectories the final altitudes are very close to the value $Z_f = 30$ which is a reasonably low altitude.

BLANK PAGE

BLANK PAGE

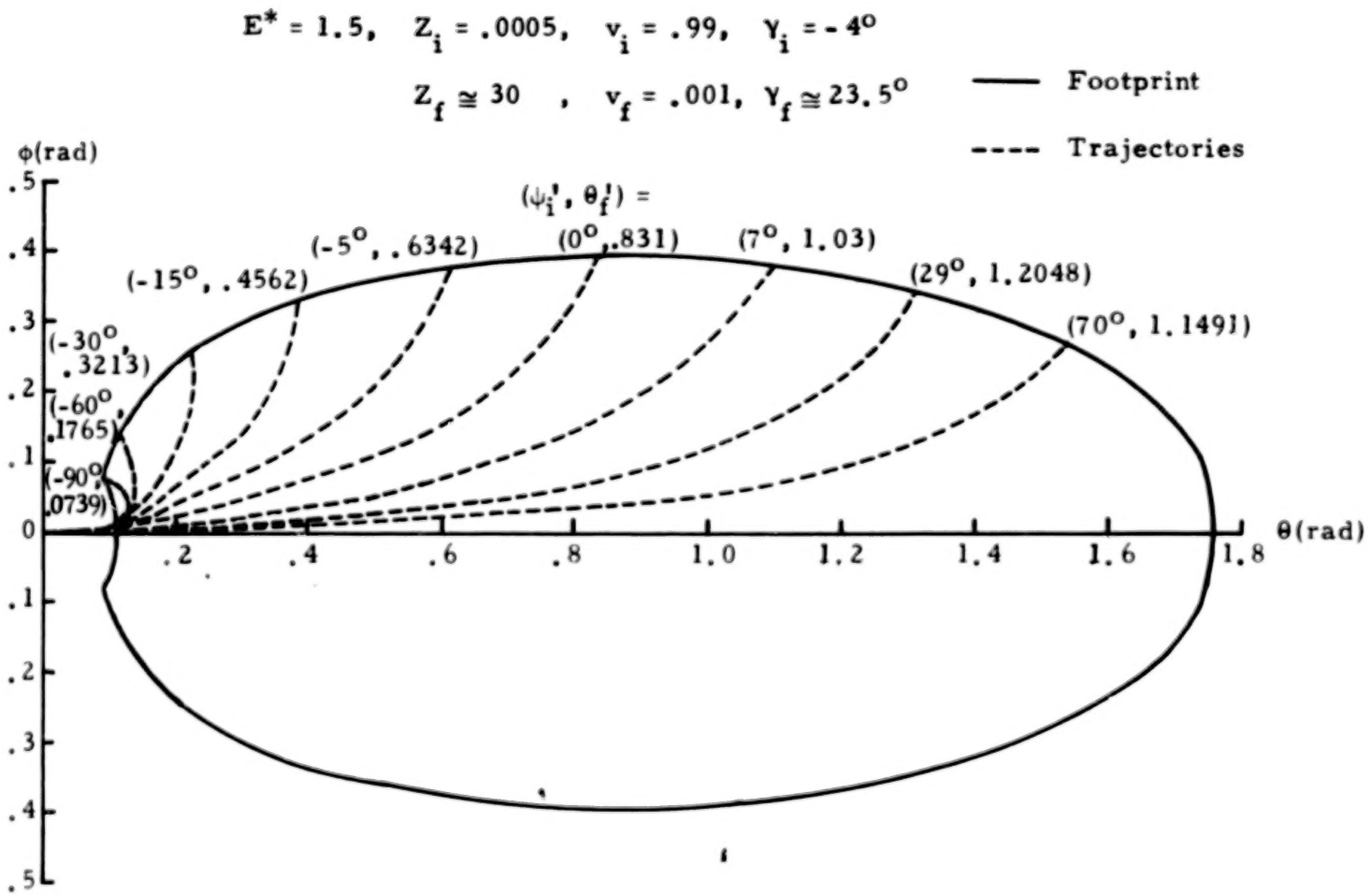

Figure 29.- Footprint for $E^* = 1.5$.

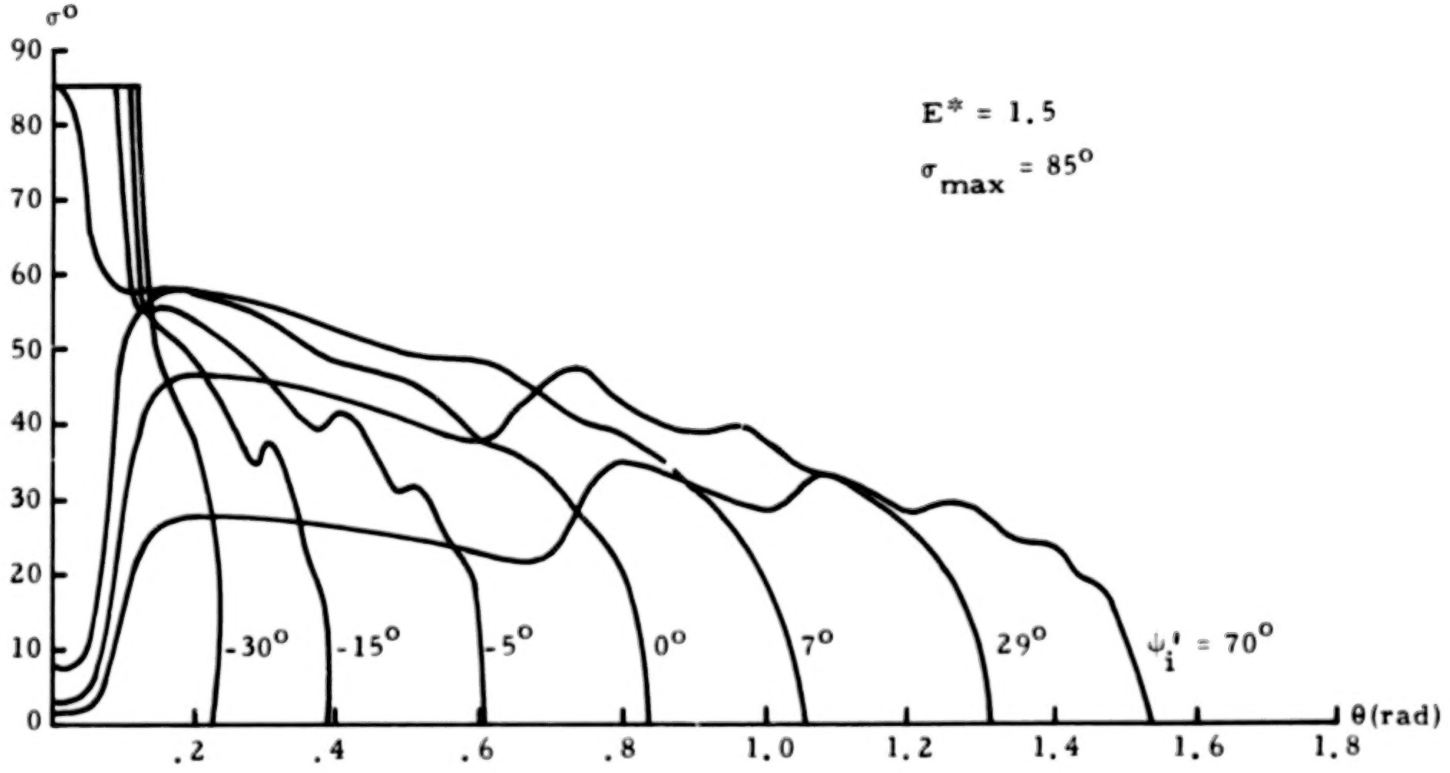

Figure 30.- Bank Control for Trajectories Leading to the Footprint, $E^* = 1.5$.

CHAPTER 9

CONCLUSIONS

A general solution for optimum reentry trajectories in a vertical plane has been presented. The three-dimensional optimal trajectories leading to a maximum cross range and the footprint are solved in a reduced problem. Unlike previous numerical studies in the published literature where physical data have to be specified numerically, here we only have to specify the most important performance parameter, namely the maximum lift-to-drag ratio E^*. The numerical results obtained are valid for all vehicles having the same maximum lift-to-drag ratio. For the other vehicles with the values of E^* around the value we have used for computation, the behavior of the optimum lift control and the trajectory variables such as altitude, speed, and flight path angle are essentially the same.

This very general study is made possible by the use of the modified Chapman's variables and a normalized lift coefficient. The planetary atmosphere is assumed to be spherical and at rest, with locally exponential variation in its density. It is found that the characteristic for any atmosphere can be specified by the average value of the dimensionless quantity $k^2 = \beta r$. For the numerical

computation, we take $k^2 = 900$ for the earth's atmosphere. The equations retain the generality and are also valid for flight in a vacuum. Hence, the totality of the optimum trajectory, from entry to landing, can be followed continuously even if at the beginning the vehicle skips out of the atmosphere repeatedly before effective entry at lower speed.

For the planar flight case, several optimum problems for flight over a spherical earth are solved and the results analyzed in detail, especially the skip trajectory. At low altitude and low speed, it is more convenient to use a flat earth model. This has been achieved by using a canonical transformation applied to the spherical equations followed by a flat earth simplification. Optimum problems for flight over a flat earth are solved using the simplified equations. The optimum gliding trajectory for maximum final range, as compared to the maximum lift-to-drag ratio gliding trajectory, has better range and smaller peak deceleration and is less oscillatory.

In three-dimensional flight, we have two more state variables, namely the latitude and the heading, one more control, namely the bank angle, and two more adjoint equations. But at the same time, we have two additional integrals. Hence, the real difficulty in three-dimensional analysis lies not in the analytical formulation but in the practical computation of a two-point boundary value problem containing three parameters instead of two as in the planar case. A

simplification is thus introduced by using the so-called equilibrium glide condition, assuming that the glide angle is small and stays nearly constant. Then, by using this simplification, the footprint of a reentry vehicle is calculated. A technique of coordinate system rotation has been used, which makes the iteration much more effective and geometrically meaningful.

A distinctive feature of the present formulation is that the equations of motion and their variational derivations are valid uniformly for flight in the dense layer of the atmosphere where the aerodynamic force is predominant and for flight in the near vacuum where the Newtonian gravitational force is predominant. Hence we can use the same equations for the investigation of the effectiveness of the optimum aerodynamic control at very high altitude. It is expected that this tenuous aerodynamic control, coupled with a thrust control with small magnitude, will be sufficient as optimum controls for the guidance of skip trajectories.

APPENDIX A

Normalized Drag Polar

Consider a generalized drag polar of the form

$$C_D = C_{D_0} + K C_L^n \tag{A.1}$$

where at very high Mach number, the zero-lift drag coefficient C_{D_0}, the induced drag factor K, and the exponent n are assumed to have their constant asymptotic values. If $E = C_L/C_D$ is the lift-to-drag ratio, then

$$\frac{1}{E} = \frac{C_{D_0}}{C_L} + K C_L^{n-1} \tag{A.2}$$

Hence, E is a maximum when

$$-\frac{C_{D_0}}{C_L^2} + (n-1) K C_L^{n-2} = 0 \tag{A.3}$$

This corresponds to the lift and drag coefficients

$$C_L^* = \sqrt[n]{\frac{C_{D_0}}{(n-1)K}} \quad , \quad C_D^* = \frac{n}{n-1} C_{D_0} \tag{A.4}$$

The maximum lift-to-drag ratio E^* is, of course,

$$E^* = C_L^*/C_D^* \tag{A.5}$$

If we define the normalized lift coefficient λ as

$$\lambda = \frac{C_L}{C_L^*} \tag{A.6}$$

then it is clear that when $\lambda = 1$, $C_L = C_L^*$ and the operating point is at the point of maximum lift-to-drag ratio. Using (A.4) and (A.6) in (A.1), we have

$$C_D = \frac{C_{D_0}}{(n-1)} \left[(n-1) + \lambda^n \right] \tag{A.7}$$

Considering (A.5) we obtain

$$C_D = C_D^* f(\lambda) \tag{A.8}$$

where

$$f(\lambda) = \frac{(n-1) + \lambda^n}{n} \tag{A.9}$$

For the case of a parabolic drag polar, $n = 2$, we have

$$C_L = \lambda C_L^* \quad , \quad C_D = C_D^* \left(\frac{1+\lambda^2}{2} \right) \quad , \quad E^* = C_L^*/C_D^* \tag{A.10}$$

APPENDIX B

Derivation of the Equations (6.31) and (6.32)

The exact Hamiltonian for the flat planet case is

$$\mathcal{H} = w p_w \tan\gamma - \frac{u p_u (1+\lambda^2)}{E^* w \cos\gamma} - 2 p_u \tan\gamma + \frac{p_\gamma \lambda}{w \cos\gamma} - \frac{p_\gamma}{u} \qquad (B.1)$$

We use the approximate solution

$$\lambda_0 = 1 \qquad (B.2)$$

to linearize $\mathcal{H}$. Then

$$\mathcal{H} = \mathcal{H}\Big|_{\lambda=\lambda_0} + \frac{\partial \mathcal{H}}{\partial \lambda}\Big|_{\lambda=\lambda_0} (\lambda - \lambda_0) + \cdots \qquad (B.3)$$

By retaining only the first order term, we have

$$\mathcal{H} = w p_w \tan\gamma - 2 p_u \tan\gamma - \frac{p_\gamma}{u} + \frac{\lambda}{E^* w \cos\gamma} (E^* p_\gamma - 2 u p_u) \qquad (B.4)$$

From the linearized Hamiltonian (B.4), we can derive the corresponding linearized state and adjoint equations. They are

$$\frac{dw}{dy} = w \tan\gamma$$

$$\frac{du}{dy} = -\frac{2 u \lambda}{E^* w \cos\gamma} - 2 \tan\gamma \qquad (B.5)$$

$$\frac{d\gamma}{dy} = \frac{\lambda}{w \cos\gamma} - \frac{1}{u}$$

and

$$\frac{dp_w}{dy} = - p_w \tan\gamma + \frac{\lambda}{E^* w^2 \cos\gamma} (E^* p_\gamma - 2 u p_u)$$

$$\frac{dp_u}{dy} = \frac{2 p_u \lambda}{E^* w \cos\gamma} - \frac{p_\gamma}{u^2} \tag{B.6}$$

$$\frac{dp_\gamma}{dy} = - \frac{w p_w}{\cos^2\gamma} + \frac{2 p_u}{\cos^2\gamma} - \frac{\lambda \sin\gamma}{E^* w \cos^2\gamma} (E^* p_\gamma - 2 u p_u)$$

respectively. Now, to maximize the Hamiltonian (B.4), we consider the switching function

$$\Phi = E^* p_\gamma - 2 u p_u \tag{B.7}$$

Then, for $\mathcal{H}$ to be maximum with respect to λ, we use $\lambda = \lambda_{max}$ if $\Phi > 0$, and we use $\lambda = \lambda_{min}$ if $\Phi < 0$. In the finite time interval during which $\Phi = 0$, we have λ = variable. Since for maximum range glide, in the plot for λ in Figure 9 there is an interval in which the optimum λ is variable and near unity, we have the approximate singular relation

$$\Phi = E^* p_\gamma - 2 u p_u = 0 \tag{B.8}$$

By taking its derivative, using Eqs. (B.5), (B.6), and (B.8) itself, we have

$$w p_w = 2 p_u \left[1 + \frac{2 \cos^2\gamma}{E^{*2}} (1 + E^* \tan\gamma)\right] \tag{B.9}$$

As the linear control does not appear in this first derivative, take

the derivative again. This time the linear control appears and is found to be

$$\lambda_1 = \frac{w \cos \gamma}{u} \tag{B.10}$$

This is the approximate but explicit control law in Eq. (6.31).

Now, let us use λ_1 as an approximate solution to linearize the Hamiltonian (B.1). Then

$$\mathcal{H} = \mathcal{H}\Big|_{\lambda = \lambda_1} + \frac{\partial \mathcal{H}}{\partial \lambda}\Big|_{\lambda = \lambda_1} (\lambda - \lambda_1)$$

$$= w p_w \tan \gamma + p_u \left(\frac{w \cos \gamma}{E^* u} - \frac{u}{E^* w \cos \gamma} - 2 \tan \gamma \right) - \frac{p_\gamma}{u}$$

$$+ \left(\frac{p_\gamma}{w \cos \gamma} - \frac{2 p_u}{E^*} \right) \lambda \tag{B.11}$$

The corresponding linearized state and adjoint equations are

$$\frac{dw}{dy} = w \tan \gamma$$

$$\frac{du}{dy} = \frac{w \cos \gamma}{E^* u} - \frac{u}{E^* w \cos \gamma} - 2 \tan \gamma - \frac{2\lambda}{E^*} \tag{B.12}$$

$$\frac{d\gamma}{dy} = \frac{\lambda}{w \cos \gamma} - \frac{1}{u}$$

and

$$\frac{dp_w}{dy} = - p_w \tan \gamma - p_u \left(\frac{\cos \gamma}{E^* u} + \frac{u}{E^* w^2 \cos \gamma} \right) + \frac{p_\gamma \lambda}{w^2 \cos \gamma}$$

$$\frac{dp_u}{dy} = p_u \left(\frac{w \cos \gamma}{E^* u^2} + \frac{1}{E^* w \cos \gamma} \right) - \frac{p_\gamma}{u^2} \tag{B.13}$$

$$\frac{dp_\gamma}{dy} = - \frac{w p_w}{\cos^2 \gamma} + p_u \left(\frac{w \sin \gamma}{E^* u} + \frac{u \sin \gamma}{E^* w \cos^2 \gamma} + \frac{2}{\cos^2 \gamma} \right) - \frac{p_\gamma \lambda \sin \gamma}{w \cos^2 \gamma}$$

respectively. Again, by putting the switching function equal to zero, we have

$$E^* p_\gamma - 2 w p_u \cos\gamma = 0 \qquad \text{(B.14)}$$

By taking the derivative of Eq. (B.14), it gives

$$E^* w p_w = p_u \left[2 E^* - \frac{2\cos^2\gamma}{E^*} + \frac{2 u^2 \cos^4\gamma}{E^* u^2} \right.$$

$$\left. - \frac{(1+2u)}{u} w \cos^2\gamma \sin\gamma + \frac{u}{w} \sin\gamma \right] \qquad \text{(B.15)}$$

Then if we take the derivative of Eq. (B.15), we can finally obtain a new explicit control law which is the one that is given in Eq. (6.32).

APPENDIX C

Derivation of Formula (8.26)

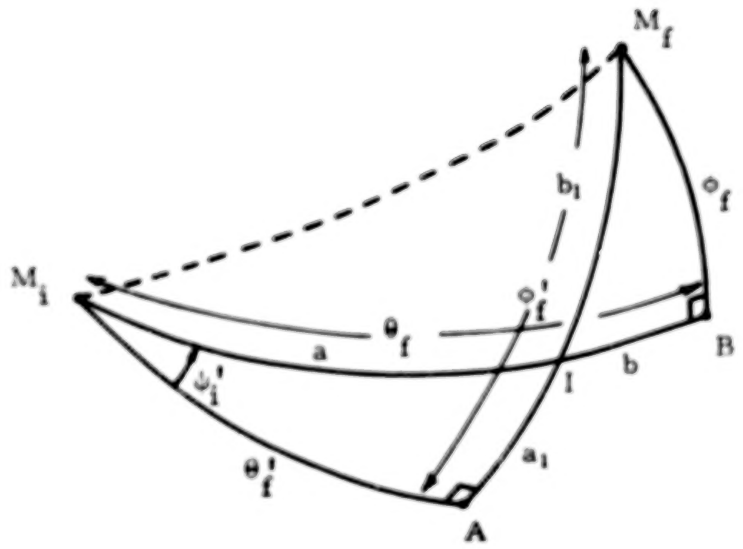

Figure C.1.- (θ'_f, ϕ'_f) and (θ_f, ϕ_f).

We have ψ'_i and (θ'_f, ϕ'_f), and we want (θ_f, ϕ_f). By considering the right spherical triangle $M_i A I$, we immediately have

$$\tan a = \frac{\tan \theta'_f}{\cos \psi'_i} \tag{C.1}$$

and

$$\tan a_1 = \sin \theta'_f \tan \psi'_i \tag{C.2}$$

Since $b_1 = \phi'_f - a_1$, taking the tangent of b_1 and using (C.2) in it, we have

$$\tan b_1 = \frac{\tan \phi_f' - \sin \theta_f' \tan \psi_i'}{1 + \sin \theta_f' \tan \phi_f' \tan \psi_i'} \qquad (C.3)$$

Now, from the right spherical triangle $M_i A I$,

$$\cos I = \cos \theta_f' \sin \psi_i' \qquad (C.4)$$

On the other hand from the other right spherical triangle $M_f B I$,

$$\cos I = \tan b \cot b_1 \qquad (C.5)$$

Solving for (tan b) from (C.4) and (C.5) and using (C.3),

$$\tan b = \frac{\cos \theta_f' \sin \psi_i' (\tan \phi_f' - \sin \theta_f' \tan \psi_i')}{1 + \sin \theta_f' \tan \phi_f' \tan \psi_i'} \qquad (C.6)$$

As $\theta_f = a + b$, again taking the tangent and using (C.1) and (C.6), we finally have

$$\tan \theta_f = \frac{\tan \phi_f' \sin \psi_i'}{\cos \theta_f'} + \tan \theta_f' \cos \psi_i' \qquad (C.7)$$

This is the first formula in (8.26).

For the second formula, from the right spherical triangle $M_f B I$,

$$\sin \phi_f = \sin b_1 \sin I \qquad (C.8)$$

and from the right spherical triangle $M_i A I$,

$$\cos \psi_i' = \cos a_1 \sin I \qquad (C.9)$$

Hence,

$$\sin \phi_f = \frac{\sin b_1 \cos \psi_i'}{\cos a_1} \qquad \text{(C. 10)}$$

Now, taking the sine on both sides of $b_1 = \phi_f' - a_1$ and then using (C. 2), we have

$$\sin \phi_f = \sin \phi_f' \cos \psi_i' - \sin \theta_f' \cos \phi_f' \sin \psi_i' \qquad \text{(C. 11)}$$

This is the second formula in (8. 26).

REFERENCES

1. Chapman, D.R., "An Approximate Analytical Method for Studying Entry into Planetary Atmospheres," NASA TR-R-11, 1959.

2. Moyer, H.G., "Integrals for Optimal Flight over a Spherical Earth," AIAA Journal, Vol. 11, No. 10, pp. 1441-1443, Oct. 1973.

3. Shkadov, L.M., Bukhanova, R.S., Illarionov, V.F., and Plokhikh, V.P., "Mechanics of Optimum Three-Dimensional Motion of Aircraft in the Atmosphere," NASA Technical Translation, NASA TT F-777, 1975.

4. Vinh, N.X., Busemann, A., and Culp, R.D., "Optimum Three-Dimensional Atmospheric Entry," Acta Astronautica, Vol. 2, pp. 593-611, 1975.

5. Fraeijs de Veubeke, B., "Canonical Transformations and the Thrust-Coast-Thrust Optimal Transfer Problem," Astronautica Acta, Vol. 11, pp. 271-282, 1965.

6. Powers, W.F. and Tapley, B.D., "Canonical Transformation Applications to Optimal Trajectory Analysis," AIAA Journal, Vol. 7, No. 3, pp. 394-399, March 1969.

7. Dunning, R.S., "Study of a Guidance Scheme Using Approximate Solutions of Trajectory Equations to Control the Aerodynamic Skip Flight of a Reentry Vehicle," NASA TN D-1923, 1963.

8. Vinh, N.X., "Optimal Singular Control with Applications to Trajectory Optimization," NASA Contractor Report 3087, 1979.

9. Fave, J., "Approche Analytique du Problème du Domaine Accessible à un Planeur Orbital," La Recherche Aérospatiale, No. 124, June 1968, pp. 3-11.

10. Dunning, R.S., "The Orbital Mechanics of Flight Mechanics," NASA SP-325, 1973.

1 Report No.	2. Government Accession No.	3. Recipient's Catalog No.
NASA CR-3236		

4. Title and Subtitle	5. Report Date
Optimum Reentry Trajectories of a Lifting Vehicle	February 1980
	6. Performing Organization Code

7. Author(s)	8. Performing Organization Report No.
Jeng-Shing Chern and Nguyen Xuan Vinh	10. Work Unit No.

9. Performing Organization Name and Address	11. Contract or Grant No.
The University of Michigan Ann Arbor, MI 48109	NSG-1448

12. Sponsoring Agency Name and Address	13. Type of Report and Period Covered
National Aeronautics and Space Administration Washington, DC 20546	Contractor Report
	14. Sponsoring Agency Code

15. Supplementary Notes

Langley Technical Monitor: Robert S. Dunning
Final Report

16. Abstract

Research results are presented of an investigation of the optimum maneuvers of advanced shuttle type spacecraft during reentry. The equations are formulated by means of modified Chapman variables resulting in a general set of equations for flight analysis which are exact for reentry and for flight in a vacuum. Four planar flight typical optimum manuevers are investigated. For three-dimensional flight the optimum trajectory for maximum cross range is discussed in detail. New techniques for calculating reentry footprints are presented.

17. Key Words (Suggested by Author(s))

shuttle trajectories
reentry
Chapman variables
optimum controls
footprints
atmospheric reentry
skips

18. Distribution Statement

Unclassified - Unlimited

Subject Category 13

19. Security Classif. (of this report)	20. Security Classif. (of this page)	21. No. of Pages	22. Price*
Unclassified	Unclassified	119	$6.50

* For sale by the National Technical Information Service, Springfield, Virginia 22161

NASA-Langley, 1980

END

June, 29, 1981